National Library of Canada
Acquisitions and Bibliographic Services Branch
395 Wellington Street
Ottawa, Ontario
K1A 0N4

Bibliothèque nationale du Canada
Direction des acquisitions et des services bibliographiques
395, rue Wellington
Ottawa (Ontario)
K1A 0N4

Your file Votre référence

Our file Notre référence

NOTICE

The quality of this microform is heavily dependent upon the quality of the original thesis submitted for microfilming. Every effort has been made to ensure the highest quality of reproduction possible.

If pages are missing, contact the university which granted the degree.

Some pages may have indistinct print especially if the original pages were typed with a poor typewriter ribbon or if the university sent us an inferior photocopy.

Reproduction in full or in part of this microform is governed by the Canadian Copyright Act, R.S.C. 1970, c. C-30, and subsequent amendments.

AVIS

La qualité de cette microforme dépend grandement de la qualité de la thèse soumise au microfilmage. Nous avons tout fait pour assurer une qualité supérieure de reproduction.

S'il manque des pages, veuillez communiquer avec l'université qui a conféré le grade.

La qualité d'impression de certaines pages peut laisser à désirer, surtout si les pages originales ont été dactylographiées à l'aide d'un ruban usé ou si l'université nous a fait parvenir une photocopie de qualité inférieure.

La reproduction, même partielle, de cette microforme est soumise à la Loi canadienne sur le droit d'auteur, SRC 1970, c. C-30, et ses amendements subséquents.

Canada

UNIVERSITY OF ALBERTA

SINGLE FREQUENCY HIGH TEMPERATURE

MICROWAVE DIELECTROMETERS

BY

BAIQIANG TIAN

A thesis submitted to the Faculty of Graduate Studies and Research in partial fulfillment of the requirements for the degree of Doctor of Philosophy.

DEPARTMENT OF ELECTRICAL ENGINEERING

EDMONTON, ALBERTA

FALL 1993

National Library of Canada
Bibliothèque nationale du Canada

Acquisitions and Bibliographic Services Branch
Direction des acquisitions et des services bibliographiques

395 Wellington Street
Ottawa, Ontario
K1A 0N4

395, rue Wellington
Ottawa (Ontario)
K1A 0N4

Your file Votre référence

Our file Notre référence

The author has granted an irrevocable non-exclusive licence allowing the National Library of Canada to reproduce, loan, distribute or sell copies of his/her thesis by any means and in any form or format, making this thesis available to interested persons.

L'auteur a accordé une licence irrévocable et non exclusive permettant à la Bibliothèque nationale du Canada de reproduire, prêter, distribuer ou vendre des copies de sa thèse de quelque manière et sous quelque forme que ce soit pour mettre des exemplaires de cette thèse à la disposition des personnes intéressées.

The author retains ownership of the copyright in his/her thesis. Neither the thesis nor substantial extracts from it may be printed or otherwise reproduced without his/her permission.

L'auteur conserve la propriété du droit d'auteur qui protège sa thèse. Ni la thèse ni des extraits substantiels de celle-ci ne doivent être imprimés ou autrement reproduits sans son autorisation.

ISBN 0-315-88117-8

Canada

UNIVERSITY OF ALBERTA

RELEASE FORM

NAME OF AUTHOR: Baiqiang Tian

TITLE OF THESIS: Single Frequency High Temperature
Microwave Dielectrometers

DEGREE: Doctor of Philosophy

YEAR THIS DEGREE GRANTED: 1993

Permission is hereby granted to the University of Alberta Library to reproduce single copies of this thesis and to lend or sell such copies for private, scholarly or scientific research purposes only.

The author reserves all other publication and other rights in association with the copyright in the thesis, and except as hereinbefore provided neither the thesis nor any substantial portion thereof may be printed or otherwise reproduced in any material form whatever without the author's prior written permission.

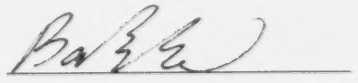

#5, 8408-105 Street
Edmonton, Alberta
Canada

Date: July 13 , 1993

UNIVERSITY OF ALBERTA

FACULTY OF GRADUATE STUDIES AND RESEARCH

The undersigned certify that they have read, and recommend to the Faculty of Graduate Studies and Research for acceptance, a thesis entitled **Single Frequency High Temperature Microwave Dielectrometers** submitted by Baiqiang Tian in partial fulfillment of the requirements for the degree of Doctor of Philosophy in Electrical Engineering.

Dr. W.R. Tinga

Dr. J.F. Vaneldik

Dr. J. Salmon

Dr. K. Nandakumar

pp Dr. S. Stuchly

Dr. C.G. Englefield

Date: June 30, 1993

ABSTRACT

Using microwaves to heat a sample in a cavity has recently been proved successful in minimizing the problems of overheating and test chamber expansion. However, two microwave channels operating at different frequencies, one for measuring and the other for heating, have to be employed. This thesis focuses on combining the measuring and the heating functions into one channel operating at a single frequency, thereby eliminating interference between channels and simplifying the instrumentation. Both passive and active dielectrometer approaches are investigated and analyzed.

This thesis shows that the Q factor is directly or inversely proportional to the input resonant resistance of a cavity when a moderate perturbation condition is satisfied. Based on this principle, a single frequency relative Q measurement method is developed, making it possible to measure the loss factor under a single frequency condition.

A modified coaxial re-entrant cavity is used as a dielectric sample heater and test chamber. In addition to an investigation of its characteristics and its design details, we analyze a re-entrant cavity with a gap arbitrarily positioned in its hollow center conductor using mode matching and equivalent circuit methods. Compared to many existing test chambers, this structure allows an easier sample access, has a lower sample air gap error and higher repeatability. We derive the theoretical model of a coupling loop at the endplate of a coaxial cavity using the mode expansion method. Based on these, a passive high temperature dielectric measurement system is constructed.

In order to eliminate mechanical tuning, we accomplish the high temperature measurement of a dielectric using an active self-oscillating loop consisting of a sample loaded cavity, amplifiers and transmission lines. A generalized oscillation condition in S-parameter notation is derived for an arbitrary loop. A subsequent theoretical model yields results within 0.05% of the measured loop oscillation frequency. From this calculated loop frequency, the dielectric constant of the sample can be predicted. A high temperature dielectrometer based on this self-oscillating loop is developed.

ACKNOWLEDGEMENT

I would like to express my gratitude to my supervisor, Dr. W.R.Tinga, for his constant encouragement, expert advice and personal help, without whom, the thesis would never have been completed. I am also grateful to my fellow graduate student, Dr. Weiguo Xi, for stimulating discussions and suggestions.

I sincerely thank Dr. W.A.G.Voss for inviting me to the Microwave Power Laboratory at the University of Alberta, which led to my doctoral program. I also thank Dr. J.F.Vaneldik, Dr. J.Salmon and Dr. C.G.Englefield for serving on the doctoral committee and reviewing the thesis.

This project was carried out with excellent support from the machine shop in the Department of Electrical Engineering.

I acknowledge the financial support provided by the Natural Science and Engineering Research Council of Canada and the Department of Electrical Engineering of the University of Alberta.

Finally, I am grateful to my family for their support and encouragement. My special thanks must go to my wife, Li Jiang, for her love and understanding.

TABLE OF CONTENTS

Chapter 1	INTRODUCTION	1
Chapter 2	SINGLE FREQUENCY Q MEASUREMENT METHOD	8
2.1	Introduction	8
2.2	Principle	9
2.2.1	Input Resonant Resistance and Q Factor	9
2.2.2	Perturbation Effect	11
2.2.3	Detuning and Retuning	14
2.3	Experimental Verification	15
2.3.1	Cavity Description	17
2.3.2	Procedures	17
2.3.3	Discussion	20
2.4	Error Analysis	21
2.5	Conclusion	23
Chapter 3	DESIGN OF SELF-HEATING DIELECTROMETER APPLICATOR	26
3.1	Introduction	26
3.2	Applicator Structure Design Considerations	28
3.2.1	General Considerations	28
3.2.2	Cavity Length, Diameter, Short Circuit Plunger, Sample Access and Inspection Holes, and Coupling Mechanism	31
3.2.3	Measurement Capability	34
3.3	Characteristics of the "Fixed Gap" Scheme	35
3.4	Conclusion	41
Chapter 4	ANALYSIS OF THE COAXIAL RE-ENTRANT CAVITY WITH AN ARBITRARILY POSITIONED GAP IN ITS CENTER CONDUCTOR	44
4.1	Introduction	44
4.2	Mode Matching Analysis	44
4.2.1	Mode Matching Formulation For Regions A and B	44
4.2.2	Mode Matching Program Verification	50

4.2.3 Variation of Field Distributions, Energy, Power Loss and Q Factor With the Gap Position 53
4.3 Equivalent Circuit Analysis 57
4.3.1 Artificial Electric Wall, Resonant and Matching Equations 57
4.3.2 Equivalent Circuit Model Verification and Matching Behavior 59
4.4 Conclusion 63

Chapter 5 THEORETICAL ANALYSIS OF A COUPLING LOOP IN A COAXIAL CAVITY 65
5.1 Introduction 65
5.2 Mode Expansion Method Formulation 66
5.3 Input Resistance Derivation 69

Chapter 6 PASSIVE SINGLE FREQUENCY DIELECTROMETER 73
6.1 Introduction 73
6.2 Dielectric Determination 73
6.3 Experimental Verification 76
6.4 High Temperature Dielectrometer 79
6.5 Conclusion 82

Chapter 7 ACTIVE SINGLE FREQUENCY DIELECTROMETER 84
7.1 Introduction 84
7.2 Oscillation Conditions of an Active Loop 87
7.3 Modeling of the Oscillation Loop Formed by a Cavity, Amplifier and Transmission Lines 89
7.4 Programming and Experimental Verification 92
7.5 Discussion of Active Loop Characteristics 95
7.6 Dielectric Constant Measurement at Room Temperature 97
7.7 Dielectric Constant Measurement at High Temperature 103
7.8 Conclusion 106

Chapter 8 CONCLUSIONS 109

Appendix A MEASUREMENT OF THE AMPLIFIER S-PARAMETERS USING AUTOMATIC NETWORK ANALYZER SYSTEM 114

Appendix B THE HP-BASIC PROGRAMS FOR ANALYSIS OF THE OSCILLATION LOOP FORMED BY AMPLIFIERS, A CAVITY AND TRANSMISSION LINES 117

Appendix C METHOD FOR Q MEASUREMENT FOR A CAVITY IN AN ACTIVE LOOP AND ASSOCIATED PROBLEMS 129

I. Method Formulation 129

II. Results and Problems 130

LIST OF TABLES

Table 2.1	Q comparison between the bandpass method and the single frequency method (circularly cylindrical cavity)	19
Table 2.2	Q comparison between the bandpass method and the single frequency method with free resonant frequency shift. (Re-entrant cavity, under coupled)	20
Table 2.3	Q comparison between the bandpass method and the single frequency method at a fixed resonant frequency using a secondary disturbance. (Re-entrant cavity, under coupled, f=2.4046 GHz)	21
Table 3.1	Typical structures of resonant cavity applicators and their major features	30
Table 4.1	Resonant wavelengths calculated from programs MMMC2 and MMMC2-AG. (d=1, L=20, r_1=1.25, r_2=4.5, ε_r=2.1 $\sigma=10^7$, N=100, M=20)	51
Table 4.2	Q factor and electromagnetic field data calculated from programs MMMC2 and MMMC2-AG. (d=1, L=20, r_1=1.25, r_2=4.5, ε_r=2.1, $\sigma=10^7$, N=100, M=20)	51
Table 6.1	Results comparison between the single frequency, manual tuning method and swept frequency method.	78
Table 7.1	Measured [S] of the experimental active oscillation loop over the 915MHz ISM band.	94
Table 7.2	Comparison of measured and calculated f_L for different f_c's.	94
Table 7.3	Dielectric constant data measured with the active oscillation loop system, compared to data from a passive swept system. Two different sets of results are shown, which are calcu ated using (6.1) with $f=f_L$ and $f=f_c$ respectively.	102
Table C1	Q-factor data measured in the active system, compared with data obtained using the passive swept frequency system.	131

Table C2 Q-factor vs Δf_L, showing the sensitivity of Q to the frequency change. ($|\Gamma|=0.3$ and $f_c=1000MHz$) 131

LIST OF FIGURES

FIGURE 1.1 Illustration of conventional and microwave high temperature dielectric measurement system 2

FIGURE 1.2 A schematic diagram of two channel microwave high temperature dielectric measurement system 3

FIGURE 2.1 Perturbed resonant cavity, the coupling device and their equivalent circuit at resonance. 10

FIGURE 2.2 Block diagram of the experimental reflectometer for verification of the single frequency Q method. 16

FIGURE 2.3 Cavity arrangement for single frequency Q method verification. 18

FIGURE 2.4 Relative Q error vs. cavity return loss using a reflectometer 23

FIGURE 3.1 Cross section of the high temperature dielectrometer using a coaxial re-entrant cavity applicator with the gap at the cavity end. 27

FIGURE 3.2 Cross section of the high temperature dielectrometer using a coaxial re-entrant cavity applicator with a movable gap 27

FIGURE 3.3 Illustration of travelling wave and resonant applicators. 29

FIGURE 3.4 Illustrative E-field distribution in a coaxial re-entrant cavity. 31

FIGURE 3.5 E and H fields for a capacitive mode in a re-entrant cavity, normalized by the TEM field. (a) Axial distribution at r=2.875cm, compared with TEM field. (b) radial distribution in the gap midplane. 36

FIGURE 3.6 E and H fields for an inductive mode in a re-entrant cavity, normalized by the TEM field. (a) Axial distribution at r=2.875cm, compared with the TEM field. (b) Radial distribution in the gap midplane. 37

FIGURE 3.7 (a) Sample energy density as a function of the gap width, d. (b) Sample energy density as a function of the dielectric constant, ε'. (c) Sample energy

density as a function of normalized sample radius. 38
FIGURE 3.8 Ez axial distribution for different dielectric constant, ε', illustrating field confinement in the hole region. 39
FIGURE 3.9 Comparison of total sample energy stored in the gap region to that stored in the hole. 40
FIGURE 3.10 Frequency shift vs. dielectric constant for the gap with and without a hole in its center conductor 40
FIGURE 4.1 Simplified cross sectional diagram of the coaxial re-entrant cavity with an arbitrarily positioned gap in its center conductor. 45
FIGURE 4.2 Resonant wavelength, λ, vs. the mode number, M, in area B. (ε'=2.1, r_o=1, r_1=1.25, r_2=4.5, L=20.0, d=1.0, L_g=1, in cm, N=100) 52
FIGURE 4.3 Resonant wavelength, λ, vs. the mode number, N, in area A. (ε'=2.1, r_o=1, r_1=1.25, r_2=4.5, L=20.0, d=1.0, L_g=1, in cm, M=11) 52
FIGURE 4.4 Normalized axial fields distributions at 915 MHz band for different gap positions. (a) L_g=0, (b) L_g=1, (c) L_g=2, (d) L_g=6, (e) L_g=8, in cm. (d=0.3, ε_r=20, r_o=0.35, r_1=1.27, r_2=4.51, λ=32.787, L≅20.7, r=2.5, in cm) 54
FIGURE 4.5 Variations of resonant frequency, f, Q factor, energy stored in the cavity, Ec, the power loss in the cavity wall, Pw, and the power loss in the sample, Ps, as a function of the gap positions, L_g 56
FIGURE 4.6 (a) Equivalent lumped elements and artificial electric wall in the gap, and (b) equivalent circuit of a coaxial cavity with a gap in its center conductor. 58
FIGURE 4.7 Resonant frequency vs. gap width, d, for different axial gap positions. Lines are calculated results using equivalent circuit model and dots are experimental data. 60

FIGURE 4.8 Resonant frequency vs. axial gap position, L_1, for different gap widths, d. Lines are calculated results using equivalent circuit model and dots are experimental data. 61

FIGURE 4.9 Tuning curve at 915MHz in terms of L_1 and L_2. solid line is calculated result using equivalent circuit model and broken line is experimental data 61

FIGURE 4.10 Reflection coefficients vs. gap position, L_1, with gap load susceptance, B_m, as a parameter and a fixed load conductance. 62

FIGURE 4.11 Reflection coefficients vs. gap position, L_1, with gap load conductance, C_m, as a parameter and a fixed load susceptance. 63

FIGURE 5.1 An adjustable coupling loop on the endplate of a coaxial cavity. 66

FIGURE 5.2 Schematic representation of the electromagnetic fields excited by a current density, J, in a cavity. 67

FIGURE 6.1 Experimental system for collecting the single frequency measurement data and the swept frequency measurement data. 77

FIGURE 6.2 Typical reflection curve on the reflectometer's CRT display. This curve includes the quantities needed for both the swept frequency method and the single frequency method. 78

FIGURE 6.3 Passive single frequency high temperature dielectrometer system with manual tuning and matching. 79

FIGURE 6.4 Dielectric constant and loss factor vs. temperature for Zeolite (13x, pellet) measured with the passive single frequency dielectrometer 81

FIGURE 6.5 Dielectric constant and loss factor vs. temperature for mullite (MV20) measured with the passive single frequency dielectrometer 81

FIGURE 7.1 (a), An oscillation loop consisting of a cavity, amplifier and transmission lines for an active dielectric measurement application, which is (b), divided into an active two-port and a passive two-port and (c), represented by an S-parameter network with its input and output ports connected together. 85

FIGURE 7.2 Equivalent circuit of a cavity with two coupling ports. 91

FIGURE 7.3 Diagram of the experimental setup for verification of the theoretical model based on S-parameter oscillation condition. 93

FIGURE 7.4 Magnitude of the loop phase vs. frequency (a) for a fixed f_c of 859MHz, labeled by O, and (b) of a cavity mode for different f_c, indicated by the vertical lines. (Loop oscillations occur at frequencies where the loop phase=0) 96

FIGURE 7.5 (a) Difference between f_L and f_c vs. f_c for a given cavity mode. $f_L=f_c$ is possible only at one particular frequency, i.e.,951MHz in this case. (b) Ratio of Δf_L to Δf_c as a function of f_c with cavity Q as a parameter. 98

FIGURE 7.6 f_L vs. variation in loop length for different f_c. The closer f_L is to f_c, the smaller the influence of the length variation on f_L. 99

FIGURE 7.7 Diagram of the active room temperature dielectric constant measurement system. 100

FIGURE 7.8 Input and output characteristic of the Avantek AM2002N amplifier, and an idealized input and output characteristic of the Avantek UTL-1001 limiter. 101

FIGURE 7.9 Diagram of the active high temperature dielectric constant measurement system, where the sample is heated in the high power region while the measuring

components are all in the low power region. 104

FIGURE 7.10 Dielectric constants vs. temperature for Mullite (MV20) and machinable alumina (Cotronics 960), measured with the self-oscillating, self-heating active dielectrometer. 105

FIGURE A1 Equipment connection diagram of automatic S-parameter network analyzer 115

FIGURE A2 The active oscillation loop for the measurement of the equivalent S-parameter of the amplifier. (a) closed loop for adjusting the oscillation loop power level, (b) measuring the [S] parameter with S-parameter measurement system at the same amplifier power level. 116

LIST OF SYMBOLS AND ABBREVIATIONS

In Chapter 1

HTDM	high temperature dielectric measurement

In Chapter 2

C	proportionality factor between Q and $\bar{R}$
E,	electric field intensity
f_0, f_1	resonant frequency of a cavity before and after perturbation
H	magnetic field intensity
n	current transformer ratio of the coupling device in a cavity
P	power loss in a cavity
Q_0, Q_1	Q factor of a cavity before and after perturbation
Q_P	Q factor obtained from the single frequency method
Q_T	Q factor obtained from a traditional method, i.e., swept frequency or time spectrum method
R	input resistance of a resonator at its resonant frequency
$\bar{R}$	normalized input resistance of a resonator at its resonant frequency
RL	return loss in dB
W	energy stored in a cavity
Γ	reflection coefficient
ε'	dielectric constant
ω	angular frequency ($=2\pi f$)

In Chapter 3

d	gap width
ISM	industrial, scientific and medical
L	cavity length
L_1, L_2	lengths of post 1 and post 2 respectively in movable gap coaxial re-entrant cavity
P_d	ratio of the energy density in the sample to the rest of the cavity
r_0	radius of the sample insertion hole

r_1 radius of center conductor

r2 radius of outer conductor

r_s sample radius

α attenuation constant

ε_r' relative dielectric constant ($=\varepsilon'/\varepsilon_0$, where ε_0 is dielectric constant of free space)

λ wavelength

In Chapter 4

a $= \frac{d}{L}$, normalized gap width with respect to the cavity length

An, Bm expansion coefficients in areas A and B respectively (in 4.2)

Bm, Gm equivalent susceptance and conductance of the dielectric in the gap (in 4.3)

Cp1, Cp2 shunt gap capacitances with respect to post 1 and post 2 respectively

Cs1, Cs2 series gap capacitances with respect to post 1 and post 2 respectively

d1, d2 distances of the artificial electric wall to post 1 and post 2 respectively

e $= \frac{Lg}{L}$, normalized distance between the gap and the endplate, with respect to the cavity length

Ec energy stored in the cavity

F_n^A, F_m^B the constants prescribed by the boundary conditions.

Jo, J1 the first and the second order Bessel function of the first kind

k, β transversal and longitudinal wave numbers

ko the wave number in free space

k_n^{A2} $= k_0^2 - \beta_n^{A2}$, transverse wave number of mode n in area A

k_m^{B2} $= k_0^2 \varepsilon_r - \beta_m^{B2}$, transverse wave number of mode m in area B

Lg $=L_1$ (in ch.3), indicating the location of the gap from the endplate of the cavity

MMMC1, MMMC2, MMMC3 and MMMC4

FORTRAN program names of the mode matching formulation for the "fixed gap" re-entrant cavity

MMMC1-AG, MMMC2-AG, MMMC3-AG and MMMC4-AG

FORTRAN program names of the mode matching formulation for the "movable gap" re-entrant cavity

n, m natural numbers numerating the respective terms in the expansion series and also indicating the different modes

N, M numbers of the modes taken into account in calculation for areas A and B respectively

N_0, N_1 the first and the second order Bessel function of the second kind

P_s power loss in the sample

P_w power loss in the cavity wall

z longitudinal distance from the tip of post 1

z' longitudinal distance from the endplate

Z_{0n}^{A}, Z_{1n}^{A}, Z_{0n}^{B} and Z_{1n}^{B} linear combinations of Bessel functions of the first and the second kind

$\beta_n^A = \frac{n\pi}{L}$, longitudinal wave number of mode n in area A

$\beta_m^B = \frac{m\pi}{aL}$ longitudinal wave number of mode m in area B

In Chapter 5

C_r proportional constant between Q and R

C_R proportional constant between Q and $\ln^2 \frac{r_2}{r_1}$

E electric field intensity in the cavity with a current density, J

E_1 electric field intensity of modes in empty cavity

H height of the coupling loop

r_1, r_2 radial distances of the inner conductor and the outer conductor of the coupling loop to the axial center of the cavity

R input resistance of the cavity at resonant frequency

R_1, R_2 radii of the cavity center and outer conductors respectively

μ permeability

ω_o ω of the mode of interest

ω' complex ω

In Chapter 6

F	filling factor of sample loaded cavity
Q_L	system Q factor
r_{10}, r_{20}	r_1 and r_2 before sample is loaded
β	coupling factor of the coupling loop
ε''	dielectric loss factor

In Chapter 7

A_c	attenuation of the cavity in dB
A_L	attenuation in the rest of the loop
A^T, A^A, A^c, A	[A] for transmission line, amplifier, cavity and the loop
AMDM	active microwave dielectric measurement
f	frequency of interest
f_c	cavity resonant frequency
f_L	loop oscillation frequency
G	Gain of the loop in dB
G_A	Gain of amplifier in dB
L	electric length of the loop
n_1, n_2	transformer ratios for coupling ports 1 and 2 respectively
S^T, S^A, S^c, S	[S] for transmission line, amplifier, cavity and the loop
Z_A, Z_P	input impedances of the active port and the passive port respectively
Γ_A, Γ_P	reflection coefficients from the active port and the passive port respectively
Φ	phase of the loop in radian

In Appendix A

A^B	[A] of an attenuator
SPARAMS	name of the automatic S parameter measurement program

Chapter 1

INTRODUCTION

Microwave material processing has been one of the most important non-communication uses of microwave energy. Microwave cooking is an example of how microwave material processing technology affects our daily lives. However, the industrial potential of microwave material processing is of even more significance. Processed using microwave energy, ceramics exhibit improved or unique microstructure and properties.[1.1,1.2] The onset of the superconductive transition occurs at a higher temperature.[1.3] Diamond synthesis is enhanced at a lower pressure.[1.4-1.8] Microwave energy has caused a major breakthrough that enables a change in the basic mechanism for heating materials.[1.9]

Microwave material processing, mostly microwave heating, started as far back as the late thirties, when microwave technology was still in its infancy.[1.10] However, substantial industrial use did not start until after World War II. During the fifties, sixties and seventies, serious efforts were made to develop microwave ovens for commercial and residential use. Since then, interest has steadily expanded into scientific, industrial and medical applications. Today, activities in this field include microwave sintering, clinkering, joining, new material synthesis, food processing, waste management and diathermy.

Some inherent differences in the microwave heating mechanism exist as compared to the conventional heating mechanism. Firstly, microwaves penetrate into a dielectric resulting in volumetric heating. As a result, a more uniform product can be fabricated due to, for example, less thermal stress. Secondly, microwave heating is faster, which leads to a shorter processing time, larger yield and less floor space. Thirdly, the nearly instantaneous interaction between microwaves and matter allows a process to be controlled more accurately. Additionally, material dependence of microwave absorption makes selective heating possible.

Because of these advantages, microwave material processing has not only undergone a further development in traditional areas, such as

food processing, but it has also expanded into more material families such as ceramics, more processing techniques, such as sintering, melting, joining, new material synthesis, and into a higher temperature range with an upper limit beyond 2000^{o} C.

These new developments need improved high temperature dielectric measurement (HTDM) techniques to predict the microwave heating response of a material, to design an effective microwave process, to control the properties and the quality of a product, and to understand the structure and the composition of a material.

Presently, there are two ways to conduct high temperature dielectric measurement, as illustrated in Figure 1.1. Measuring a sample heated by conventional means, such as an electrical furnace or a gas flame, is one way; measuring the sample heated by microwave energy is the other way. Three facts hamper the use of a conventional method. Firstly, over-heating, that is, not only is the sample itself heated but its surroundings also, which will deteriorate the performance of measurement equipment such as a cavity or a probe.

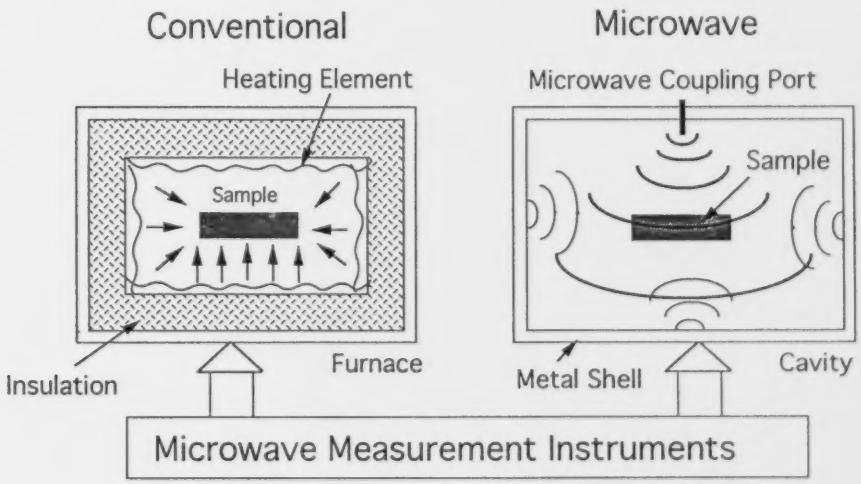

FIGURE 1.1 Illustration of conventional and microwave high temperature dielectric measurement systems

Secondly, non-uniform heating is inevitable. The temperature of the surface closest to the heating source is always higher than other parts of the sample. In addition, attaining a high temperature, say more than $1000^{o}C$, can be extremely difficult. On the contrary, microwave heating performs excellently in all these aspects due to its nature in selectivity, uniformity and fast heating. Therefore in this thesis we choose to use microwave energy for the sample heating.

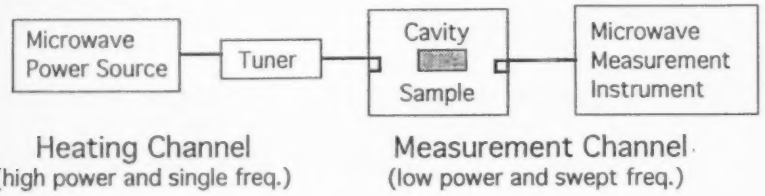

FIGURE 1.2 A schematic diagram of two channel microwave high temperature dielectric measurement system

Typical of a microwave HTDM system in use today is the two channel system as shown in Figure 1.2. On the one hand, to heat a sample to a high temperature, sufficient microwave power needs to be applied to a resonant cavity through a so called heating channel, which usually operates under a high power single frequency condition. On the other hand, to determine the dielectric constant and the loss factor of the sample, the resonant frequency shift and Q factor variation caused by the sample have to be measured. These measurements are usually made under a low power swept frequency condition. Consequently, a low power swept frequency channel has to be added to the system for the purpose of measurement.

There are various problems associated with such a system. Firstly, the need for two channels complicates the instrumentation. Secondly, the existence of high and low power electromagnetic fields in the same cavity can cause interference between the two channels. Besides, there is a conflict in system optimization because in the heating channel, adjustments, such as tuning and matching, are necessary to assure effective power delivery, whereas in the measuring

channel, stability is required to secure an accurate measurement.

To eliminate these problems, we propose a single frequency microwave measuring and heating approach, by which a sample is heated and measured using one power channel at a single frequency. This thesis describes the theoretical basis of the proposed method, solutions to the technical difficulties encountered, method implementation, experimental verification and discussion of the remaining problems.

A fundamental obstacle in the single frequency approach is the lack of a method to measure the Q factor at a single frequency, since Q variation measurement is so essential for loss factor determination. In principle, the techniques used for Q measurement, so far, can be grouped into two categories. One is the frequency spectrum technique, which is based on an observation of the reflection or the transmission characteristics of a cavity over a frequency band near the resonant frequency. The popularly used half power bandwidth method belongs to this category. The other is the time spectrum technique, which requires an observation of the decay time of an oscillation after a sudden removal of a power source from a cavity. For our case, the frequency spectrum technique is ruled out because of the single frequency requirement; and the time spectrum technique cannot be applied either because of the continuous heating requirement.

In response to these constraints, chapter 2 is devoted to the development of a single frequency Q measurement method. Starting with the general definition of Q factor, we comprehensively examine the quantities involved under a perturbation condition. The result of this effort is the establishment of a relation between the Q factor and the input parameters of the cavity, proving that the measurement of Q at a single frequency is not only possible theoretically but is also feasible practically. This chapter also includes the experimental verification and the error analysis. Even though derived to solve our specific problem, the method of the single frequency Q measurement is generally applicable to any cavity, provided that the perturbation condition is satisfied.

Serving as a microwave heater and a test chamber, the applicator

is the heart of any microwave measuring and heating system, including, of course, the single frequency measuring and heating system. Currently used geometries for the applicators are the rectangular cavity, a modified microwave oven or a cylindrical cavity. Not satisfied with the performance of these cavities for various reasons, we propose a new structure, that is, a coaxial re-entrant cavity with a gap in its hollow center conductor. The applicator design, the discussion of its characteristics and its experimental performance are presented in chapter 3. To expand the tuning and the matching range to make the applicator more suitable for diverse samples, this structure is modified by allowing the gap to be positioned arbitrarily along the center conductor. Chapter 4 is focused on the analysis of this structure by modifying an existing mode matching formulation and computer program. It has led to a wide range tunable and matchable high temperature microwave applicator.

One of the keys in the single frequency method is the establishment of a relation between the Q factor and the geometric dimensions of the coupling device. A coupling loop is analyzed using the mode expansion method in chapter 5. The input resistance for the principal mode is then derived. This formulation has eventually made it possible to measure the loss factor under a matched resonator condition.

The first five chapters are mainly focused on dealing with the theory and techniques necessary for the single frequency method. In chapter 6, we apply the theory and the techniques to high temperature dielectric measurement, whereby a passive high temperature dielectrometer is developed. A set of dielectrometer formulas related to specific cavity dimensions are given. Experiments at room temperature verify the validity of the method. A set of high temperature ($>1200^{0}C$) experiments further demonstrates its satisfactory high temperature performance. However, it is found that the required manual, mechanical tuning and matching procedures are too slow to respond to the dramatic incremental change in the properties of a high temperature sample.

In order to overcome the difficulties of mechanical tuning in the

above passive dielectrometer, we develop, in chapter 7, a single frequency dielectrometer using an active oscillation loop. The active oscillation loop incorporates the dielectric material to be measured into a microwave oscillation loop, so that the oscillation frequency is determined by the material's dielectric properties. Therefore, the dielectric constant can be obtained through the measurement of the oscillation frequency. Still retaining the feature of the one channel and single frequency, this active system no longer needs separate microwave sources nor a tuning system. In this chapter, we present a theoretical analysis of the oscillation loop using the S-parameter representation, including the oscillation condition formulation, the analysis of the loop characteristics, model development and programming. The dielectric constant measurements are conducted at both room and high temperature, demonstrating the feasibility of the oscillation loop method as a high temperature dielectrometer. Owing to the elimination of the separate microwave source and the mechanical applicator tuning, this active dielectrometer is much simpler.

Chapter 8 summarizes the pertinent conclusions.

Because of the diversity of the topics covered in this thesis, most chapters have been presented in a self-contained fashion and therefore stand relatively independent among the others.

References

[1.1] W.H.Sutton, "Microwave Processing of Ceramic Materials", Ceramic Bulletin, Vol.68, No.2, 1989, p376-386.

[1.2] Y.L.Tian, D.L.Johnson, "Ultrafine Microstructure of Al_2O_3 Produced by Microwave Sintering", Ceramic Trans. Ceramic Powder Science 2. P925-932.

[1.3] I. Almad, "Processing of Superconducting Ceramics Using Microwave Energy", Microwave Processing of Materials, Vol. 124, 1988, p137-148

[1.4] M. Kamo, Y. Sato, S. Matsumoto and N. Selaka, "Diamond Synthesis From Gas phase in Microwave Plasma", J. of Crystal

Growth 62, 1983, P642-644

[1.5] -, "Diamond Films Synthesized at Low Pressures", Materials and Processing Report, July,1986, P2-p386

[1.6] P.K.Bachmann, W. Drawl, D.Knight, R. Weimer, and R.F.Messier, "Diamond Nucleation and Growth in a Bell Jar Microwave Plasma CVD Reactor", Diamond and Diamond-like Materials Synthesis, edited by G.H.Johnson, A.R.Badziam, M.W.Geis. P99-102

[1.7] T.Hartnett, A.R.Badzian, and K.E.Spear, "Characterization of Diamond Deposition in a Microwave Plasma", ibid, P103-105.

[1.8] B.E.Williams, J.T.Glass, R.F.Davis, K.Kobashi and Y.Kawaate, "Electron Microscopy of Diamond Films Grown By Microwave PECVD", ibid, P59-62

[1.9] -, "Microwave Processing Symposium Report", Material and Processing Report, Vol.3, No.4, July 1988, P1 1988, P1

[1.10] J. M. Osepchuk, "A History of Microwave Heating Applications", IEEE, MTT-32, pp 1200-1223

Chapter 2

SINGLE FREQUENCY Q MEASUREMENT METHOD[1]

2.1 Introduction

This chapter is devoted to the development of a new single frequency Q measurement method. In a cavity dielectric measurement method, the loss factor of a sample is usually determined through a Q measurement. Since, in this thesis, the sample heating is performed in a resonating cavity, the Q measurement becomes indispensable to the loss determination of the sample. In fact, an accurate determination of a dielectric constant also needs the Q measurement. This can be shown explicitly through the second order influence of the Q on ε' expressed by[2.1]

$$\frac{F}{2}(\varepsilon'-1)=\frac{f_o-f_1}{f_1}+\frac{1}{4Q_1}\left(\frac{1}{Q_1}-\frac{1}{Q_o}\right) \qquad (2.1)$$

where F is the filling factor, f_o, Q_o and f_1, Q_1 are the resonant frequency and Q factor before and after the introduction of the sample into the cavity respectively. Moreover, the relationship between the Q and the material properties is so interrelated that the Q measurement is used not only for the determination of the electromagnetic properties like permittivity and permeability, but also for non-electromagnetic properties including moisture content, density, size and mechanical deformation.

Over the past fifty years, a great variety of Q measurement methods have been developed.[2.2] They may be divided, in principle, into two categories, namely, the frequency spectrum technique and the time spectrum technique. In the frequency spectrum technique, the Q is measured by an observation of the reflection or the transmission characteristics of a cavity over a frequency band, such as the 3 dB bandwidth, the 10 dB bandwidth and so forth. On the other hand, Q characterizes the damping time constant of a resonance as shown, for

---

[1] A version of this chapter has been accepted for publication. IEEE Trans. Microwave Theory and Tech. vol 41, 1993.

example, by the equation:

$$E=Eo\ e^{-\frac{\omega}{Q}t} \tag{2.2}$$

where E is the electric field intensity, Eo is the E when t=0, ω is the angular resonant frequency, and t is the time. Obviously, according to equation (2.2), Q can also be measured by an observation of the decay time of an oscillation after a sudden removal of an exciting source from the cavity. The so-called decrement methods are based on this principle.

Unfortunately, neither method can be applied under continuous single frequency operating conditions, the situation involved in this thesis. The reason is that the time spectrum technique cannot be applied in a continuous operation nor the frequency spectrum technique in a single frequency operation. In order to solve this problem, we propose a method for the Q measurement applicable in a single frequency operation, which involves only an input resistance measurement of a cavity at its resonant frequency, while a moderate perturbation condition is satisfied. This chapter includes the principle, the experimental verification and the error analysis.

2.2 Principle

2.2.1 Input Resonant Resistance and Q Factor

It is well known that the input resonant resistance, R, on the cavity side of the equivalent coupling plane, see Figure 2.1, is defined as

$$R=\frac{2\ P}{\left(\oint_c \bar{H}\cdot d\bar{L}\right)^2}=\frac{2\ P}{I^2} \tag{2.3}$$

or

$$R=\frac{\left(\int_a^b \bar{E}\cdot d\bar{L}\right)^2}{2\ P}=\frac{V^2}{2\ P} \tag{2.4}$$

where P is the power dissipated in the cavity, I and V are the equivalent current and the equivalent voltage on the cavity side of the coupling device respectively. $\bar{E}$ is the electric field vector and $\bar{H}$ is the magnetic field vector. The integration path for $\bar{H}$ encloses the path where the current, I, is defined. Similarly, the integration limits, a and b, are the points between which the equivalent voltage,

V, is defined. The nature of the coupling mechanism prescribes the choice of the definition to be used, that is, Eq. (2.3) is employed for magnetic coupling while Eq. (2.4) is used for electric coupling. However, we need to analyze only one of the two cases since the results of the other can be obtained by the principle of duality. Here we choose to analyze the magnetic coupling case.

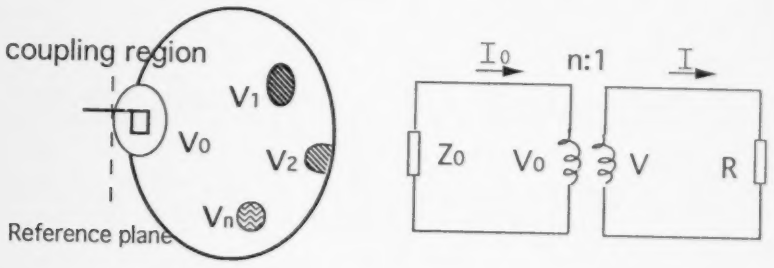

(a) A Cavity Containing Disturbances $V_1, V_2, \ldots V_n$

(b) The Equivalent Circuit at Resonance

FIGURE 2.1 The perturbed resonant cavity, the coupling device and their equivalent circuit at resonance. V_0 is the volume before introduction of the perturbation. V_1, V_2, V_n are far from the coupling region.

By definition, the Q factor is

$$Q \equiv \frac{\omega W}{P} \tag{2.5}$$

where ω is the angular resonant frequency and W is the energy stored in the cavity. Substituting for P from Eq. (2.5) into Eq. (2.3), the internal resistance at resonance is represented by

$$R = \frac{2 \omega W}{\left(\oint_c \bar{H} \cdot d\bar{L} \right)^2 Q} \tag{2.6}$$

Transforming through the coupling device and normalizing with respect to the characteristic impedance of the input transmission line, Z_0, (see Figure 2.1(b)), we can obtain the normalized input resistance, $\bar{R}$, looking into the cavity from the outside as

$$\bar{R} = \frac{n^2 R}{Z_0} = \frac{2 n^2 \omega S}{Z_0 Q} \tag{2.7}$$

where n is the current transformer ratio of the coupling mechanism and

S is defined as the ratio of the stored energy in the cavity to the square of the integrated magnetic field around the coupling device, i.e. , the square of the RF current in the coupling device in the cavity, so that

$$S \equiv \frac{W}{\left(\oint_c \bar{H} * d\bar{L} \right)^2} \tag{2.8}$$

Alternatively, Q can also be written as a function of $\bar{R}$

$$Q = \frac{2 n^2 \omega S}{Zo\bar{R}} \tag{2.9}$$

Up to this point, no approximations have been made. Therefore, an absolute value of Q can be obtained by measuring the input resistance, $\bar{R}$, under the resonant condition provided that Z_o, n, ω and S are known. However, this is realistic only for some well-defined resonator geometries such as the circularly cylindrical cavity, the rectangular cavity and the coaxial cavity, with coupling mechanisms that can be fully analyzed to obtain the values for n and S.

However, the real significance of Eq. (2.9) is the fact that it reveals how a Q can be measured without resorting to a band of frequencies or a given time increment. What may, practically, be even more significant is that a relative value of Q can be obtained with sufficient accuracy by simply measuring $\bar{R}$ even without solving for n, S, and ω if a moderate perturbation condition is satisfied, as we will proceed to prove next.

2.2.2 Perturbation Effect

In most microwave dielectric measurements, including the high temperature microwave dielectric measurement we are interested in, the variations of the parameters of the dielectric are well within the perturbation range. Therefore, the analysis of the relationship between Q and $\bar{R}$ under a perturbation condition is significant in this sense.

Eq. (2.9) shows that, besides $\bar{R}$, the four quantities Zo, n, ω and S would affect Q. Since Zo is a known constant, we only need to examine how n, ω and S vary when a resonator is perturbed.

The value of the transformer ratio, n, is decided by the

geometric structure of a coupling mechanism for a given field configuration in the coupling region. In other words, n will not vary as long as the field configuration in the neighborhood of the coupling mechanism remains unchanged. Notice that this is a weaker requirement than demanded in conventional perturbation theory where invariance of the fields throughout the whole cavity is required except in the locally perturbed region. If the coupling mechanism is situated far enough from the disturbed field region, as is usual in practice, the above perturbation condition is satisfied quite rigorously. Moreover, when the dominant fields at the coupling port are different from those in the perturbed region, the effect of the perturbation on the coupled field will be still further reduced[2.3] and hence can be assumed negligible. So, the conclusion drawn from this is that n would remain a constant as long as a moderate perturbation condition is satisfied.

Let us look at how the perturbation affects S. Perturbation theory requires that, on introducing disturbances, the fields may change considerably in magnitude but the field configurations or the patterns will not change appreciably except in the region of the disturbances.[2.4] Say that, due to the disturbances, the existing field magnitude changes from Ho to

$$H = h\, Ho \tag{2.10}$$

where h is a simple scale factor. By Eq. (2.8) we then have

$$S=\frac{\mu\, h^2 \int_v \bar{H}o^2 dV}{2h^2\left(\oint_c \bar{H}o^* d\bar{L}\right)^2}=So \tag{2.11}$$

where So is the S for the undisturbed resonator and V=Vo. It is evident that the parameter S is invariant under the perturbation assumption. Now Q can be expressed as

$$Q = \frac{2}{Zo} no^2 So\ \omega o\left(1+\frac{\Delta\omega}{\omega o}\right)\frac{1}{\bar{R}}=\frac{Co}{\bar{R}}\left(1+\frac{\Delta\omega}{\omega o}\right) \tag{2.12}$$

where

$$Co=\frac{2}{Zo} no^2\ So\ \omega o$$

is a constant for a resonator satisfying the perturbation assumptions. The subscript 0 refers to the quantities before perturbation.

In order to examine the perturbation effect on ω, consider that the field is disturbed and redistributed thereby altering the resonant

frequency. The variation of the resonant frequency can be represented by the well-known cavity perturbation formula

$$\frac{\Delta\omega}{\omega_o} = \frac{\int_{V_o}\left[(\bar{E}_1\cdot\bar{D}_o - \bar{E}_o\cdot\bar{D}_1)+(\bar{H}_1\cdot\bar{B}_o-\bar{H}_o\cdot\bar{B}_1)\right]dV}{\int_{V_o}\left[\bar{E}_o\cdot(\bar{D}_o+\bar{D}_1)-\bar{H}_o\cdot(\bar{B}_o+\bar{B}_1)\right]dV} \tag{2.13}$$

where $\bar{E}_1$, $\bar{D}_1$, $\bar{H}_1$ and $\bar{B}_1$ are the small incremental changes in $\bar{E}_o$, $\bar{D}_o$ and $\bar{H}_o$ and $\bar{B}_o$ due to the perturbation. The results for many specific cases can be found in the literature[2.4]. It is this frequency shift that is the essential quantity in the standard perturbation theory and in its applications. Yet, from the point of view of the Q relation in Eq. (2.12), the shift of the frequency is negligible because, in any perturbation case, the frequency shift $\Delta\omega/\omega$ is much smaller than unity. For example, 2% of $\Delta\omega/\omega$ may be considered as a quite large perturbation for a microwave cavity, but it contributes a Q error of only 2% according to Eq. (2.12). For this reason, neglect of $\Delta\omega/\omega$ has little impact on the Q value. Consequently, the Q is very simply related to the normalized input resistance of a resonating cavity by

$$Q=\frac{C_o}{\bar{R}} \tag{2.14}$$

For the electric coupling case, using the principle of duality, we find that

$$Q=C_o\bar{R} \tag{2.15}$$

Moreover, note that $\bar{R}$ is related to the absolute reflection coefficient, $|\Gamma|$, by

$$\bar{R} = \frac{1\pm|\Gamma|}{1\pm|\Gamma|} \tag{2.16}$$

where the choice of the sign depends on whether the cavity is overcoupled or undercoupled respectively. So, the Q of a cavity can be obtained simply by measuring the reflection coefficient at

resonance.

Applying Eqs (2.14), (2.15) and (2.16), we can determine the relative Q-factor through the measurement of reflection coefficient. Of course, if an absolute value of Q needs to be found, then the parameter Co has to be determined independently.

2.2.3 Detuning and Retuning

In perturbation applications, two cases are very common. One is that of detuning, where a dielectric disturbance, V_1 as in Figure 2.1, causes a resonant frequency shift. And the other is the retuning case, where, after a first disturbance, the resonant frequency is retuned via a second disturbance, say V_2 (see Figure 2.1), to the original unperturbed resonator frequency. Therefore, the retuning can be considered as a true single frequency operation since a fixed frequency has been maintained. What concerns us here is whether the previous conclusion regarding the Q relation still holds for the retuning case, for there is a double disturbance applied.

For the detuning case, the frequency shift can be derived from Eq. (2.13) as

$$\frac{\Delta\omega}{\omega_o}\Big|_{V_1} = \frac{\int_{V_1}\left(\bar{E}_1 \cdot \bar{D}_o^* - \bar{E}_o^* \cdot \bar{D}_1\right) dV}{4\, W_o} \tag{2.17}$$

where

$$W_o = \frac{1}{4}\int_V \left(\bar{E}_o^* \cdot \bar{D}_o + \bar{H}_o^* \cdot \bar{B}_o\right) dV$$

is the energy in the unperturbed cavity.

For the retuning case, suppose we slightly change the volume of the cavity by an appropriate second disturbance of volume V_2 to pull the disturbed resonant frequency back to its undisturbed value. In a practical case, this is usually done by adjusting a short circuit plunger or a tuning stub. According to perturbation theory, the frequency shift due to a volume variation is given by[2.4]

$$\frac{\Delta\omega}{\omega_o}\Big|_{V_2} = \frac{\int_{V_2}\left(\bar{H}_o^* \cdot \bar{B}_o - \bar{E}_o^* \cdot \bar{D}_o\right)}{4\, W_o} \tag{2.18}$$

Maintaining the resonant frequency constant requires

$$\frac{\Delta\omega}{\omega_o}\Big|_{V_1} = -\frac{\Delta\omega}{\omega_o}\Big|_{V_2} \tag{2.19}$$

By comparing Eqs. (2.17) and (2.18) and assuming Wo constant, we have

$$\int_{V_1}\left(\bar{E}_1^*\bar{D}_o - \bar{E}_o^*\bar{D}_1\right) dV = -\int_{V_2}\left(\bar{H}_o^*\bar{B}_o - \bar{E}_o^*\bar{D}_o\right) dV \tag{2.20}$$

that is,

$$\int_{V_1}\left(\bar{E}_1^*\bar{D}_o - \bar{E}_o^*\bar{D}_1\right) dV + \int_{V_2}\left(\bar{H}_o^*\bar{B}_o - \bar{E}_o^*\bar{D}_o\right) dV = 0 \tag{2.21}$$

This equation shows that, to maintain a fixed resonant frequency, the addition of the energy variations caused by the two disturbing sources must be zero. In other words, the energy in the twice disturbed cavity is equal to that of the undisturbed cavity. Therefore, not only does the frequency remain unchanged but so does the factor S since the energy, W, remains invariant as does the coupling loop current given by $\oint_c \bar{H}^* d\bar{L}$, due to the assumption that the coupling region is far away from the disturbances. Consequently, the Q measured in the retuned case will be more accurate than that measured in the detuned case. In the above derivation, a dielectric permittivity or magnetic permeability variation is also allowed as the secondary disturbance in lieu of a physical volume variation.

In summary, it is found that Q is directly or inversely proportional to the input resistance $\bar{R}$ once the perturbation conditions are satisfied. To achieve this, the critical stipulation is that the field configuration in the coupling region remains undisturbed even though the field amplitudes change. Besides, maintaining a fixed frequency by introducing a secondary disturbance further improves the accuracy. Therefore, the relative Q can then be obtained from a reflection measurement at a single frequency.

2.3 Experimental Verification

In this section, the conclusions based on the theoretical

analysis in the previous section are verified experimentally. In order to ensure the credibility, not one but two cavities, different in structure and Q range, have been employed in the verification experiment. One is a circularly cylindrical TM_{013} mode cavity and the other is a re-entrant coaxial cavity. The experiments were conducted in S-band. Comparison data for the Q factor were obtained from the traditional bandpass method.

A typical swept frequency reflectometer was used for the bandpass Q measurement, as shown in Figure 2.2. Using this method, we can obtain the cavity Q, Q_T, by

$$Q_T = (1+\beta)Q_L \tag{2.22}$$

where β is the coupling coefficient. The loaded Q, Q_L, is given by

$$Q_L = k\frac{fo}{\Delta f} \tag{2.23}$$

where k depends on the power level at which Δf is measured. For example, if the 3 dB power level is chosen, k=1.

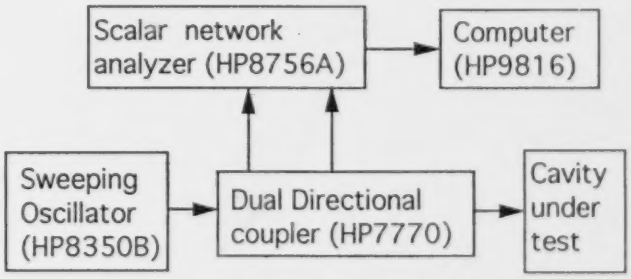

FIGURE 2.2 Block diagram of the experimental reflectometer for verification of the single frequency Q method.

On the other hand, the cavity Q obtained through the single frequency method is designated as Q_P, and is given by (2.14), i.e.,

$$Q_P = \frac{Co}{\bar{R}} \tag{2.24}$$

with the constant Co determined by a prior separate measurement

procedure. $\bar{R}$ is obtained through Eq. (2.15) by an absolute reflection coefficient measurement at the resonant frequency. A novel HP BASIC program for the HP8756 scalar network analyzer[2.5] was used for collecting the data of the pertinent resonant curve including Δf, f_o and $|\Gamma|$ which simultaneously contains the information for both the bandpass and the single frequency method, ensuring identical electromagnetic conditions for both tests. Therefore, any source frequency and power instability will not affect the relative comparison between these two different methods, making the comparison more direct and reliable.

2.3.1 Cavity Description

The geometrical structures of the two cavities are shown in Figure 2.3. Two things about the construction of the cavities should be mentioned. Firstly, they both have a hole for introducing the disturbances, mostly lossy materials, by which the Q variation can be realized without changing the cavity geometry. Secondly, the coupling mechanisms are located far from the disturbing sources and both are loop coupled to the H-field to achieve as high an isolation as possible between the coupling mechanisms and the disturbances placed in a maximum E-field. Two different procedures for introducing the disturbances were used for the cylindrical cavity and the reentrant coaxial cavity. The first was designed to confirm the validity of the single frequency method and the second to confirm the validity of the method as well as to compare the results of the detuned and the retuned cases.

2.3.2 Procedures

1. Circularly Cylindrical Cavity

In order to verify Eq. (2.14), we wish to keep the frequency shift and the field disturbance as small as possible while the Q factor varies during the introduction of the loss into the cavity. To achieve this, about 0.13 g of dry table salt, NaCl, was placed in a glass tube, which was inserted into the cavity and its resonant performance was recorded. Subsequently, a very small drop of water

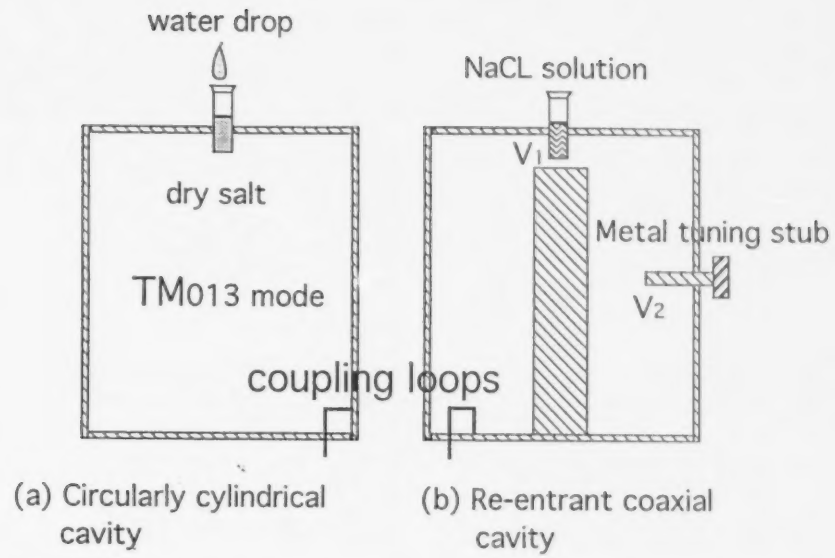

FIGURE 2.3 Cavity arrangement for single frequency Q method verification. (a) A small drop of water sliding into dry salt greatly increases the loss factor resulting in a significant Q drop, while the resonant frequency remains constant. (b) Insertion of 0.1N NaCl solution (V_1) into the cavity in the high E-field gap region changes both Q and resonant frequency. The metal tuning stub, as a secondary disturbance (V_2), pulls the resonant frequency back to the unperturbed value.

was added by letting it slide slowly along the inner surface of the tube wall as illustrated in Figure 2.3. On absorbing the water, the loss of the salt increases dramatically but the dielectric constant of the mixture does not change much. This leads to a significant Q reduction with little variation in resonant frequency and field configurations. During this period, the Q measurements, using both the bandpass and the single frequency methods, were performed automatically via the previously mentioned computer program. The results are listed in Table 2.1 for different coupling conditions. It shows that the results for the single frequency Q measurement method compare very favorably with those of the bandpass method. It should

be pointed out that the resonant data on which the tables are based were acquired semi-continuously, one reading for about every 0.25 second, as the salt was absorbing the water. As expected, the percentage difference between the two methods increases as the disturbance becomes larger.

Table 2.1 Q comparison between the bandpass method and the single frequency method (circularly cylindrical cavity)

f(GHz)	$\|\Gamma\|$	Q factor			Coupling Condition
		Bandpass	Single freq.	Difference(%)	
2.9550	0.469	7129	7122	0.1	over coupled
2.9550	0.425	6408	6374	0.5	
2.9549	0.348	5414	5322	1.7	
2.9549	0.332	5247	5136	2.1	
2.9549	0.297	4880	4751	2.6	
2.9549	0.293	4829	4706	2.6	
2.9549	0.032	2850	2749	3.7	
2.9450	0.177	1768	1770	0.1	under coupled
2.9450	0.190	1712	1772	0.6	
2.9450	0.227	1581	1594	0.8	
2.9449	0.352	1174	1213	3.3	
2.9449	0.414	997	1048	5.2	
2.9448	0.521	724	797	10.0	
2.9447	0.563	626	708	12.9	
2.9447	0.684	398	476	19.6	

2. Re-Entrant Coaxial Cavity

With this cavity, the validity of Eq. (2.14) was again confirmed and, in addition, dissimilarities of the results under perturbation conditions after the manner of the detuning and the retuning were revealed. The secondary disturbance was provided by a metal tuning stub as shown in Figure 2.3. We inserted a 0.1N NaCl solution in a glass tube through the cavity hole into the high E-field region in the gap. Because of the high dielectric constant and the high loss tangent of the sample, the Q factor as well as the resonant frequency were altered significantly as the sample was being inserted. During this insertion period, resonant data was again obtained on a

semi-continuous basis. To obtain the data for the retuning case, we repeated the Q measurements and retuned the cavity after each change in disturbance to its original resonant frequency by adjusting the metal stub tuner as the secondary disturbance. The Q, the resonant frequency and the reflection coefficient for the detuning and the retuning cases are listed in Tables 2.2 and 2.3 respectively for the comparison.

Table 2.2 Q comparison between the bandpass method and the single frequency method with free resonant frequency shift. (re-entrant cavity, under coupled)

f(GHz)	$\|\Gamma\|$	Q Factor		
		Bandpass	Single Freq.	Difference(%)
2.4042	0.154	1082	1110	2.6
2.4028	0.199	981	1012	3.2
2.4012	0.243	908	922	1.5
2.4003	0.267	857	876	2.3
2.3998	0.282	818	848	3.7
2.3983	0.324	711	774	8.8
2.3969	0.361	632	712	12.6
2.3958	0.387	568	670	17.8
2.3934	0.451	462	573	24.0

2.3.3 Discussion

The results show that the Q values from the single frequency method agree well with those from the standard bandpass method over a wide range of Q values. For example, the difference is less than 3.7% for a Q range of 7000 to 3000 and less than 20% for a Q range of 1800 to 400. The discrepancy from the standard bandpass method data increases with the increase of the perturbation.

As a large disturbance is introduced, the difference in the measured Q increases rapidly in the detuned case whereas the difference remains relatively constant in the retuned case This confirms the prediction made in the previous theoretical analysis that

Table 2.3 Q comparison between the bandpass method and the single frequency method at a fixed resonant frequency (re-entrant cavity, under coupled, f=2.4046 GHz).

$\|\Gamma\|$	Q Factor		
	Bandpass	Single Freq.	Difference(%)
0.131	1129	1195	5.9
0.165	1032	1085	5.1
0.232	879	943	7.3
0.254	854	900	5.4
0.290	772	833	7.9
0.335	696	753	8.3
0.366	645	702	8.8
0.417	568	622	9.5
0.498	460	507	10.2
0.607	338	371	9.5

the Q measured in the retuned case will be more accurate than that measured in the detuned case. This extension of the effective valid perturbation range can be attributed to the rebalancing of the cavity energy by the second disturbance and the removal of the energy change effect on the parameter S.

2.4 Error Analysis

In the foregoing, the perturbation theory for the single frequency Q measurement is proved to be valid theoretically and experimentally within a certain error. This error is analyzed more fully in this section. From the Q expression of Eq. (2.9), we can write the general form for the relative error in Q as

$$\frac{\Delta Q}{Q} = \frac{\Delta\omega}{\omega} + \frac{\Delta S}{S} + 2\frac{\Delta n}{n} - \frac{\Delta Zo}{Zo} - \frac{\Delta \bar{R}}{R} \qquad (2.25)$$

where $\Delta Zo/Zo$ can be considered to be zero. Specific forms for $\Delta S/S$ and $\Delta n/n$ affecting the constant C can be determined, at least in principle, only when the cavity and coupling structure geometry are

specified. The accuracy with which the constant C is obtained will largely determine the accuracy of the absolute Q value. If, on the other hand, the relative variation of Q is of interest, as is true in many practical cases, the error is equal to the $\Delta\bar{R}/\bar{R}$ term and is independent of the cavity geometry. This resonant input resistance error is related to the reflection coefficient by

$$\frac{\Delta\bar{R}}{\bar{R}} = \frac{2\,\Delta|\Gamma|}{1-|\Gamma|} \tag{2.26}$$

Since

$$|\Gamma| = 10^{\frac{RL}{20}}$$

where RL is the return loss in dB, Eq. (2.26) becomes

$$\frac{\Delta\bar{R}}{\bar{R}} = \frac{|\Gamma|\ln 10}{10(1-|\Gamma|)}\,\Delta(RL) \tag{2.27}$$

For a dual directional coupler of 30 dB directivity, the lower and upper limits of RL are[2.6]

$$\Delta(RL)^{-} = -0.336 - 0.0025|RL|^{2.373} \tag{2.28}$$

and

$$\Delta(RL)^{+} = 0.354 + 0.0028|RL|^{2.223} \tag{2.29}$$

respectively. Based on Eqs. (2.27) - (2.29) the relative error of $\bar{R}$ vs. RL is plotted in Figure 2.4 for a 30 dB directivity coupler. For comparison, the curve for a 40 dB directivity dual directional coupler is presented in Figure 2.4 also.

These curves demonstrate that the relative error is less than $\pm$ 8% for a 30 dB directivity coupler and a minimum return loss of 5 dB. If a 40 dB directivity coupler is used, however, a substantial accuracy improvement can be achieved with the error remaining nearly constant over a large return loss range. This contrasts with the error behavior of Q for the typical bandpass method as revealed in a study done in [2.7] in which they show a minimum error of $\pm$10% for the 30 dB directivity case over only a narrow return loss range. The error of the single frequency Q measurement tends to decrease when the cavity input impedance approaches a matching condition. This is an

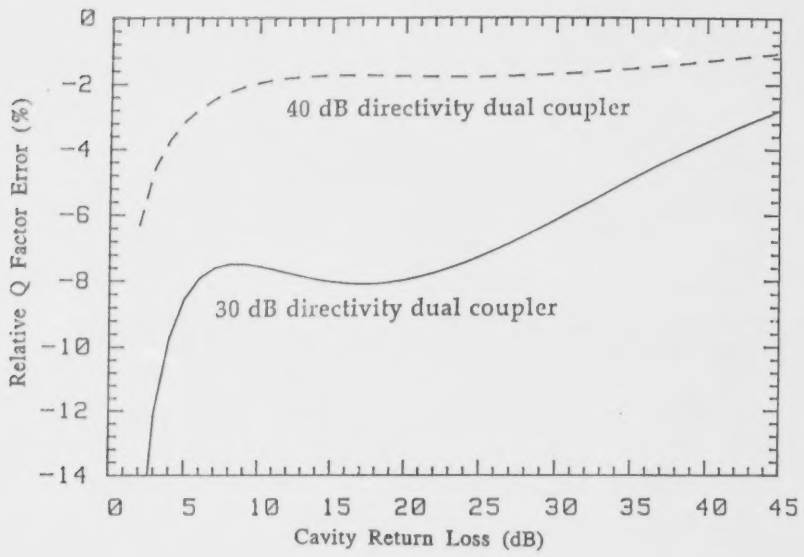

FIGURE 2.4 Relative Q factor error vs. cavity return loss using a reflectometer.

obvious advantage for resonant systems operating near their matched condition. More importantly, the present method eliminates the need for fo and Δfo measurements. Therefore, the power and the frequency variations of the source would have no direct effect on the measured relative Q factor. Moreover, a single frequency reflectometer can be tuned to give a much higher effective directivity at the fixed frequency, thereby further decreasing the error.

2.5 Conclusion

It has been proved that the Q factor can be calculated from parameters measured at the resonant frequency, i.e, a single frequency condition. Moreover, perturbation theory has been applied to the measurement of Q factor, proving that the Q factor is directly or inversely proportional to the input resonant resistance of a cavity when a moderate perturbation condition is satisfied. This principle has led to the development of the single frequency relative Q measurement method. In addition, the perturbation condition of the

invariance of the field configuration is required strictly only for the, usually small, coupling region in the cavity, which is a less stringent condition than that required in the traditional perturbation approach. It is found that a retuned perturbed resonator can yield a more accurate relative Q factor result. The experimental data from a cylindrical and a coaxial cavity confirms the validity of this method over a wide range of Q factor. An error analysis shows a more favorable performance compared to the bandpass method. As a relative method, the single frequency method can be applied to arbitrary cavities satisfying the perturbation stipulation. The principle of the single frequency Q measurement proposed in this chapter lays the basis for the loss measurement in our single frequency microwave heated dielectrometer.

References

[2.1] M. Martinelli, P.A.Rolla and E. Tombari, "a Method for Dielectric Loss Measurements by a Microwave Cavity in Fixed Resonance Condition", IEEE, MTT-33, No.9 sept. 1985, pp 779-783

[2.2] M. Sucher and J.Fox, Handbook of Microwave Measurement, 3rd Edition, Vol. II, Polytechnic Press of the Polytechnic Institute of Brooklyn, New York, 1963ork, 1963

[2.3] W. Xi, W. R. Tinga, W. A. G. Voss and B. Q. Tian, "New Results for Coaxial Re-Entrant Cavity with Partially Dielectric Filled Gap", IEEE. MTT-40(4) April, 1992, pp747-753

[2.4] R.A. Waldron, "Theory of Guided Electromagnetic Waves, Van Nostrand Reinhold, London, 1969

[2.5] W. Xi, "Notes on the Program DIELEC1-0", Lab. Rept., Department of Electrical Eng., University of Alberta, Edmonton, Canada, 1991

[2.6] HP8756A Scalar Network Analyzer Operating Manual, System Specification, p. 9, Hewlett-Packard, 1986

[2.7] W.Tinga and W.Xi, "Reflectometer Q Factor Measurements and Errors", Lab. Rept., Department of Electrical Eng., University of Alberta, Edmonton, Canada, 1991.

Chapter 3

DESIGN OF SELF-HEATING DIELECTROMETER APPLICATOR

3. 1 Introduction

A dielectrometer applicator is a device that provides a means for applying microwave energy from a microwave source to a dielectric sample. In our high temperature dielectrometer, the applicator serves as both a microwave heater and a measurement chamber, i.e. a self-heating dielectrometer applicator. In this chapter, we will discuss design considerations for the applicator, highlight its key elements and summarize its characteristics, and thereby confirm its usefulness as a high temperature dielectric applicator.

To allow for different applications, two different structures are considered for the applicators. Both are coaxial re-entrant cavities with a gap in their hollow center conductor, where, in one applicator, the gap is fixed at the endplate , as shown in Figure 3.1, while in the other, the gap is movable along the center conductor, as shown in Figure 3.2. A sample, held inside a quartz tube, is placed in the gap and extended into the adjacent hole region. In the movable gap scheme, the change of the gap position is realized through two movable short circuit plungers, while the center and outer conductor cylinders remain stationary. This arrangement maintains a fixed sample setup and a fixed gap position with respect to the inspection hole and the temperature monitoring holes. The applicator is designed at the ISM frequency of 915MHz.

Comparing the two schemes, the fixed gap scheme has easier sample access and a more stable cavity construction. Nevertheless, as we will show in the next chapter, changing the gap location is an effective way to control the loading without changing the sample volume or the gap width. In turn, this leads to widening the

1

A version of this chapter has been published. Mat. Res. Soc. Symp. proc. vol 189, pp. 111-116, 1991.

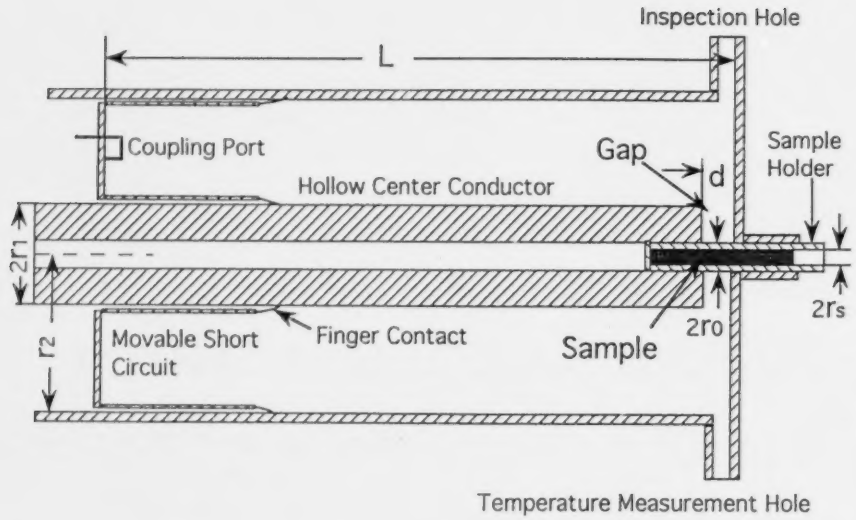

FIGURE 3.1 Cross section of the high temperature dielectrometer using a coaxial re-entrant applicator with the gap at the cavity end. (r_s=0.24, r_0=0.35, r_1=1.27, r_2=5.08, d=0.25 cm)

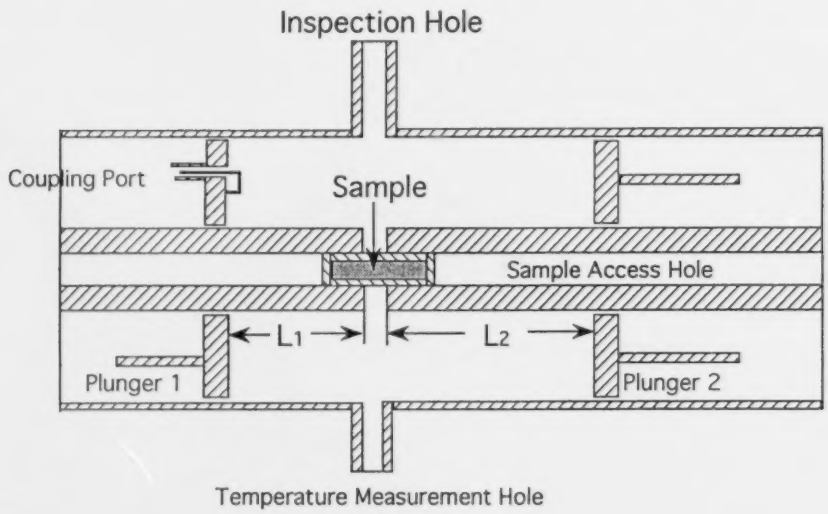

FIGURE 3.2 Cross section of the high temperature dielectrometer using a coaxial re-entrant cavity applicator with a movable gap. The movable plungers are designed as non-contact choke structure.

applicator's matching range to accommodate more diverse samples. For this reason, the movable gap scheme is a substitute for the fixed gap scheme for heavier loading cases.

Extensive analysis of the "fixed gap" scheme using the mode matching technique has been reported in the literature [3.1-3.4]. Here, we will still briefly present its characteristics because they are important for understanding the applicator's performance. A theoretical analysis of the "arbitrarily positioned gap" structure will be given in the next chapter.

3.2 Applicator Structure Design Considerations

3.2.1 General Considerations

In general, there are two types of dielectrometer applicators, i.e., travelling wave applicators and resonant applicators, as shown in Figure 3.3. A travelling wave applicator allows microwaves to travel through the dielectric without significant resonance occurring. This kind of applicator may have a uniform field distribution. But few, if any, are used in very high temperature dielectric heating because of the lack of a focused electromagnetic field. A resonant applicator refers to an applicator in which the microwave field forms a resonant wave pattern, where some regions contain focused fields, such as that at point A in Figure 3.3(b), which is useful to heat a dielectric sample effectively. For this reason, we chose a resonant cavity as our dielectrometer applicator.

Some major types of resonant cavity applicators currently used are shown in Table 3.1, along with a summary of their important features. Considering the overall heating and measuring requirements discussed in the following, we chose to use a coaxial re-entrant cavity, instead of the structures listed.

To heat samples effectively, we should consider not only the field distribution but also the heated sample's effects on the cavity's performance. Property variations of a heated sample may alter the electromagnetic fields, and thereby its resonant frequency and matching conditions. In order to maintain proper operation, either the sample loading or the physical cavity dimensions must be

adjustable.

From the measurement point of view, the establishment of the relationship between the dielectric properties and the measurable parameters, the stability of the applicator and the heating rate are the important factors to be considered. Firstly, an applicator chosen for measuring the properties of a dielectric should preferably be analysable so that the relation between the properties of the dielectric and the measurable parameters can be obtained. So far, the

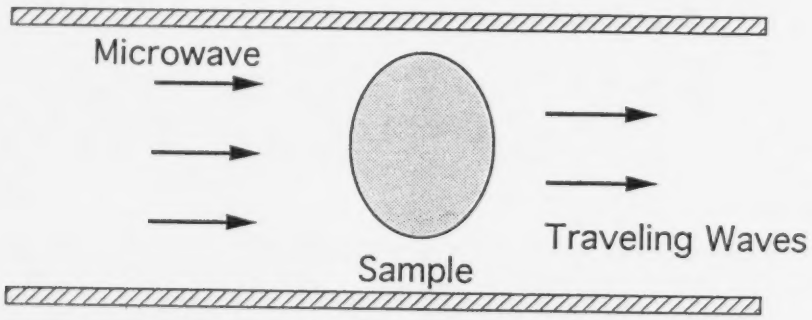

(a) A Traveling Wave Applicator

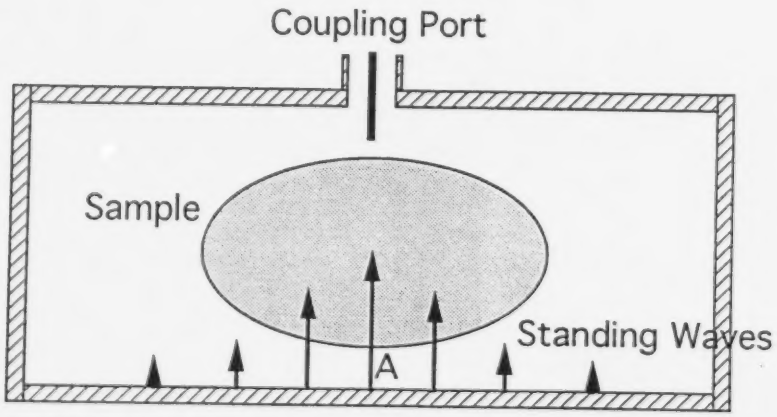

(b) A Resonant Applicator

FIGURE 3.3 Illustration of a traveling wave and a resonant applicators

Table 3.1 Typical structures of resonant cavity applicators and their major features

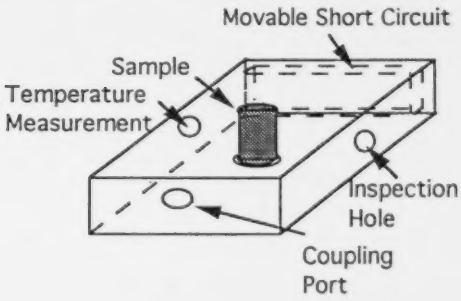

A rectangular waveguide applicator used in 1976 [3.5]. The first direct microwave sintering applicator. TE111 mode, E-field concentrates in the treatment zone.

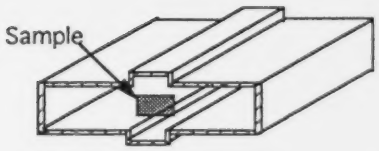

The groved waveguide applicator, a modified rectangular applicator, used in 1979 [3.6]. Quasi-TE111. Higher Q and larger sample allowed.

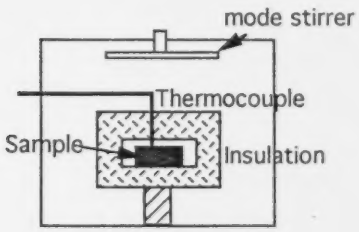

A modified microwave oven applicator used for ferrite sintering in 1981 [3.7]. Difficult to control field, tuning and matching.

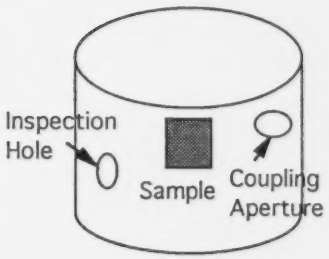

A cylindrical applicator used for ferrite sintering in 1986 [3.8]. TE011 mode, internal E-field in the sample increases from its center to its surface.

structures that can be fully analyzed are limited to rectangular, circularly cylindrical, spherical and coaxial cavities. Secondly, to satisfy perturbation conditions, sample loading is usually restricted, which, in turn, leads to a limitation in the measurement sensitivity. This requires an applicator stable enough to ensure that meaningful information about the sample can be extracted. A fixed sample mount and repeatable sample replacement are helpful means to achieve this stability. Thirdly, the heating rate also influences the accuracy of the measurement through the thermal expansion of the cavity and its

surface deterioration caused by overheating, resulting in a resonant frequency shift and Q drop. Since the analysis of these effects are usually quite difficult, it is preferable to have the sample heating rate high enough to allow the completion of a measurement cycle before cavity temperature rise has any significant effects on the resonant frequency and Q. To achieve this, a small sample and focused fields are essential.

Bearing these considerations in mind, we now take a look at how well our proposed structure can satisfy these heating and measuring requirements.

3.2.2 Cavity Length and Diameter, Short Circuit Plungers, Sample Access and Inspection Holes and Coupling Mechanism

As suggested by its construction, the quasi-TEM mode is the dominant mode, i. e. , a TEM field exists in the large coaxial portion, while hybrid TM and TEM fields exist in the gap and the gap-coaxial line transition region, the illustrative field pattern of which is depicted in Figure 3.4. In order to have a strong electric field in the gap, the length of the cavity, L, is designed with $\lambda/2 < L < 3\lambda/4$. As we will see later, an intense electric field can be produced in the gap, which aids the sample heating function. The width of the gap can be adjusted from 0-1.5 cm so that the sample's

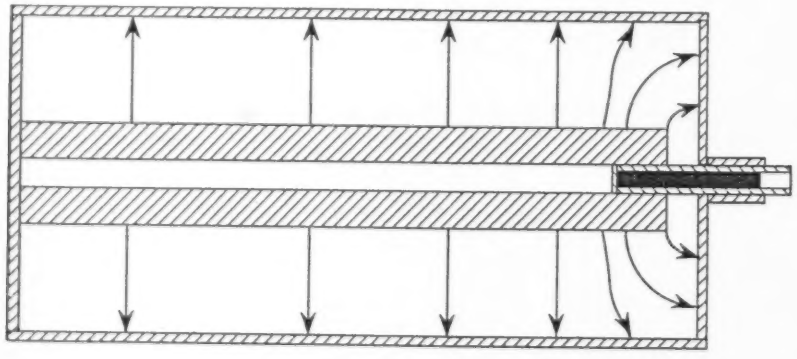

FIGURE 3.4 Illustrative E-field distribution in a coaxial re-entrant cavity.

heating zone can be controlled. To obtain a maximum Q factor, the ratio of the outer to inner conductor diameters is[3.9]

$$\frac{r2}{r1}=3.6 \tag{3.1}$$

Holes in the center conductor and on the endplate improve the performance and extend the usefulness of the cavity. Firstly, the hole provides the sample with an easy access to the gap, eliminating the need to open the cavity for sample replacement, thereby increasing measurement repeatability. Secondly, sample contact uncertainty is avoided. Because the gap completely cuts the conductive current flowing along the center conductor, the continuity of the current is sustained only by the displacement current in the gap. Thus, a small air gap between the sample end and the center conductor would cause appreciable measurement uncertainty.[3.10-3.12] The presence of the hole removes the contact and therefore eliminates this uncertainty.

Since the property variations of the sample alter the resonant frequency, a mechanism able to tune the cavity is needed. For the proposed structure, there are a number of methods which can be used to realize the frequency alteration, such as adjustment of a metal disk at a peak of the electric field, change of the gap width or the cavity length. However, our experiments showed that the metal disk at the maximum electric field severely disturbs the normal TEM mode pattern and the fields in the gap region, making an analytical field formulation impossible. Besides, the tuning range it can provide is too limited. On the contrary, the movement of the short circuit plunger does not change the cavity's coaxial structure, therefore adding no complexity to the cavity analysis. Meanwhile, the resonant frequency varies almost linearly with the displacement of the short circuit, leading to convenient tuning. For these reasons, a movable short circuit plunger is used as the tuning mechanism. Considering the maximum possible shifts of the frequency caused by the variations in the dielectric constant and the gap width, we designed the movable range of the plunger to be approximately 4 cm. To eliminate any effects caused by an erratic contact between the sliding plunger and the cavity wall as well as by any power leakage, we designed the

plunger in a bucket shape with finger contacts at a current node which occurs at a quarter wavelength away from the short. Our tests show that very stable electrical performance and a Q up to 4000 can be obtained at 915MHz.

Loops and probes are the most widely used coupling devices. We use a loop, instead of a probe, as our coupling device for two reasons. Firstly, the probe, which is required to be positioned at the maximum electric field, disturbs the existing electric field in the gap region. Secondly, the input impedance of a probe will change as the short circuit tuning plunger moves because the maximum E-field position varies with this movement. Since the loop is required to be located in a maximum H-field region, it can be mounted on the short circuit bucket and would move along with it. This arrangement is advantageous because the field pattern in the loop region will remain invariant when the bucket moves, and maximum isolation between the coupling port and the gap is achieved. The former leads to a stable input impedance condition and the latter reinforces the required perturbation condition for the single frequency Q measurement discussed in the previous chapter.

There are three radially mounted tubes, 1.5 cm in diameter and 3 cm in length, on the outer conductor wall. One is for insertion of an optical thermometer probe and the others for visual inspection of the gap region. Treating the tubes as cylindrical waveguides acting below their TM_{01} mode cutoff frequency, their attenuation constant is

$$\alpha = \frac{2\pi}{\lambda}\sqrt{(\frac{\lambda}{\lambda_c})^2 - 1} = 28 \text{ dB/cm} \qquad (3.2)$$

where λ is the wavelength and λ_c is the cutoff wavelength of TM_{01} mode. For the given guide diameter at 915MHz, λ=32.3cm and λ_c=2.613(1.5/2). Suppose that 100 Watts power is incident on one of the guides, the power reaching the opening of these tubes is only

$$P = 100\, e^{-2\alpha l} = 1.2*10^{-71} (W) \qquad (3.3)$$

which is obviously much lower than the recommended safe level of 10^{-3} Watts/cm^2.

3.2.3 Measurement Capability

Finally, let's briefly evaluate the capability of this applicator as a measuring chamber. In fact, without the hole in the center conductor and on the endplate, the structure proposed is the same as a standard re-entrant cavity, which has already had a long history in dielectric measurement. C.N.Works first used this cavity for measuring dielectric properties at ultra-high frequencies in 1945.[3.13] Following that, S.I.Reynolds (1947),[3.14] C.N.Works (1947)[3.15] and J.V.L.Parry (1951)[3.16] further improved the re-entrant cavity method. Until a theoretical field analysis of the cavity was done by O.V.Karpova using the mode-matching method in 1959,[3.17] all the measurements were based on experimental calibrations. Karpova's work was significant in terms of his replacing the approximate lumped circuit approach by a rigorous field approach. He also replaced the reference sample dependent experimental calibration measurement by a calculation based absolute measurement. Using the same approach, A. Milewski[3.18] and A. Kaczkowski[3.19] investigated the double post re-entrant cavity and the re-entrant cavity with a sample having a diameter smaller than that of the center conductor in 1975 and in 1980 respectively. Besides the field approach, the lumped circuit approach was also employed in many measurements in the past four decades.[3.20-3.22]

To sum up, as a measurement chamber, the re-entrant cavity has the following features:

1. Accurate. Attributed to the rigorous field solution, the error in determination of the permittivity can be less than 1%.[3.17] Milewsk claimed that the deviations in the measurement were less than 0.2% and 5% $\pm 5*10^{-5}$ for the relative dielectric constant and the loss tangent respectively.[3.18]

2. Wide frequency range. Initially, this cavity was proposed to operate in the frequency range from 0.1 to 1 GHz to cover the band that many other measurement methods could not.[3.15] A single cavity of this type can be designed to cover the frequency band as wide as 200-1000MHz.[3.23] By virtue of its quasi-TEM mode, the cavity can be easily scaled down or up for measuring dielectric properties at other

microwave frequencies.

3. High sensitivity. Among the methods for dielectric measurements, the resonant cavity method is one of the most sensitive ones. The sample being immersed in an intense gap field, the re-entrant cavity further enhances this sensitivity. [3.20]

3.3 Characteristics of the "Fixed Gap" Scheme

The fixed gap scheme has been best analyzed by W. Xi et al with the mode matching technique.[3.1] For a better understanding of the performance of the applicator, we summarize its major electromagnetic characteristics based on this analysis.

Its field distributions are reproduced here in Figures 3.5 and 3.6. These figures reveal that 1) the fields in the cavity are basically no different from the pure TEM coaxial fields except in the gap region. Therefore, the coupling loop on the short circuit plunger is immersed in basically pure TEM fields regardless of the field variations in the gap. 2) Due to the presence of the gap, the TEM mode fields are converted into a hybrid TM mode. The E_z component of the TM mode in the gap is the major source for heating a sample in the gap. 3) Depending on the gap width and the permittivity of the dielectric sample, the fields in the gap may be electrically dominant, i.e., a capacitive mode or magnetically dominant, i.e., an inductive mode. Since a dielectric sample interacts mainly with electric fields, therefore, to achieve a high sensitivity and effective heating, we always adjust the cavity length to obtain a capacitive mode in the gap. In the following discussion, a capacitive mode is always assumed.

We have pointed out that the field intensity in the gap is much higher than in the rest of the cavity. The magnitude of this intensification can be characterized by a density ratio of the energy, P_d, as

$$P_d = \frac{\frac{W_D}{V_D}}{\frac{W_E}{V_c}} \tag{3.3}$$

where W_D and W_E are the energy stored in the sample and in the rest of

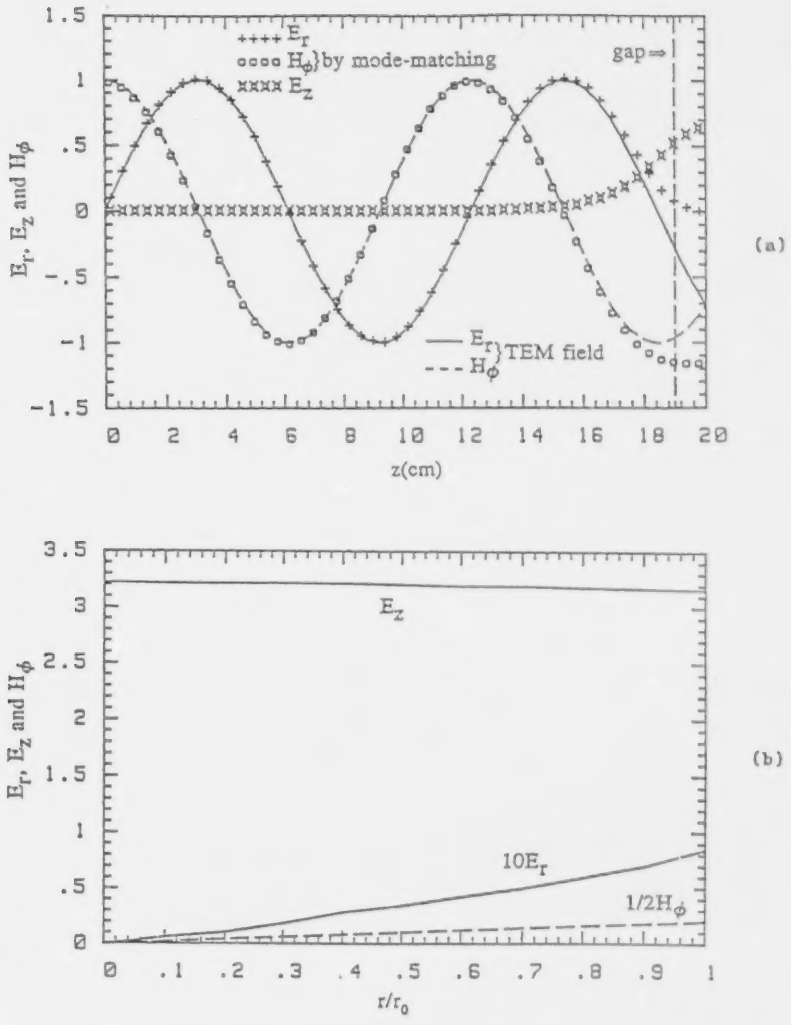

FIGURE 3.5 E and H fields for a capacitive mode in a re-entrant cavity, normalized by the TEM field. (a) Axial distribution at r=2.875cm, compared with TEM field. (b) Radial distribution in the gap midplane [3.1].

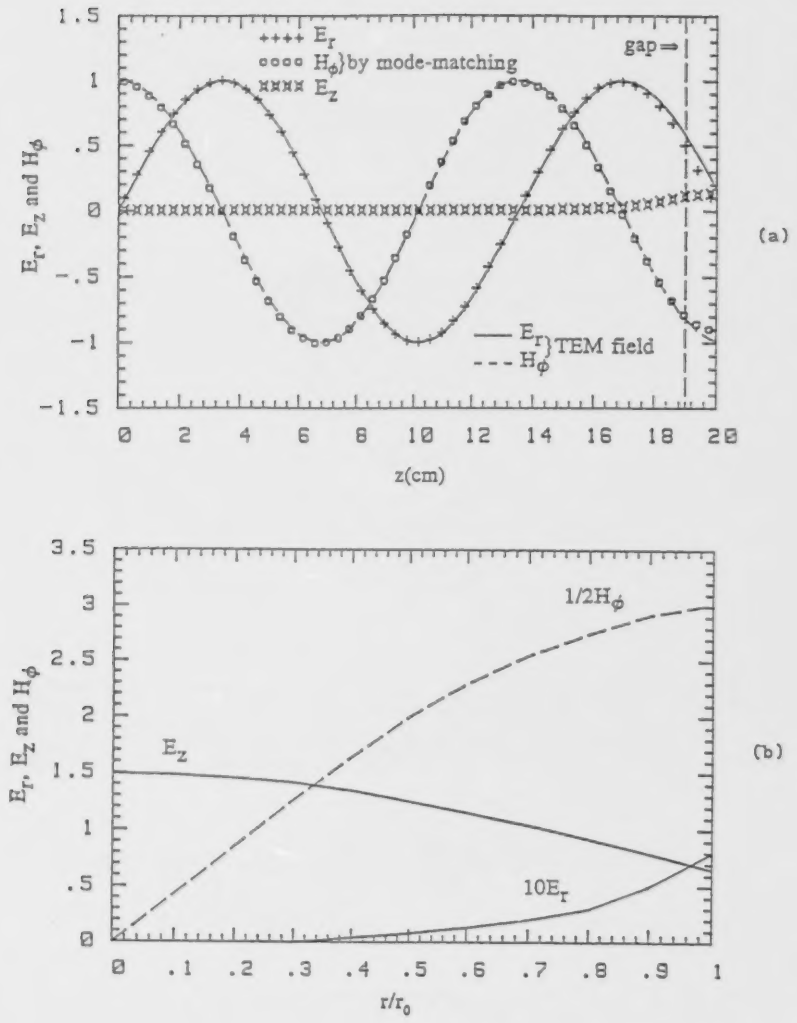

FIGURE 3.6 E and H fields for an inductive mode in a re-entrant cavity, normalized by the TEM field. (a) Axial distribution at r=2.875cm, compared with TEM field. (b) Radial distribution in the gap midplane [3.1].

the cavity; V_D and V_c are the volumes of the sample and the cavity respectively. Figures 3.7(a), (b) and (c) show the magnitude of this energy density. As we can see, eventhough P_d varies with gap width, dielectric constant and sample diameter, a P_d of more than one hundred can be easily obtained in a normal case. Such strong concentration of the electric fields will benefit the heating rate and the measuring sensitivity. In turn, this requires careful control of the heating process to avoid thermal runaway.

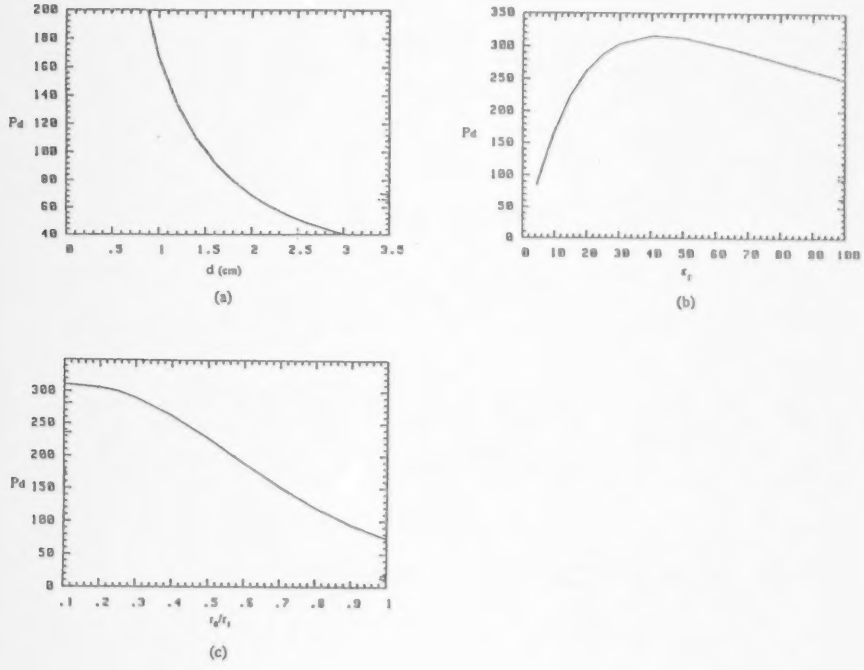

FIGURE 3.7 (a) Sample energy density as a function of the gap width, d, (b) the dielectric constant, ε', and (c) normalized sample radius. [3.24]

The hole affects the electromagnetic behavior of the cavity in three aspects:

1. Field confinement As we have mentioned, the hole is so designed that the fields in it are evanescent, thereby they are, practically, confined to a limited depth in the hole, as shown in

Figure 3.8. The advantage of this is that the region of interaction between the sample and the fields is confined without the physical presence of metal end walls.

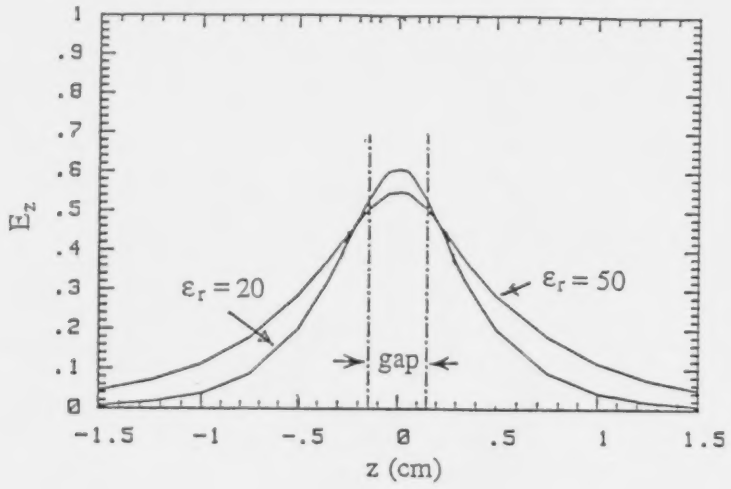

FIGURE 3.8 Ez axial distribution for different dielectric constant, ε', illustrating field confinement in the hole region. [3.24]

2. Energy redistribution The holes store appreciable energy. This is shown in Figure 3.9, where more than half of the total sample energy is seen to be stored in the holes. As the value of the dielectric constant of the sample increases, the increase of the energy stored in the holes tends to accelerate.

3. Linearization of frequency shift Without the holes, the frequency shift would start to saturate at a certain value of dielectric constant, as shown in Figure 3.10. With the holes, the frequency shift saturation is offset by the acceleration of the increase in the energy storage in the holes, resulting in a more linear relation between f and ε_r.

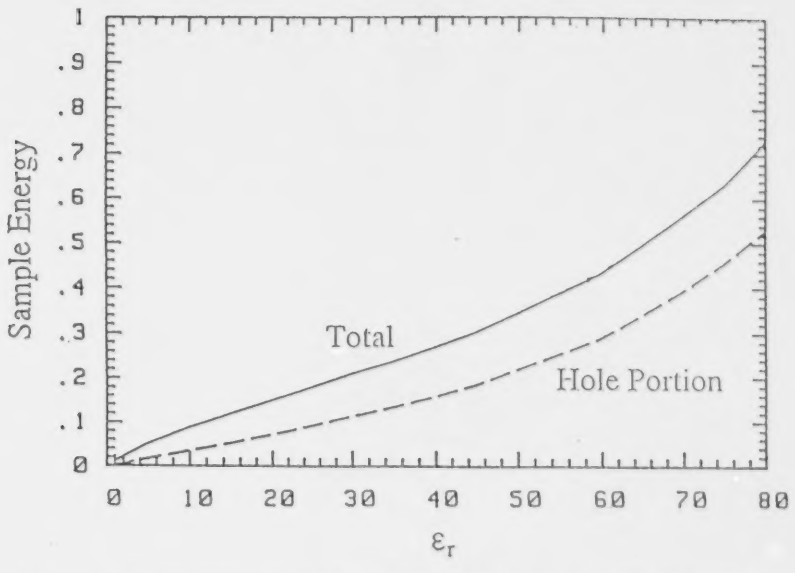

FIGURE 3.9 Comparison of total sample energy stored in the gap region to that stored in the hole. [3.24]

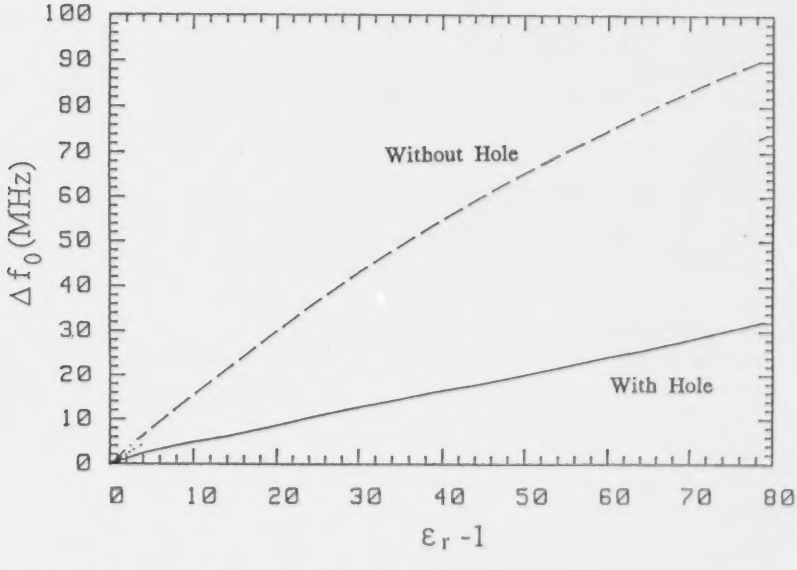

FIGURE 3.10 Frequency shift vs. dielectric constant for the gap in a re-entrant cavity with and without a hole in its center conductor. [3.24]

3.4 Conclusions

This chapter focused on the design of the self-heating dielectrometer applicator, including a survey of basic resonator structures, applicator design considerations, useful modifications to the coaxial re-entrant cavity and a summary of its enhanced characteristics.

Compared to other dielectrometer applicators, the coaxial re-entrant cavity has high sensitivity and wide bandwidth. More importantly, if an appropriate amount of microwave energy is applied, the intensified gap electric field can be used to heat a dielectric sample in the gap. By measuring the resultant frequency shift and Q factor variation, we can determine the sample's dielectric constant and loss factor as a function of temperature. Therefore, a self-heating dielectrometer applicator can be realized using these design principles.

References

[3.1] W. Xi, W. R. Tinga, W. A. G. Voss, B. Q. Tian, "New Results for Coaxial Re-Entrant Cavity with Partially Dielectric Filled Gap", IEEE Trans. Microwave Theory and Tech., vol. MTT-40, pp 747-753, 1992.

[3.2] B.Q.Tian, W.R.Tinga, "A Wide Range Tunable And Matchable High Temperature Applicator", Cera. Trans. Vol 21, p647-654, 1991.

[3.3] W.R.Tinga, B.Q.Tian and W.A.G.Voss, "New High Temperature Multi-Purpose Applicator", Mat.Res.Soc., vol.189, pp 111-116, 1991.

[3.4] W.Xi and W.R.Tinga, "A High Temperature Microwave Dielectrometer", Cera.Trans. Vol 21, pp 215-224, 1991

[3.5] A. J. Berteaud, "High Temperature Thermal Treatment of Refractory Oxides with Microwave Heating", J. of Microwave Power, Vol. 11, No.2, 1976, p 199

[3.6] J.M.Thiebaut, "A New Microwave Resonant Applicator", J. of Microwave Power, Vol.14, No.3, 1976, p217-222

[3.7] M.K.Krage, "Microwave Sintering of Ferrites", Cera. Bull., Vol.60, No. 11, 1981, p1232-1234

[3.8] F.Okada, "Microwave Sintering of Ferrite", Advances in Cera., Vol.15, 14th International Conf. On Ferrites, Part 1, p201-205

[3.9] Montgomery, Technique of Microwave Measurement p 307

[3.10] S.B.Wilson, "Modal Analysis of the 'Gap Effect' in Waveguide Dielectric Measurements", IEEE Trans. Microwave Theory Tech., Vol MTT-36, pp752-756,1988-756,1988-756,1988

[3.11] K.S.Champlin and G.H.Glover, "'Gap Effect' in Measurement of Large Permittivities", IEEE Trans. Microwave Theory Tech. Vol MTT-14, pp 397-398, 1966398, 1966

[3.12] K.S.Champlin and G.H.Glover, "Influence of Waveguide Contact On Measured Complex Permittivity of Semiconductors", J. Applied Phys. Vol 37, no.6, pp 2355-2360, 1966

[3.13] C. N. Works, T. W. Dakin and F. W. Boggs " A Resonant-Cavity Method for Measuring Dielectric Properties at Ultra-High Frequencies", Proc. I. R. E. April, 1945, p245-254

[3.14] S. I. Rynolds, "Improved Reentrant Cavity", General Electric Review, Sept. 1947, p34-394-39

[3.15] C. N. Works, "Resonant Cavity for Dielectric Measurements", J. of Applied Physics, Vol. 18, July, 1947, p605-612 p605-612

[3.16] J. V. L. Parry, " the Measurement of permittivity and Power Factor of Dielectrics at Frequencies From 300 to 600 Mc/s", Proc. IEE., Vol 98, no. 54, pp303-311, 1951311, 1951

[3.17] O. V. Karpova, "On an Absolute Method of Measurement of Dielectric Properties of a Solid Using a π Shaped Resonator", (in Russian), Fiz. Twerd, Tela. Vol 1, pp246-255, Feb, 1959, Moscow

[3.18] A. Milewsk, "Coaxial Lumped Capacitance Resonators for the Investigations of Dielectrics", Electron Techn. Vol. 10, pp71-98, Jan., 1977, Warsaw

[3.19] A. Kaczkowski and A. Milewski, "High Accuracy Wide-Range

Measurement Method for Determination of Complex Permittivity in Reentrant Cavity, Part A -- Theoretical Analysis of the Method", IEEE. Trans. MTT-28, pp225-228, Mar., 1980

[3.20] I. L. Eldumiati, G. I. Haddad, "Cavity Perturbation Techniques for Measurement of the Microwave Conductivity and Dielectric electric Constant of a Bulk Semiconductor Material", IEEE Trans., MTT-20, No.2, pp 126-132, Feb. 1972.

[3.21] I. L. Eldumiati, G. I. Haddad, "Microwave Properties of n-Type InSb in a Magnetic Field between 4 and 300^{0} K", J. of Appl. Phys. , Vol.44, No.1, pp 395-405, Jan., 1973

[3.22] Susanta Sen, P. K. Saha and B. R. Nag, "New Cavity Perturbation Technique for Microwave Measurement of Dielectric Constant", Rev. Sci. Instrum. 50(12), Dec., 1979, pp 1594-1597

[3.23] A. Kaczkowski and A. Milewski, "High-Accuracy Wide-Range Measurement Method for Determination of Complex Permittivity in Reentrant Cavity: Part B -- Experimental Analysis of Measurement Errors", IEEE. Tran., MTT-28, No. 3, pp 228-231, Mar.,1980

[3.24] Weiguo Xi and Wayne R. Tinga, "Field Analysis of New Coaxial Dielectrometer", IEEE Trans. Microwave Theory and Tech., vol MTT-40(10), pp1927-1934, 1992.

Chapter 4

ANALYSIS OF COAXIAL RE-ENTRANT CAVITY WITH AN ARBITRARILY POSITIONED GAP IN ITS CENTER CONDUCTOR[1]

4.1 Introduction

In this chapter, we will concentrate on the theoretical analysis of the movable gap structure, or more strictly, on the coaxial re-entrant cavity with an arbitrarily positioned gap in its center conductor. Two approaches will be used in the analysis, namely, a field analysis by modifying an existing mode matching formulation for the fixed gap structure, and an equivalent circuit analysis based on a novel artificial electric wall concept. Using the mode matching model, we will calculate and discuss the fields, the energy distribution, the resonant frequency and the Q factor. Matching performance is discussed on the basis of the equivalent circuit model.

4.2 Mode Matching Analysis

For the convenience of the mode matching formulation, the actual structure of the movable gap coaxial re-entrant cavity shown in Figure 3.2 has been redrawn in the simpler form of Figure 4.1. Note that, except for the addition of one more post, the construction of the movable gap structure is the same as the fixed gap one, for which the mode matching formulation is available [4.1, 4.2]. Therefore, we need only to add new formulas pertinent to the two new subareas created by the addition of the post, i.e., the regions A and B in the figure. Only one new symbol is added here, namely, the dimension of the gap position, L_g.

4.2.1 Mode Matching Formulation For Regions A And B

Fields in the subareas A and B can be expanded in a series of TM_{0n} modes in a circular waveguide as suggested by the axially symmetrical structure, that is,

---

[1] A version of this chapter has been published. Amer. Cer. Soc. Trans.vol 21, "Microwave: Theory and Applications In Material Processing", pp 647-654, 1991.

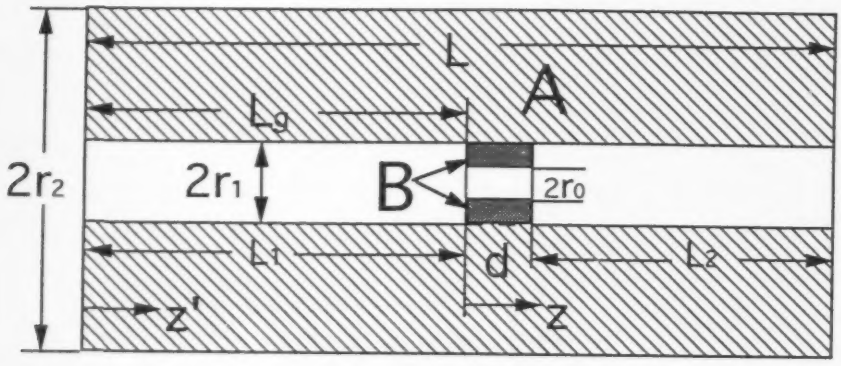

FIGURE 4.1 Simplified cross section diagram of the coaxial re-entrant cavity with an arbitrary positioned gap in its center conductor. The shaded areas A and B are the regions of interest.

$$\begin{cases} E_z^A = \sum_{n=0}^{N-1} A_n \, Z_{0n}^A(k_n^A r) \cos\beta_n^A z' & (4.1a) \\ H_\phi^A = \sum_{n=0}^{N-1} A_n \, \frac{j\omega\varepsilon_0}{k_n^A} \, Z_{in}^A(k_n^A r) \cos\beta_n^A z' & (4.1b) \end{cases} \quad \text{in A}$$

$$\begin{cases} E_z^B = \sum_{m=0}^{M-1} B_m \, Z_{0m}^B(k_m^B r) \cos\beta_m^B z & (4.2a) \\ H_\phi^B = \sum_{m=0}^{M-1} B_m \, \frac{j\omega\varepsilon_0}{k_m^B} \, Z_{im}^B(k_m^B r) \cos\beta_m^B z & (4.2b) \end{cases} \quad \text{in B}$$

where

n, m = natural numbers numerating the respective terms in the expansion series and also indicating the different modes

A_n, B_m = expansion coefficients

k, β= transversal and longitudinal wave numbers

ko = the wave number in free space

$k_n^{A2} = k_0^2 - \beta_n^{A2}$ = transverse wave number of mode n in area A (4.3a)

$\beta_n^A = \frac{n\pi}{L}$ = longitudinal wave number of mode n in area A (4.3b)

$k_m^{B2} = k_0^2\varepsilon_r - \beta_m^{B2}$ =transverse wave number of mode m in area B (4.3c)

$\beta_m^B = \frac{m\pi}{aL}$ = longitudinal wave number of mode m in area B (4.3d)

$a = \frac{d}{L}$ = normalized gap width with respect to the cavity length (4.3e)

$e = \frac{L_g}{L}$ = normalized distance between the gap and the endplate, with respect to the cavity length (4.3f)

We define Z_{0n}^A, Z_{1n}^A, Z_{0n}^B and Z_{1n}^B as the linear combinations of Bessel functions of the first and the second kind as follows.

$$Z_{0n}^A(k_n^A r) = J_0(k_n^A r) - F_n^A N_0(k_n^A r) \quad (4.4a)$$

$$Z_{1n}^A(k_n^A r) = J_1(k_n^A r) - F_n^A N_1(k_n^A r) \quad (4.4b)$$

$$Z_{0m}^B(k_m^B r) = J_0(k_m^B r) - F_m^B N_0(k_m^B r) \quad (4.4c)$$

$$Z_{1m}^B(k_m^B r) = J_1(k_m^B r) - F_m^B N_1(k_m^B r) \quad (4.4d)$$

where

J_0, J_1 = the first and the second order Bessel function of the first kind

N_0, N_1 = the first and the second order Bessel function of the second kind

F_n^A, F_m^B = the constants prescribed by the boundary conditions.

By the boundary condition $E_z^A|_{r=r2}=0$, we obtain, from (4.1a) and (4.4a),

$$F_n^A = \frac{J_0(k_n^A r_2)}{N_0(k_n^A r_2)} \quad (4.5)$$

The boundary condition at $r=r_1$ requires $E_z^A = E_z^B$. By equating (4.1a) to (4.2a) for $r=r_1$, we get

$$\sum_n^{N-1}{}' A_n \cos\beta_n^A z' = \begin{cases} \sum_{m=0}^{M-1}{}' B_m \cos\beta_m^B z & z \in (0,d) \\ 0 & -L_g<z<0,\ d<z<L-L_g-d \end{cases} \quad (4.6)$$

where $A_n' = A_n Z_{0n}(k_n^A r_1)$ and $B_m' = B_m Z_{0m}^B(k_m^B r_1)$. (4.7)

Noting $z=z'-L_g$ as shown in Figure 4.1, we replace z on the right hand side of (4.6) by $z'-L_g$, so that the two sides of this equation include the same longitudinal variable, i.e.,

$$\sum_{n}^{N-1} A_n' \cos\beta_n^A z' = \begin{cases} \sum_{m=0}^{M-1} B_m' \cos\beta_m^B (z'-L_g) & z \in (0,d) \\ 0 & -L_g<z<0,\ d<z<L-L_g-d \end{cases} \tag{4.8}$$

In order to obtain the relation between A_n' and B_m', and thereby A_n and B_m using (4.7), we must expand $B_m' \cos\beta_m^B(z'-L_g)$ on the right hand side of (4.8) into $\cos\beta_n^A z'$ over z' from 0 to L using Fourier series. Fourier expansion coefficient A_n' can be obtained by multiplying the two sides by $\cos\frac{m\pi}{L}z'$ and integrating each term over the interval 0 to L. Note that, in the interval $-L_g < z < 0$ and $d < z < L-L_g-d$, the right hand side is zero. As a result, the remaining integration is limited from L_g to L_g+aL and so

$$A_n' = \frac{2}{L}\int_{L_g}^{L_g+aL} \sum_{m=0}^{M-1} B_m' \cos\frac{m\pi}{aL}(z'-L_g)\cos\frac{m\pi}{L}z'\,dz' \tag{4.9}$$

β_n^A and β_m^B have been substituted by $n\pi/L$ and $m\pi/aL$ respectively according to (4.3b) and (4.3d). Working out the integration for each term in the series, we obtain

$$A_n' = \frac{2n}{\pi}\sum_{m=0}^{M-1} B_m' \frac{(-1)^m \sin(e+a)n\pi - \sin(en\pi)}{n^2-(\frac{m}{a})^2} \tag{4.10}$$

Substituting A_n' and B_m' using (4.7), an explicit relation between A_n and B_m can be expressed as

$$A_n \frac{2n}{\pi}\sum_{m=0}^{M-1} B_m \frac{Z_{0m}^B(k_m^B r_1)}{Z_{0n}^A(k_n^A r_1)} \cdot \frac{(-1)^m \sin(e+a)n\pi - \sin(en\pi)}{n^2-(\frac{m}{a})^2} \tag{4.11}$$

For neatness, we write this equation in a matrix form as

$$\mathcal{A}=\mathcal{P}\mathcal{B} \tag{4.12}$$

where $\mathcal{A}=[A_0,\ A_1,\ A_2,\ldots.A_n]^T$, $\mathcal{B}=[B_0,\ B_1,\ B_2,\ldots.B_m]^T$, $\mathcal{P}=[p_{nm}]$ and

$$p_{nm} = \frac{2n\, Z_{0m}^B(k_m^B r_1)\ (-1)^m \sin(e+a)n\pi - \sin(en\pi)}{\pi Z_{0n}^A(k_n^A r_1)\ [n^2-(\frac{m}{a})^2]} \tag{4.13}$$

Since the azimuthal component of the magnetic field should also be continuous at the boundary between A and B, that is, $H_\phi^A = H_\phi^B$ at $r=r_1$, by equating (4.1b) to (4.2b) and using (4.3d) and (4.3e), we obtain,

$$\sum_{n=0}^{N-1} A_n \frac{j\omega\varepsilon_0}{k_n^A} Z_{1n}(k_n^A r_1) \cos(\frac{n\pi}{L}z') = \sum_{m=0}^{M-1} B_m \frac{j\omega\varepsilon_0}{k_m^B} Z_{1m}(k_m^B r_1) \cos(\frac{m\pi}{d}z) \tag{4.14}$$

Substituting $z+L_g$ for z' on the left hand side, so that the longitudinal variables are the same on the two sides, results in

$$\sum_{n=0}^{N-1} A_n \frac{j\omega\varepsilon_0}{k_n^A} Z_{1n}(k_n^A r_1) \cos\frac{n\pi}{L}(z+L_g) = \sum_{m=0}^{M-1} B_m \frac{j\omega\varepsilon_0}{k_m^B} Z_{1m}(k_m^B r_1) \cos(\frac{m\pi}{d}z) \tag{4.15}$$

For this case, we can expand the left hand side of the equation in $\cos\frac{n\pi}{d}z$ over z from 0 to d using another Fourier series. Similar to the previous manipulation, we obtain another equation set defining the relation between B_m and A_n as follows

$$B_m = \frac{2}{a\pi}\sum_{n=0}^{N-1} A_n \frac{k_m^B Z_{1n}(k_n^A r_1)}{k_n^A Z_{1m}(k_m^A r_1)} \frac{n}{(\frac{m}{a})^2-n^2} [\sin(en\pi)-(-1)^m \sin(e+a)n\pi] \tag{4.16}$$

This equation can also be written in a matrix form as

$$\mathcal{B}=Q\mathcal{A} \tag{4.17}$$

where $Q=[q_{mn}]_{MN}$ and (4.18)

$$q_{mn} = \frac{2}{a\pi} \frac{k_m^B Z_{1n}(k_n^A r_1)}{k_n^A Z_{1m}(k_m^A r_1)} \frac{n}{(\frac{m}{a})^2-n^2} [\sin(en\pi)-(-1)^m \sin(e+a)n\pi] \tag{4.19}$$

Substituting for $\mathcal{A}$ in Eq. (4.17) using Eq. (4.12), we obtain

$$\mathcal{B}=Q\mathcal{P}\mathcal{B} \tag{4.20}$$

or $$(Q\mathcal{P}-\mathcal{J})\mathcal{B}=0 \tag{4.21}$$

where $\mathcal{J}$ is a unit matrix of $(M+1)\times(M+1)$.

Let $$\mathcal{G}=Q\mathcal{P}-\mathcal{J} \tag{4.22}$$

then (4.21) becomes $$\mathcal{G}\mathcal{B}=0 \tag{4.23}$$

where $\mathcal{G}=[g_{ij}]_{(M+1)(M+1)}$. Substituting $\mathcal{P}$ and Q in (4.22) by (4.13) and (4.19) respectively, multiplying Q and $\mathcal{P}$ and subtracting $\mathcal{J}$, we obtain the expression for g_{ij} as

$$g_{ij} = a\alpha_i \frac{k_i^B Z_{oj}^B(k_j^B r_1)}{Z_{i1}^B(k_i^B r_1)} \sum_{n=0}^{N-1} \alpha_n U_{ni} U_{nj} S_n - \delta_{ij} \tag{4.24}$$

where $\alpha_i = \begin{cases} \frac{1}{2} & i=0 \\ 1 & i\neq 0 \end{cases}$

$\alpha_n = \begin{cases} \frac{1}{2} & n=0 \\ 1 & n\neq 0 \end{cases}$

$\delta_{ij} = \begin{cases} 1 & i=j \\ 0 & i\neq j \end{cases}$

$$U_{nm} = \frac{2an}{\pi[(an)^2-m^2]} [(-1)^m \sin(e+a)n\pi - \sin(en\pi)] \qquad an\neq m \tag{4.25}$$

$$S_n = \frac{Z_{in}(\hat{k_n} r_1)}{\hat{k_n} Z_{in}(\hat{k_n} r_1)} \tag{4.26}$$

It is noted, in Eq (4.25), that U_{nm} will be undefined when $(an)^2-m^2 \Rightarrow 0$. Therefore, special treatment for this case is needed. Considering that

$$\lim_{an\Rightarrow m\neq 0} U_{nm} = \frac{2}{\pi} \lim_{an\Rightarrow m} \frac{an\,[(-1)\sin(an+\frac{e}{a}an)\pi - \sin\frac{e}{a}an\pi]}{(an)^2-m^2}$$

$$= 2\cos\frac{e}{a}m\pi \tag{4.27}$$

and

$$\lim_{n=m\Rightarrow 0} U_{nm} = \lim_{n\Rightarrow 0}(\lim_{m\Rightarrow 0} U_{nm})$$

$$= \lim_{n\Rightarrow 0} \frac{2\,an\,[(-1)\sin(a+e)n\pi - \sin en\pi]}{\pi\,(an)^2} = 2 \tag{4.28}$$

we now have obtained U_{nm} for all cases, that is

$$U_{nm}=\begin{cases} \dfrac{2an}{\pi[(an)^2-m^2]}[(-1)^m\sin(e+a)n\pi-\sin(an\pi) & an\neq m \\ 2\cos\dfrac{e}{a}m\pi & an=m\neq 0 \\ 2 & n=m=0 \end{cases} \quad (4.29)$$

The major objective of the entire formulation is to obtain the determinant equation (4.23) and the expression for $\mathcal{G}$, so that we can obtain the resonant frequency, the fields, the Q factor, the energy and the power loss. If (4.23) is to have a non-zero solution for B_m, we must require the determinant of $\mathcal{G}$ to be zero. The wave number, k_o, and therefore the resonant frequency, can be found from the solution of the determinant equation set. Once k_o is determined, so are the expansion coefficients, B_m, as the solutions of (4.23), the transversal wave numbers using (4.3), and A_n using (4.11). Then the fields are obtained with Eqs. (4.1) and (4.2). The Q factor is calculated with $Q=\omega W/P$, where W is the electromagnetic energy stored in the cavity, P is the power loss in the cavity, including the loss in the cavity wall and in the dielectric sample. W and P are all readily calculable since all the field expressions have been found.

To implement the above calculations, all the derived formulas are coded into a set of FORTRAN programs named MMMC1-AG, MMMC2-AG, MMMC3-AG and MMMC4-AG, in which, AG, an abbreviation of Arbitrary Gap, is added to distinguish them from their fixed gap counterparts, MMMC1, MMMC2, MMMC3 and MMMC4, which are available at the Microwave Power Lab of the University of Alberta. In the movable gap scheme, the determination of a sample's dielectric constant can be performed under a fixed resonant frequency condition, from which we can obtain ε_r from the variation of the cavity length, ΔL, instead of from Δf as in the fixed gap case.

4.2.2 Mode Matching Program Verification

Since the results from MMMC1 to MMMC4 have been carefully checked

against experimental data with a maximum difference of 0.22%,[3.1] programs MMMC1-AG to MMMC4-AG were verified by comparing the calculated data to those from MMMC1 to MMMC4. Only the calculated data from MMMC2-AG and MMMC2 are given in Tables 4.1 and 4.2 to show the typical values of the calculation results. Table 4.1 gives the calculated resonant wavelength for different modes, showing a maximum difference of 0.012%, while Table 4.2 gives the calculated Q and electromagnetic field components with a maximum difference of 8%.

Table 4.1 Resonant wavelengths calculated from programs MMMC2 and MMMC2-AG (d=1, L=20, r_1=1.25, r_2=4.5 cm, ε'=2.1).

Modes N	Modes M	MMMC2-AG (cm)	MMMC2 (cm)	Differences (%)
5	3	12.53290	12.53229	0.0049
100	5	12.53370	12.53311	0.0047
100	20	12.30662	12.30510	0.0120

Table 4.2 Q factor and electromagnetic field data calculated from MMMC2 and MMMC2-AG (d=1, L=20, r_1=1.25, r_2=4.5, N=100, M=20).

	Q	Er	Ez (r=0.3,z=0.4)	H	Er	Ez (r=2.0,z=2.0)	H
MMMC2-AG	3424.8	-0.00621	0.983	0.000415	0.158	0.0943	0.00121
MMMC2	3415.6	-0.00675	0.983	0.000415	0.158	0.0952	0.00121
Difference (%)	0.0023	8	0	0	0	0.95	0

The calculated resonant wavelength versus the mode number, N, in area A and the mode number, M, in area B are depicted in Figures 4.2 and 4.3 respectively. As shown in Figure 4.2, the resonant wavelength value approaches its asymptotic value after M=5. If we take the final

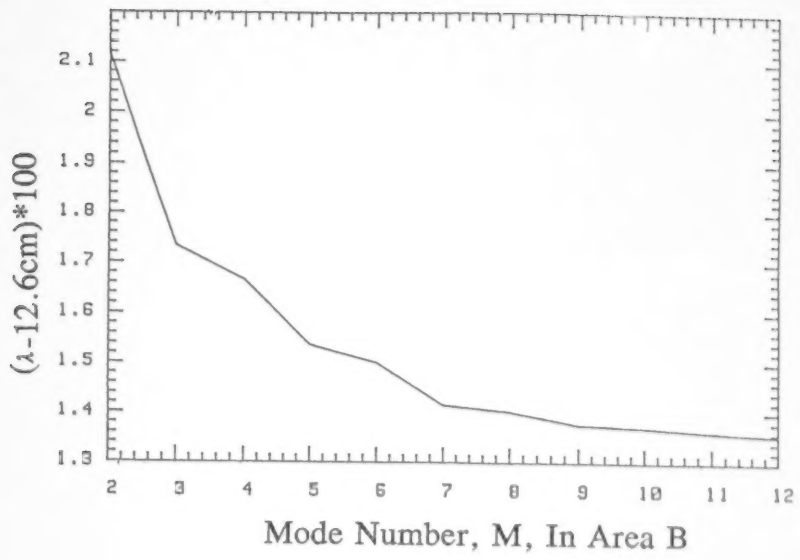

FIGURE 4.2 Resonant wavelength, λ, vs. the mode number, M, in area B (ε'=2.1, r_o=1, r_1=1.25, r_2=4.5, L=20.0, d=1.0, L_g=1 cm, N=100).

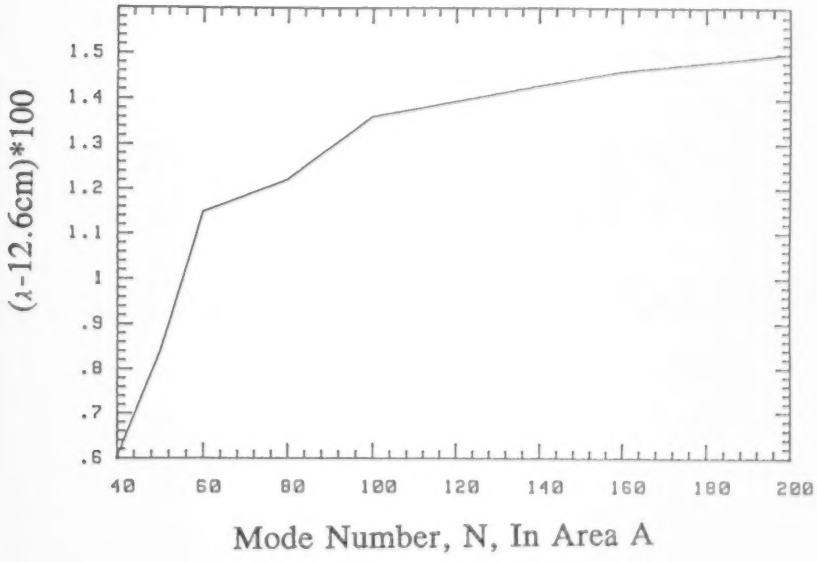

FIGURE 4.3 Resonant wavelength, λ, vs. the mode number, N, in area A (ε'=2.1, r_o=1, r_1=1.25, r_2=4.5, L=20.0, d=1.0, L_g=1 cm, M=11).

asymptotic value as the "accurate" value for the wavelength, say at M=12, the truncation error in the calculated wavelength using M=5 will be only 0.0000013%. A similar consideration shows that the truncation error of the resonant wavelength would be less than 0.000002% for the calculation with N>80. Therefore, in most of our calculations, we use M=5 and N=80 respectively.

Figures 4.2 and 4.3 also reveal some field characteristics related to the cavity's geometric structure. Firstly, to reach the same order of truncation error, we need to calculate many more modes in area A than in area B, i.e., N>>M. This is simply because the longitudinal length of area A is much longer than that of area B, since L>>d. Secondly, an odd mode, i.e., 1, 3, 5....contributes more to the wavelength calculation than an even mode, because, as shown in Figure 4.2, the slope of wavelength versus M for an odd mode is steeper than that of an even mode. This is attributed to the fact that the gap (Here, L_g=1 cm from the endplate) is off the cavity center, resulting in stronger odd mode fields.

4.2.3 Variations Of Field Distributions, Energy, Power Loss And Q Factor With The Gap Positions

With the calculated results from programs MMMC1-AG to MMMC4-AG, we can investigate the variations of the field distributions, the energy, the power loss and the Q factor as the gap moves along the center conductor.

As demonstrated in Figures 4.4 (a-e), when the gap moves towards the cavity center, the peak of Ez follows the gap until it gets close to the center. However, as shown in Fig.4.4(e), when the gap is moved right into the center, the E_r component reaches a peak, instead of E_z.

Gap location affects the resonant frequency, f, the Q factor, the energy stored in the cavity, E_c, the power loss in the cavity walls, P_w, and in the dielectric sample, P_s, as depicted in Figure 4.5. As the gap moves towards the center, f, Q and P_s vary little while E_c and P_w increase dramatically. To grasp the quantitative relations among these parameters, notice the large differences in the multiplying factors of these curves. For example, as the gap moves from L_g=5 to

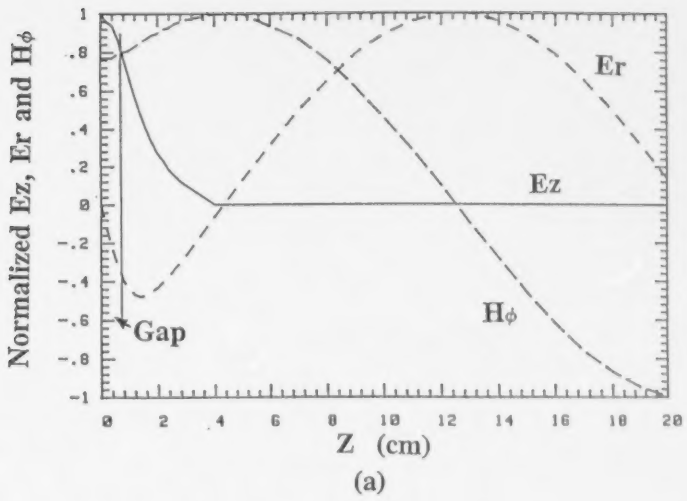

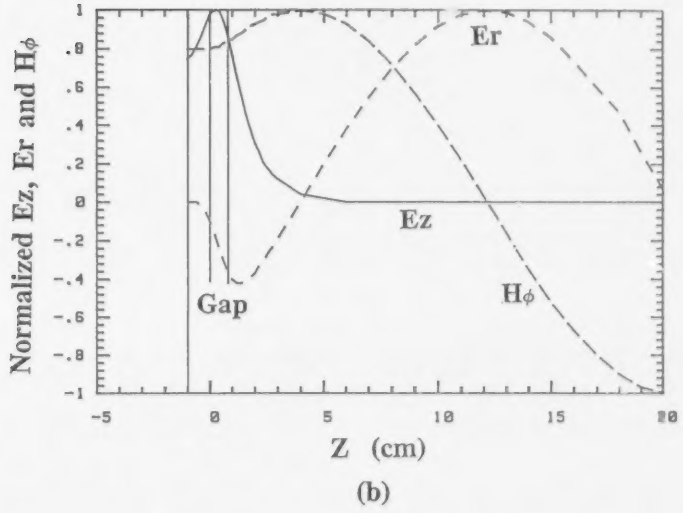

FIGURE 4.4 Normalized axial fields distributions at 915 MHz band for different gap positions. (a) L_g=0, (b) L_g=1, (c) L_g=2, (d) L_g=6, (e) L_g=8 cm. (d=0.3, r_o=0.35, r_1=1.27, r_2=4.51, L=20.0, L≅20.7, r=2.5, λ=32.787 cm, ε'=20)

L_g=7, E_c increases by about 10 times from 0.5 to 5 while P_s stays relatively the same in this region. (actually, P_s drops a little). But, when comparing the absolute increase in E_c to that in P_s, because of the difference of 1000 in their multiplying factors, we find that

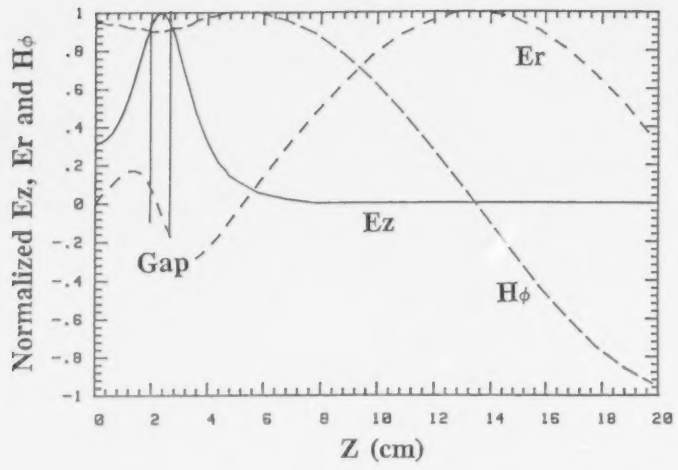

(c)

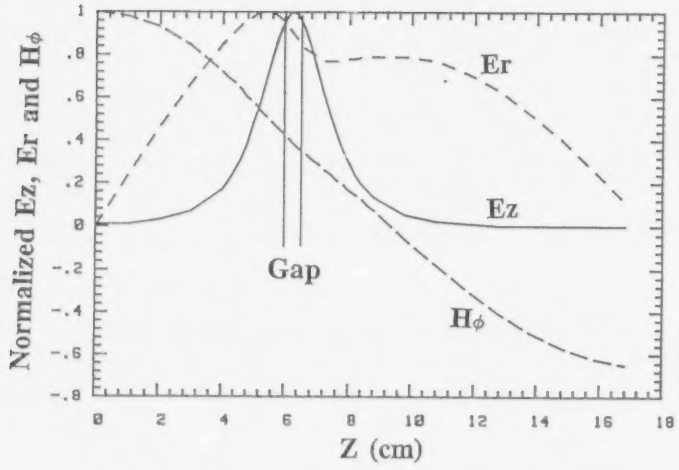

(d)

FIGURE 4.4 (Continues)

the increase of E_c is actually 10,000 times that of P_s. This implies that, for a given sample, the energy dissipated in the sample would be approximately 10,000 times less when the gap moves 2 cm from L_g=5 to L_g=7 towards the cavity center, resulting in a tremendous decrease in cavity loading.

The energy redistribution due to the gap location change has a

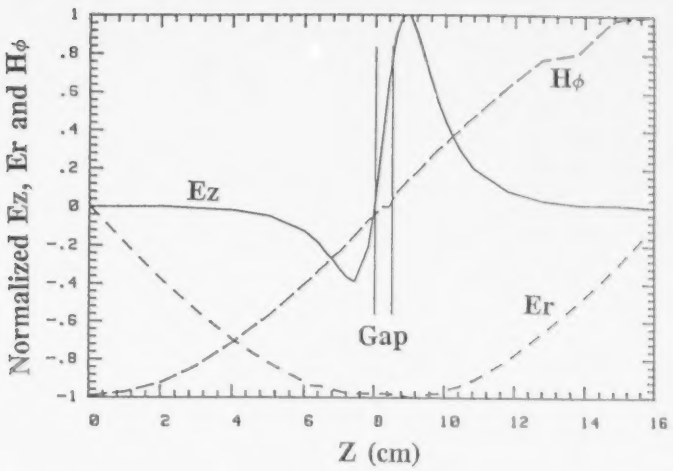

FIGURE 4.4 (continues)

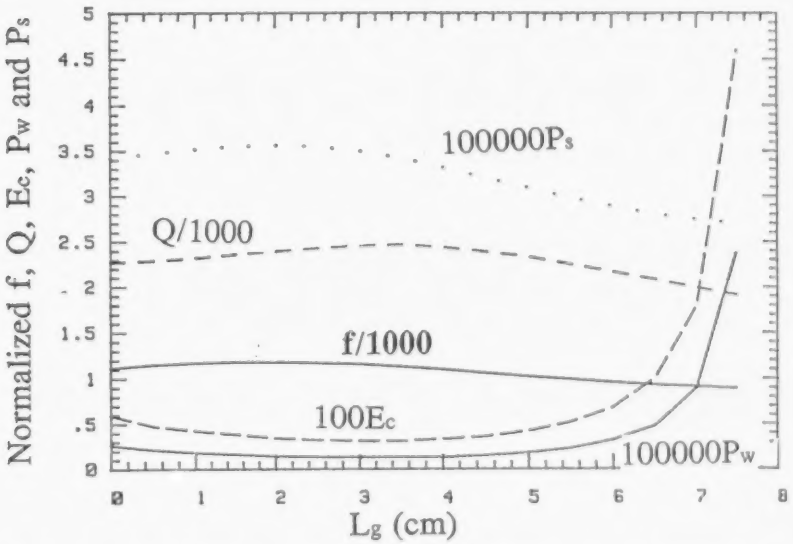

FIGURE 4.5 Variations of resonant frequency, f, Q factor, energy stored in the cavity, Ec, the power loss in the cavity wall, Pw, and the power loss in the sample, Ps, as function of the gap positions, Lg.

direct impact on the application of the movable gap structure. Firstly, since the matchable impedance range for a given cavity is always limited by its loading range, a mechanism able to adjust cavity loading to an extremely low level is the key to extending the cavity's matching range to allow the measurement of high loss dielectrics. In this sense, the controllable loading provided by the movable gap scheme is substantially advantageous over the fixed gap one. Secondly, the controllable energy distribution in the applicator leads to a controllable heating rate because the energy absorption competition between the sample and the rest of the cavity exists all the time in the applicator. Finally, the cavity with the gap close to its center can no longer be as sensitive to the sample as that with the gap close to the endplate. In summary, with the movable gap scheme, much more flexibility can be achieved in the cavity loading control, its matching adjustment and measurement sensitivity.

4.3 Equivalent Circuit Analysis

Even though a complete field solution of the movable gap structure can be obtained using the mode-matching method, it is complex both in formulation and programming. Moreover, the physical meanings of the formulas are not readily understood until a great number of calculations are done and unless the calculated data are correctly interpreted. In order to understand the cavity characteristics from a different perspective, and more importantly, in order to analyze its matching behavior, the equivalent circuit approach is employed here. Compared to the mode matching method, the equivalent circuit method is much simpler in formulation, more efficient in calculation and allows a clearer physical understanding of this cavity's behavior.

4.3.1 Artificial Electric Wall, Resonant And Matching Equations

There are no simple analytic formulas of lumped circuit parameters for a gap positioned arbitrarily in the center conductor. However, lumped capacitance formulas for a gap at the end of a coaxial cavity are available.[4.4] Interestingly, we found that once an artificial electric wall concept is established, these end-gap

formulas could be adapted to the case of a gap at an arbitrary position on the center conductor. Thus an equivalent circuit model can be developed based on this procedure. For convenience, instead of using L_g, we will use L_1 and L_2 to designate the gap position, where L_1 and L_2 are the lengths of the two posts respectively. (See Figure 4.1).

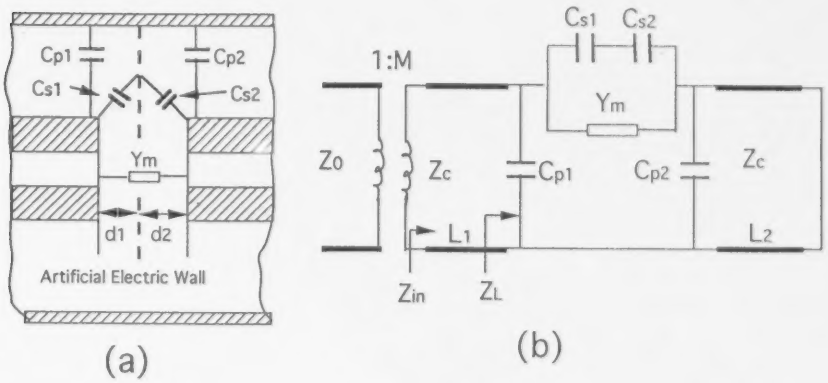

FIGURE 4.6 (a) Equivalent lumped elements and artificial electric wall in the gap, and (b) the equivalent circuit of a coaxial cavity with a gap in its center conductor.

As shown in Figure 4.6(a), the position of an imaginary electric wall in the gap, relative to the post, is designated by d_1 and d_2. To determine d_1 and d_2, two special cases can be considered. First, if $L_1=L-d$, that is, the gap is positioned at the end of the cavity (see Figure 4.1), the electric wall is simply the endplate itself, thus $d_2=0$ and $d_1=d$. Secondly, if $L_1=(L-d)/2$, i.e. the gap is located at the midplane of the cavity and the electric wall at the midplane of the gap, then $d_1=d_2=d/2$, due to the symmetry of even modes.[2] This fact suggests that an artificial electric wall may move from the gap's midplane to the gap end as the actual gap moves from the axial cavity

[2] Even for an odd mode, the gap hardly has any effect on the TEM mode when the gap approaches the axial cavity center. For this reason, we will not distinguish between an even and an odd mode any longer.

midplane to the cavity end. For simplicity, we assume d_1 and d_2 vary with L_1, approximately, in a linear fashion, that is

$$d_1=\frac{d}{L-d}L_1 \quad \text{and} \quad d_2=d-d_1 \tag{4.30}$$

Based on the imaginary electric wall, the gap discontinuity can be represented by the following lumped parameters as shown in Figure 4.6(b), two series capacitances, C_{s1} and C_{s2}, two shunt capacitances, C_{p1} and C_{p2}, and an admittance, Y_m, which accounts for the effects of the sample and the hole present in the gap. The series gap capacitances can be written as[4.4]

$$C_{s1}=4r_2\varepsilon_0\ln(\frac{r_3-r_2}{d_1})+\frac{\varepsilon_0\pi r_2^2}{d_1} \tag{4.31}$$

$$C_{s2}=4r_2\varepsilon_0\ln(\frac{r_3-r_2}{d_2})+\frac{\varepsilon_0\pi r_2^2}{d_2} \tag{4.32}$$

Shunt capacitances, C_{p1} and C_{p2}, are omitted here since they are 100 times less than C_{s1} and C_{s2} for a narrow gap.[4.5] Therefore, the only remaining unknown is $Y_m=G_m+B_m$, determined by the hole and the sample's electromagnetic properties.

Based on this equivalent circuit representation, the input impedance is given by

$$Z_{in}=Z_c\frac{Z_L+jZ_c\tan(\frac{2\pi}{\lambda}L_1)}{Z_c+jZ_L\tan(\frac{2\pi}{\lambda}L_1)} \tag{4.33}$$

where Z_L, a function of L_2, G_m and B_m, is readily obtained using the equivalent circuit in Figure 4.6(b).

Finally, resonance is established when the input reactance vanishes

$$Im(Z_{in})=0 \tag{4.34}$$

and a matching condition is obtained by requiring

$$M^2Re(Z_{in})=Z_0 \tag{4.35}$$

where M is the coupling loop's transformer ratio.

4.3.2 Equivalent Circuit Model Verification And Matching Behavior

In order to verify the above equivalent circuit model, we compare the calculated resonant and matching behavior to the measured behavior. Theoretical and experimental resonant frequency variations versus gap width for three different axial gap positions are depicted in Figure 4.7 which indicates agreement to better than 3.1% for a gap

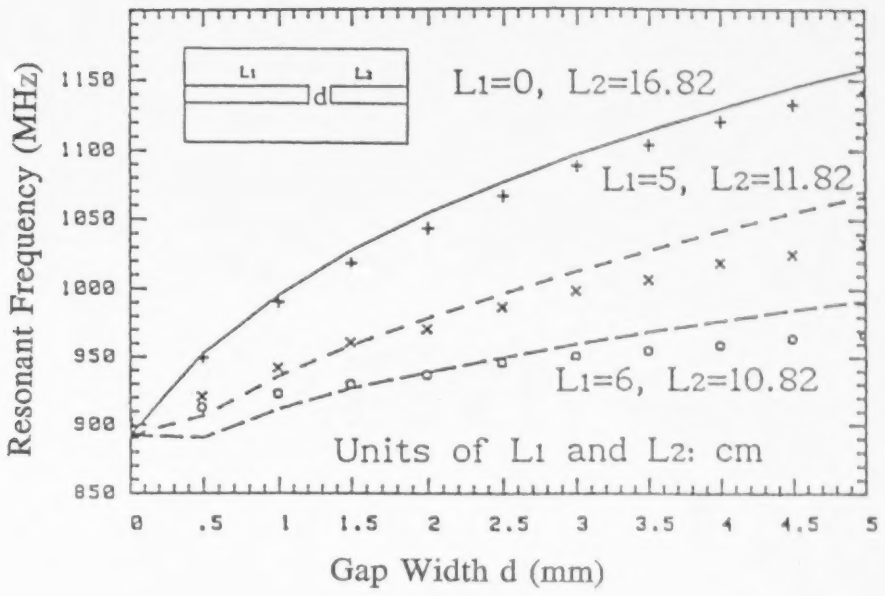

FIGURE 4.7 Resonant frequency vs. gap width, d, for different axial gap positions. Lines are calculated results using equivalent circuit model and symbols are experimental data.

width range of 0-5 mm. Figure 4.8 shows the resonant frequency versus axial gap position, L_1, for three commonly used gap widths of 1 mm, 2 mm and 3 mm, indicating a maximum discrepancy of 2.1%. By adjusting L_1 and L_2, we will be able to keep the cavity resonating at a fixed frequency. Figure 4.9 shows the calculated and the measured tuning curves at 915 MHz as a relationship between L_1 and L_2. The discrepancy between the calculated and the measured results is less than 3.5%. These three figures prove the validity of the equivalent circuit model based on the artificial electric wall concept.

It is desirable to maintain a matched input impedance to obtain a maximum power delivery and to fix the resonant frequency at a given source frequency regardless of the variation in the sample properties. With the fixed gap scheme, we can not achieve this because any variation in sample properties invariably alters the resonant frequency and the input impedance.

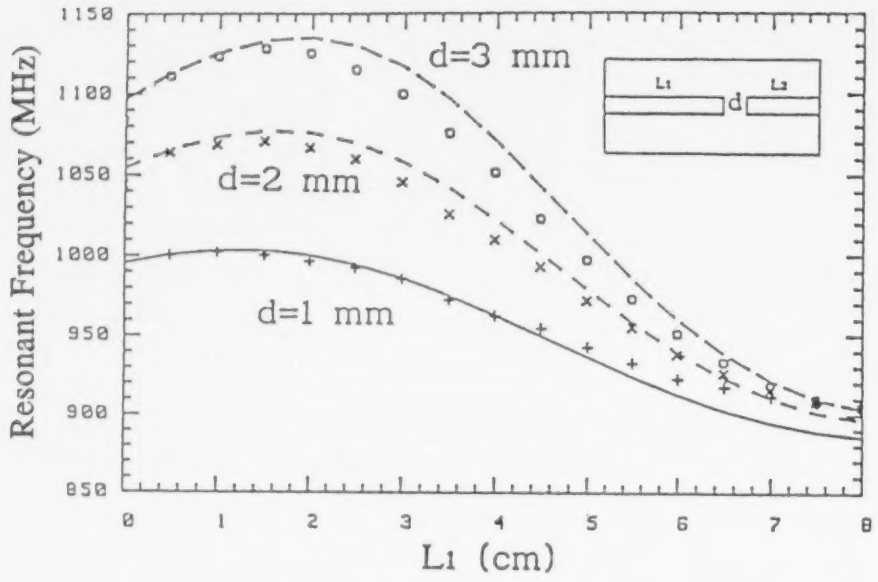

FIGURE 4.8 Resonant frequency vs. gap width, d, for different gap widths, d. Lines are calculated results using equivalent circuit model and symbols are experimental data.

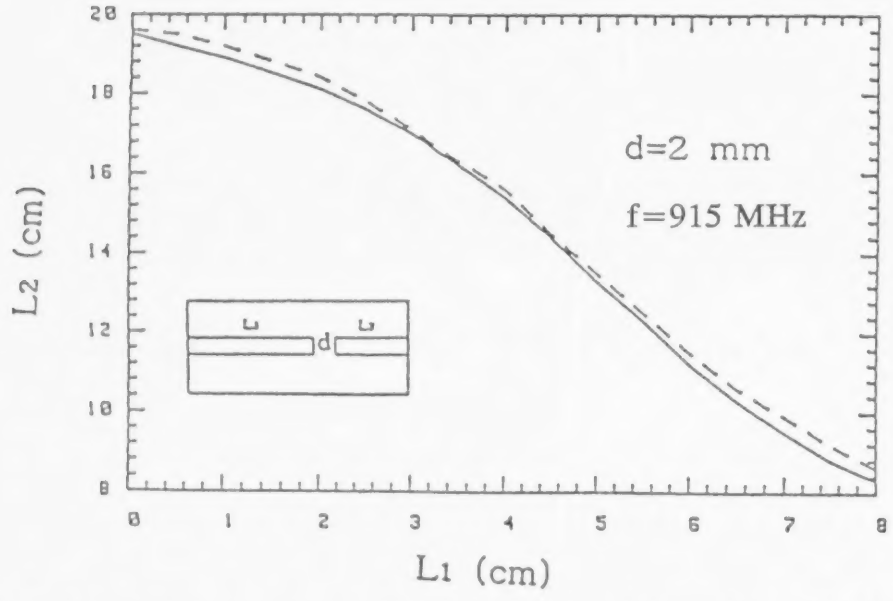

FIGURE 4.9 Tuning curve at 915MHz in terms of L_1 and L_2. Solid line is calculated result using equivalent circuit model and broken line is experimental data.

The movable gap scheme allows us to maintain a matched input impedance condition at a chosen resonant frequency regardless of the property variation of the sample. In other words, it allows us to satisfy both the resonant and the matching conditions, i.e., Eqs. (4.34) and (4.35), simultaneously regardless of the changes in G_m and B_m, where G_m represents the loss in the sample and B_m its dielectric constant. Mathematically, this requires two independent variables which are allowed to take on arbitrary values in the two equations. According to the cavity's structure, we can choose L_1 and L_2 as the two independent variables, i.e., choose to change the gap position. With this approach, a simultaneous solution of (4.34) and (4.35) will be guaranteed for any given frequency, sample loss and dielectric constant. The physical mechanism allowing this matching approach is that the sample, along with the gap, may be moved from a maximum field region to a nearly zero field region, as explained previously.

Our calculated data shown in Figures 4.10 and 4.11 exhibit the

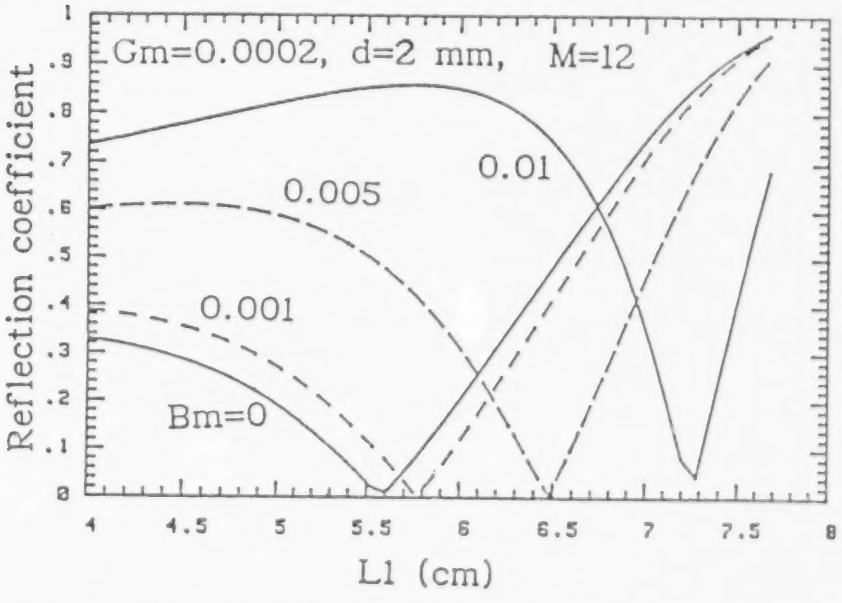

FIGURE 4.10 Reflection coefficient vs. gap position, L_1, with gap load susceptance, B_m, as a parameter and a fixed load fixed load conductance.

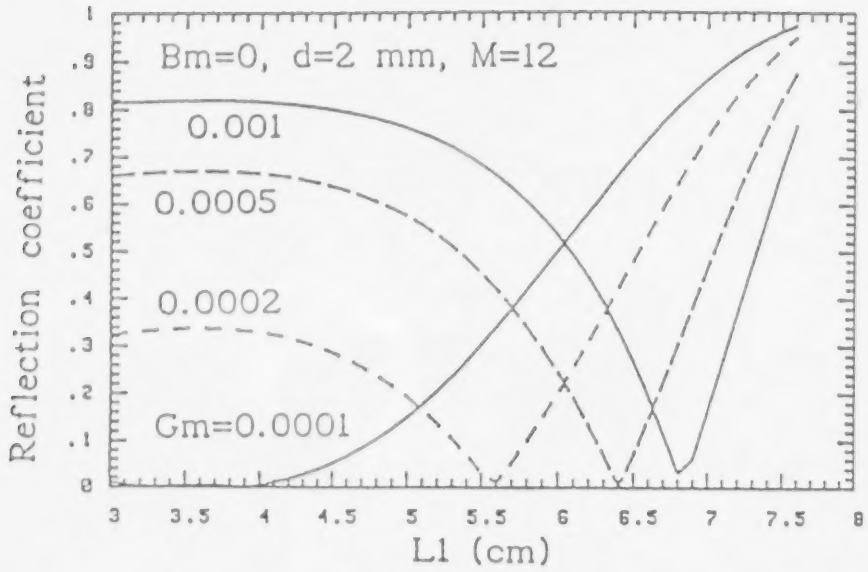

FIGURE 4.11 Reflection coefficient vs. gap position, L_1, with gap load conductance, C_m, as a parameter and a fixed load fixed load susceptance.

cavity's matching characteristics at 915 MHz for different gap susceptance, B_m, and conductance, G_m. For each curve, the bottom of the valley is the match point where the reflection $|\Gamma|=0$. In these figures, an increase in L_1 means that the gap moves towards the cavity center. It is clear that, as the susceptance or conductance is increased, matching can always be obtained by moving the gap closer to the cavity center.

4.4 Conclusion

In this chapter, we have analyzed the coaxial re-entrant cavity with an arbitrarily positioned gap using the mode matching and the equivalent circuit methods respectively. The mode matching analysis characterizes the field distributions, the resonant frequency, the Q factor and the energy density while the equivalent circuit analysis mainly characterizes the matching behavior. These two analyses complement each other, presenting a comprehensive understanding of the

structure. As we will show, such a structure is eminently suitable as part of a self-heating dielectrometer.

References

[4.1] W. Xi, "Theoretical Analysis of Re-entrant Coaxial Cavity by the Mode Matching Method", internal report, Microwave Power Lab. Dept. of Electrical Engineering. Univ. of Alberta, 1990

[4.2] W. Xi, "Mode-Matching Analysis of Re-entrant Cavity, Report One", internal report, Microwave Power Lab. Dept. of Electrical Engineering.

[4.3] W.Xi, "High Temperature Microwave Dielectrometer Using A Re-Entrant Cavity", Ph.D thesis, Dept. of Electrical Engineering, University of Alberta, Edmonton, Canada, Fall 1992.

[4.4] N. Marcuvitz, Waveguide Handbook, McGRAW-HILL, New York, 1951, p 178.

[4.5] Susanta Sen and P. K.Saka, "Equivalent Circuit of a Gap In the Center Conductor of a Coaxial Line", IEEE Tran. Microwave Theory and Tech. MTT-30, pp 2026-2029, 1982.

Chapter 5

THEORETICAL ANALYSIS OF A COUPLING LOOP IN A COAXIAL RE-ENTRANT CAVITY

5.1 Introduction

To determine dielectric loss using a resonator requires a Q measurement of the dielectrically loaded resonator. In chapter 2, we proved that this Q is simply related to a cavity's resonant input resistance. That resistance, in turn, is determined by the mechanism used to couple energy to the resonator. Therefore, this chapter is devoted to the theoretical analysis of a coupling loop on the endplate of a coaxial re-entrant cavity. From this analysis, a relationship between the coupling loop's geometrical dimensions and the input resistance of the cavity can be established.

To use the single frequency Q measurement method, one must allow the input impedance to vary with the variation of the loss factor of the dielectric. On the other hand, to get maximum power delivery to the cavity requires that we maintain the input impedance at a matched condition regardless of the variation in the loss factor. For example, in the applicator we used, where a radially adjustable coupling loop is employed, as shown in Figure 5.1, this matching condition is realized by constantly varying the location of the coupling loop as the loss factor of the sample varies. Unfortunately, as expected, once the input impedance is fixed by this procedure, the information for the loss factor determination from the reflection coefficient is lost.

Our solution to this dilemma is explained as follows. To maintain a fixed input resistance, we must adjust the coupling loop location. If we can find the relationship between this loop location and the cavity's input resonant resistance, we can then obtain the equivalent variation in the input resistance from the adjusted loop location, and hence the Q and the loss factor, while maintaining a fixed matching condition. Obviously, to find that relationship requires a theoretical analysis of the coupling loop.

Generally, the method of the Green's function can be used to

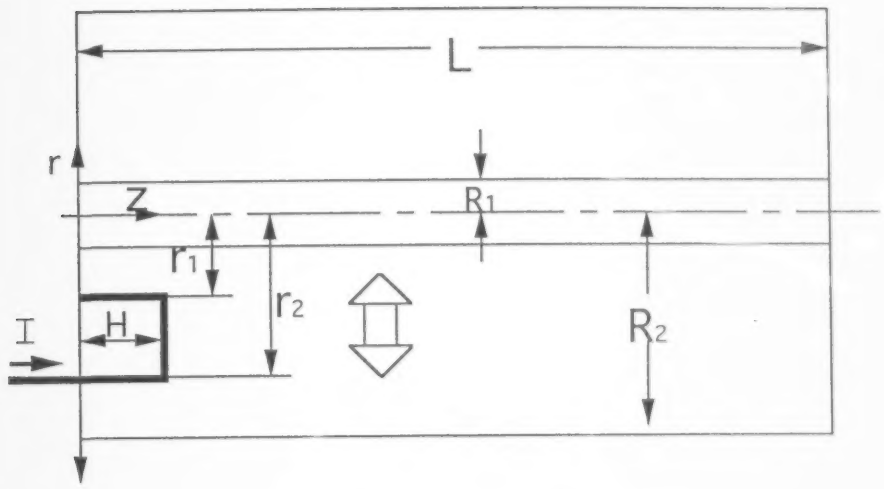

FIGURE 5.1 An adjustable coupling loop on the endplate of a coaxial cavity.

calculate the input impedance of a cavity. Unfortunately, except for some simple structures, the implementation of this method can be extremely difficult. An alternative is the mode expansion method, which can be much easier provided the mathematical expressions of the basic modes are obtainable. For a coaxial cavity, these expressions can be readily obtained. For this reason, the mode expansion method is employed in this coupling loop analysis.

As a general approach for determination of the impedances for the principal and the higher order modes, the mode expansion method was proposed in 1941,[5.1] in which, however, only the impedance related to the principal mode was derived. Ten years later, this approach was further developed and the input impedance as a sum of the mode impedances of all modes was reported.[5.2] To date, the most complete and explicit description of this method has been given by R.F.Harrington,[5.3] whose methodology we will follow.

5.2 Mode Expansion Method formulation

It is well known that the electric field vector, E, excited by a current source, J, as shown in Figure 5.2, is governed by the

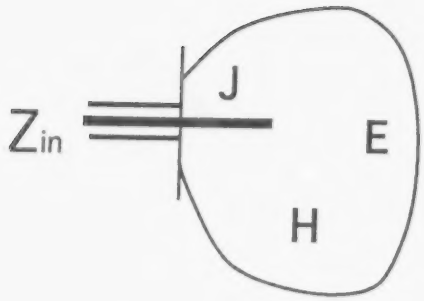

FIGURE 5.2 Schematic representation of the electromagnetic fields excited by a current density, J, in a cavity.

Helmholtz equation

$$\nabla\times(\mu^{-1}\nabla\times E)-\omega^2\varepsilon E=-j\omega J \tag{5.1}$$

Suppose that the E_i's are the basic elements of the electric field vector in the same cavity but without the current source, J. Then, E_i should satisfy

$$\nabla\times(\mu^{-1}\nabla\times E_i)-\omega_i^2 E_i=0 \tag{5.2}$$

and the orthogonality and normalization condition

$$\iiint_v \varepsilon E_i\cdot E_j^* dv=\begin{cases}0 & i\neq j\\ 1 & i=j\end{cases} \tag{5.3}$$

where ω_i are the eigen frequencies, dv is the volume element and v is the internal cavity volume.

Since these E_i's constitute a complete function set, an arbitrary field vector, E, can always be expressed in terms of them as an infinite series

$$E=\sum_{i=0}^{\infty} A_i E_i \tag{5.4}$$

where A_i are the coefficients of the series.

Substituting this into (5.1), we obtain[5.3]

$$\sum^{\infty} A_i[\nabla\times(\mu^{-1}\nabla\times E_i)-\omega^2\varepsilon E_i]=-j\omega J \tag{5.5}$$

$i=0$

which, by Eq. (5.2), can be written as

$$\sum_{i=0}^{\infty} A_i(\omega_i^2-\omega^2)\varepsilon E_i=-j\omega J \tag{5.6}$$

If each side is now multiplied scalarly by E_j^* and integrated over the cavity volume, all terms except i=j vanish because of orthogonality, and we have

$$(\omega_i^2-\omega^2)A_i= -j\omega\iiint J\cdot E_i^* d\tau \tag{5.7}$$

which determines the coefficients, A_i. Hence Eq. (5.4) becomes

$$E=\sum_{i=0}^{\infty} \frac{j\omega E_i}{\omega^2-\omega_i^2}\iiint J\cdot E_i^* d\tau \tag{5.8}$$

On the other hand, the complex power generated by the current, J, is given by

$$P=-\iiint(E\cdot J^*)\cdot d\tau \tag{5.9}$$

The input impedance can be written as

$$Z_{in}=\frac{P}{I^2}=-\frac{1}{I^2}\iiint(E\cdot J^*)\cdot d\tau \tag{5.10}$$

Substituting **E** from Eq. (5.8) into (5.10), we get

$$Z_{in}=-\frac{1}{I^2}\sum_{i=0}^{\infty}\frac{j\omega}{\omega^2-\omega_i^2}b_i^2 \tag{5.11}$$

where $b_i=\left|\iiint E_i\cdot J^*\cdot d\tau\right|$ (5.12)

and ω is the complex angular resonant frequency.

For a high Q cavity operating in the vicinity of a given frequency, say ω_o, its complex resonant frequency, ω', can be expressed as[5.3]

$$\omega'^2=\omega_o^2(1+\frac{j}{Q}) \tag{5.13}$$

This equation implies that the loss is caused only by the resonant mode of interest. This assumption is close to the actual situation in a real cavity.

Substituting ω_1 in (5.11) by ω' and separating (5.11) into its real and imaginary parts results in

$$R=\frac{\omega\omega_o^2(\frac{b_o}{I})^2 Q}{Q^2(\omega^2-\omega_o^2)+\omega_o^4} \tag{5.14}$$

$$X_o=-\frac{\omega(\omega^2-\omega_o^2)Q^2(\frac{b_o}{I})^2}{Q^2(\omega^2-\omega_o^2)+\omega_o^4} \tag{5.15}$$

$$X=-\frac{\omega}{I^2}\sum_{i\neq o}\frac{b_i^2}{\omega^2-\omega_i^2} \tag{5.16}$$

so that $Z_{in}=R+j(X_o+X)$ (5.17)

where the quantities with subscript 0 are for the mode of interest.

5.3 Input Resistance Derivation

The formulas above suggest a simple way to find the relation between the resonant input resistance and the Q-factor. Firstly, Eq. (5.14) shows that R is independent of the higher order modes. Secondly, the higher order mode reactances are not related to Q, as shown by Eq. (5.16). Finally, X_o actually vanishes when resonance occurs at $\omega=\omega_o$. As a result, the relation between R and Q can be determined without dealing with the higher order modes.

To find the bo/I used in Eqs (5.14) and (5.15), we assume that the coaxial cavity resonates in the mth TEM mode. Then, the normalized principal mode can be expressed as

$$E_r=\frac{A}{r}\sin(\frac{m\pi}{L}z) \tag{5.18}$$

where r is the radius at which the field is desired. Then

$$\iiint \varepsilon E_r^2 dv = \varepsilon A^2 \int_0^{2\pi} \int_{R1}^{R2} \int_0^L r \left[\frac{1}{r}\sin\left(\frac{m\pi}{L}\right)\right]^2 dz dr d\theta \tag{5.19}$$

$$= A^2 \varepsilon \pi L \ln\frac{R2}{R1} \tag{5.20}$$

where we assume ε to be independent of r, z and θ, and R_1 and R_2 are defined in Figure 5.1.

According to Eq. (5.3), the above equation equals unity, so that

$$A = \frac{1}{\sqrt{\varepsilon \pi L \ln\frac{R2}{R1}}} \tag{5.21}$$

For a loop with a filamentary current, I, as shown in Figure 5.1, and noting that $I = \iint_s J^* ds$, where s is the cross section of the loop, we can derive from (5.12)

$$b_o = I \int_{r1}^{r2} \frac{A}{r} \sin\left(\frac{m\pi}{L}H\right) dr \tag{5.22}$$

i.e.,
$$\frac{b_o}{I} = \frac{\sin\left(\frac{m\pi}{L}H\right) \ln\frac{r2}{r1}}{\sqrt{\pi \varepsilon_o L \ln\frac{R2}{R1}}} \tag{5.23}$$

Substituting $\frac{b_o}{I}$ into (5.14), we find the input resistance related to the cavity parameters by

$$R = \frac{Q \sin^2\left(\frac{m\pi}{L}H\right) \ln^2\frac{r2}{r1}}{\left\{Q^2\left[\left(\frac{\omega}{\omega_o}\right)^2 - 1\right] + 1\right\} \pi \varepsilon_o L \ln\frac{R2}{R1}} \cdot \frac{\omega}{\omega_o^2} \tag{5.24}$$

At resonance, $(\omega/\omega_o)=1$, and we have

$$R = R(\omega_o) = \frac{Q \sin^2\left(\frac{m\pi}{L}H\right) \ln^2\frac{r2}{r1}}{\pi \varepsilon_o L \ln\frac{R2}{R1}} \tag{5.25}$$

For the purpose of our particular application, the parameters of

interest are R, Q and r_2/r_1. All the rest are fixed values. To emphasize the relations between R and Q and between r_2/r_1 and Q, we write (5.25) in the following two different simple forms as

$$Q=\frac{R}{C_r} \tag{5.26}$$

and

$$Q=\frac{C_R}{\mathrm{Ln}^2\frac{r_2}{r_1}} \tag{5.27}$$

where

$$C_r=\frac{\sin^2(\frac{m\pi}{L}H)\ \mathrm{Ln}^2\frac{r_2}{r_1}}{\pi\varepsilon_0 L\ \mathrm{Ln}\frac{R_2}{R_1}} \tag{5.28}$$

and

$$C_R=\frac{R\ \pi\varepsilon_0 L\ \mathrm{Ln}\frac{R_2}{R_1}}{\sin^2(\frac{m\pi}{L}H)} \tag{5.29}$$

As we can see, the parameter, C_r, is a constant when the geometrical dimensions and the location of the coupling loop are fixed. This means that Q is proportional to the input resistance at resonance for a given coupling loop. This is the same conclusion as drawn in chapter 2, where the analysis was based on the perturbation method. It is interesting and important to note, eventhough the two approaches in deriving Eq. (2.15) and Eq. (5.26) are totally different, these two equations take exactly the same form. Of course, in chapter 2, the equations derived based on the perturbation theory are more general, while in this chapter, this relation is derived based on the mode expansion theory for a specific structure.

For a given coupling loop, the second parameter, C_R, defined by (5.29) becomes a constant when the input resistance, R, and the loop length is fixed. As a result, the Q is simply related to the loop's radial position. Therefore, we can obtain the Q factor for a given input resistance, from (5.27) by measuring the loop's radial position.

In summary, according to Eqs. (5.26) and (5.27), we now have two means to determine the Q variation. One is to fix the coupling loop and measure the resulting variation in the input resonant resistance.

The other is to fix the input resistance, possibly at the matched value, and measure the required variation in the location of the coupling loop . While the former is easier and mechanically more stable, the latter provides a better matched condition. The implementation of these measurements will be discussed in the next chapter.

References

[5.1] E.V.Condon, "Forced Oscillations In Cavity Resonators", J. of Applied Physics, Vol.12, Feb. 1941, p129-132.

[5.2] T.Teichmann, "Completeness Relations for Loss Free Microwave Junctions", J. of Applied Physics. Vol.23, no.7, 1952,p701-710.

[5.3] R.F.Harrington, "Time-Harmonic Electromagnetic Fields", McGraw-Hill Book Company, Ch. 8, 1961.

Chapter 6

PASSIVE SINGLE FREQUENCY DIELECTROMETER[1]

6.1 Introduction

In the previous chapters, we focused on the different aspects of techniques that are essential for developing the single frequency high temperature dielectrometer, including the single frequency Q measurement method in chapter 2, the self-heating dielectrometer applicator in chapter 3 and chapter 4 and the coupling loop analysis in chapter 5. In this chapter, we will use these results to build an experimental dielectrometer to test the feasibility of our proposed single frequency high temperature dielectrometer. We first derive the formulas for the dielectric determination, and then construct an experimental dielectrometer which can perform a dielectric measurement at room temperature using a standard swept frequency or single frequency method, so that we can compare their results. After the room temperature verification of the measurement method, a single frequency self-heating high temperature dielectrometer is built to demonstrate the high temperature capability of the single frequency method. In order to distinguish it from the active dielectrometer, which will be studied in the next chapter, the dielectrometer designed in this chapter is called a passive single frequency dielectrometer.

6.2 Dielectric Determination

Once a sample is introduced into the cavity shown in Figure 3.1, the cavity's resonant frequency will shift. By adjusting the cavity length with the short circuit plunger, we can offset the resulting resonant frequency shift to return the cavity to its original resonant frequency after the introduction of the sample. Naturally, the cavity length variation required to offset the resonant frequency variation, ΔL, is related to the dielectric constant of the sample, ε'. Once this relationship is found, the dielectric constant is determined. In

1 A version of this chapter has been published. Mat. Res. Soc. Symp. proc., vol. 269, pp 83-89. 1992

this process, tuning the cavity to a single frequency and determining the sample's dielectric constant are accomplished simultaneously.

Running MMMC4-AG, the previously developed mode matching program, we can produce the numerical data relating ε' and ΔL at any given resonant frequency. A calibration curve obtained by a least square fit of the numerical data can be expressed as

$$\varepsilon' = 1.0 + 4.09245\Delta L + 0.46555\Delta L^2 + 0.05964\Delta L^3. \tag{6.1}$$

This equation corresponds to the cavity dimensions shown in Figure 3.1 and to the resonant frequency of 915MHz, at which all our measurement and heating experiments were conducted.

It is common practice to determine the loss factor from the Q factor drop of the cavity, caused by the loss of the inserted sample[6.1] and given by

$$\varepsilon'' = \frac{\varepsilon'}{F}\left(\frac{1}{Q} - \frac{1}{Q_o}\right) \tag{6.2}$$

where Q_o and Q are the cavity Q before and after the sample is loaded respectively. F is the filling factor, which can be calculated also by MMMC4-AG, and can be expressed in a polynomial form as

$$\frac{\varepsilon'}{F} * 10^{-3} = 0.4873 + 0.026666\varepsilon' - 0.73027 * 10^{-4}\varepsilon' \tag{6.3}$$

It is obvious that once ε' is known and the Q_o and the Q are measured, ε'' will be determined. As shown in Eqs.(5.26) and (5.27), there are two ways to measure Q, resulting in the following two cases for determining ε''.

Case A Determine ε'' by Reflection (Reflection Method)

In this case, ε'' is determined by a reflection coefficient measurement for a given coupling loop location.

Substituting the Q from Eq.(5.26) for the Q in Eq.(6.2), we obtain

$$\varepsilon'' = C_r \frac{\varepsilon'}{F}\left(\frac{1}{R} - \frac{1}{R_o}\right) \tag{6.4}$$

or

$$\varepsilon'' = C_r \frac{\varepsilon'}{F}\left(\frac{1 \mp |\Gamma|}{1 \pm |\Gamma|} - \frac{1 \mp |\Gamma_o|}{1 \pm |\Gamma_o|}\right) \tag{6.5}$$

since

$$R=\frac{1\mp|\Gamma|}{1\pm|\Gamma|} \text{ and } R_o=\frac{1\mp|\Gamma_o|}{1\pm|\Gamma_o|} \tag{6.6}$$

where Γ_o and Γ are the reflection coefficients at the resonant frequency before and after the sample is loaded. Depending on whether the cavity is over or under coupled, the - or + sign, respectively, is used.

It is noted that, in this case, the coupling loop is required to be fixed. Therefore, C_r will be a constant, which can be determined using the known Q value of the empty cavity. Then ε'' can be determined according to the measured reflection coefficients, $|\Gamma|$ and $|\Gamma_o|$ by (6.5). Since the coupling loop is fixed and a reflection measurement is easy, the Reflection Method for ε'' determination is convenient. However, in this case, it is inherently impossible to provide the maximum power delivery because the reflection of the cavity varies as the variation in sample loss factor. In this sense, the requirements for heating and measuring are in conflict. Therefore, the Reflection Method is not suitable for the self-heating dielectrometer, where an effective power delivery to the cavity is critical for sample heating.

Case B Determine ε'' From Loop Location (Loop Location Method)

Upon the introduction of a sample, the reflection of the cavity will be altered. Adjusting the location of the coupling loop radially, as proved in the previous chapter, can offset the reflection alteration, thereby fixing the reflection coefficient at its original reflection level. If the original reflection is initially adjusted to zero, a matched input impedance is realized. The amount of the radial displacement required to offset the reflection alteration is decided by the sample's loss factor. The relation between ε'' and the radial loop location, defined by r_2/r_1, can be obtained by substituting the Q factor from Eq. (5.27) for the Q in Eq. (6.2), resulting in

$$\varepsilon''=\frac{\varepsilon'}{C_R F}\left(\mathrm{Ln}^2\frac{r_2}{r_1}-\mathrm{Ln}^2\frac{r_{20}}{r_{10}}\right) \tag{6.7}$$

where r_{20}/r_{10} defines the radial location of the coupling loop before the sample is inserted. After the sample is inserted, the location is adjusted to offset the reflection variation where r_2/r_1 defines the

new radial location.

In this case, since a constant reflection coefficient is maintained, C_R will be a constant (see Eq. (5.29)). Therefore, it can be determined, again, from the empty cavity Q. Now ε'' is determined according to the loop locations, r_2/r_1 and r_{20}/r_{10}. Because the input impedance of the cavity can be maintained at a matched condition, the Loop Location method will be most suitable for the self-heating dielectrometer. Unlike the Reflection method, the Loop Location method harmonizes the requirements for heating and measuring.

6.3 Experimental Verification

In order to verify the above dielectric determination formulas, we will compare the dielectric constants and loss factors determined using the above formulas and the standard swept frequency method. To carry out this verification, we need three sets of data. The first set is for the swept method, which includes the resonant frequency shift, Δf, caused by the introduction of the sample, and the 3dB bandwidth, Δf_{3db}. Using these data we can obtain the dielectric constant, the Q factor and therefore the loss factor.[6.1] The second set is for the Reflection Method, which includes the cavity length shift, ΔL, and the reflection coefficients, $|\Gamma_o|$ and $|\Gamma|$, for the empty and the loaded cavity. Substituting these data in Eqs. (6.1) and (6.4-6.6), we can obtain the dielectric constant and the loss factor. The third set is for the Loop Location Method, which includes, again, the ΔL and the locations of the coupling loop, r_{20}/r_{10} and r_2/r_1. Employing Eqs. (6.1) and (6.7), we can again obtain the dielectric constant and the loss factor.

Figure 6.1 shows the block diagram of the experimental system for the dielectric measurement using the standard swept frequency method. Again, the cavity used is the one discussed in chapter 3. A scalar network analyzer (SNA) (HP8756A), a swept source (HP8350B) and a dual directional coupler (HP775D) constitute a standard swept frequency reflectometer. Both the resonant frequency shift, Δf_0, and the 3dB bandwidth, Δf_{3dB}, can be read from the SNA display, as shown in Figure 6.2. From these data, the dielectric constant and the loss factor of

the sample can be readily obtained.

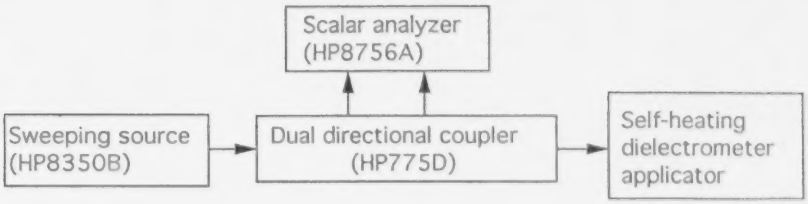

FIGURE 6.1 Experimental system for collecting the single frequency measurement data and the swept frequency measurement data.

It is noted that the reflection, $|\Gamma|$, needed for both the Reflection Method and the Location Method, can also be obtained from the SNA display, because, as can be seen in Figure 6.2, the data includes not only f_0 and Δf_{3dB} but also $|\Gamma|^2$. Therefore, we can use the same measurement setup to obtain the data needed for both the swept and the single frequency methods. This not only avoids building one more setup but, more importantly, makes the method verification more reliable. Data needed for the two methods would be taken at one time using exactly the same sample, sample holder and the same measurement hardware. Mechanical displacements such as ΔL, r_{20}/r_{10} and r_2/r_1 are all measured with the micrometers mounted on the movable short circuit plunger and the movable coupling loop respectively.

Experimental results for five different samples, with a dielectric constant range of 5-80 and loss factor range of 0.30-4.2, are presented in Table 6.1. The results for the single frequency method show a maximum difference of 9% from those for the swept frequency method. One source of that difference can be the deviation of the actual dimensions of the cavity from the ideal dimensions by which the calibration curves were calculated. As can be seen from Figure 3.1, the short circuit bucket section is obviously smaller in diameter than the rest of the cavity. The frequency drift of the source may also contribute some errors. The resolution of ε' in the 915MHz band is limited to about 0.05 by the resolution of the cavity length variation measurement. The differences in ε'' are mostly due to

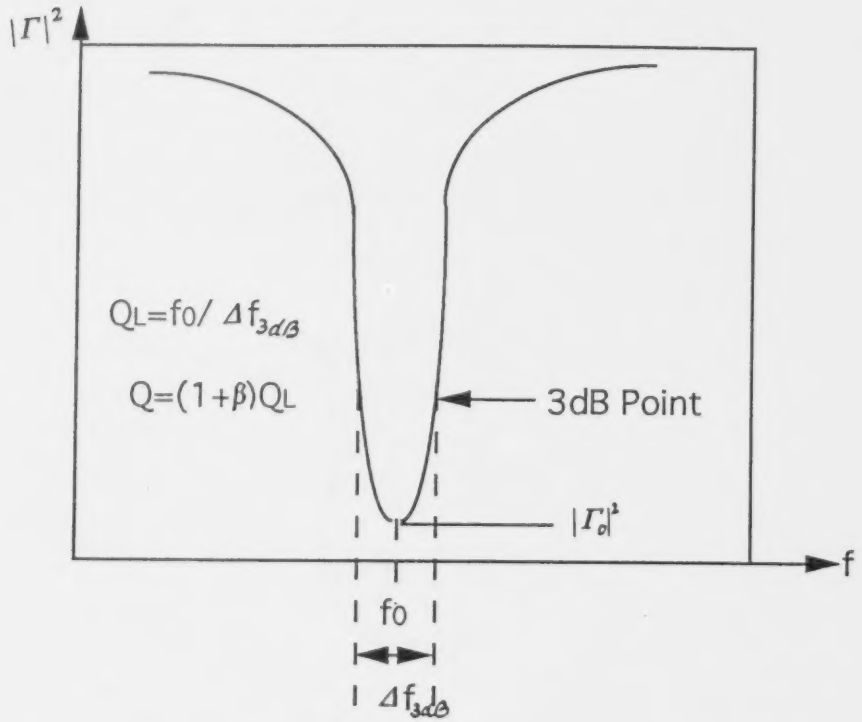

FIGURE 6.2 Typical reflection curve on the reflectometer's CRT display. This curve includes the quantities needed for both the swept method and the single frequency method such as f_0, Δf_{3dB} and $|\Gamma|$.

Table 6.1 Result comparison between the single frequency, manual tuning method and swept frequency method.

Sample No.	$\varepsilon'-j\varepsilon''$			Difference(%)			
	Present method		Swept Freq. Method	Reflection method		Loop location Method	
	Relection method	Loop location method		ε'	ε''	ε'	ε''
1	5.3-j0.34	5.3-j0.31	4.9-j0.33	8.2	3.0	8.2	-6.1
2	8.1-j1.33	8.1-j1.29	7.5-j1.19	7.9	12.0	7.9	8.4
3	12.5-j1.58	12.5-j1.58	11.7-j1.42	7.0	11.0	7.0	8.5
4	19.8-j0.51	19.8-j0.49	20.0-j0.43	1.2	19.0	1.2	14.0
5	81.4-j4.2	81.4-j4.47	78.6-j5.3	3.5	26.0	3.5	15.7

the differences in Q values obtained by the two different Q measurement methods. Reflectometer directivity errors may be as large as ± 10% for either method.[6.1] Considering that ε'/F is the same for both the swept frequency and the single frequency methods, we can estimate that the reflection coefficient errors are of the same order for both methods.

6.4 High Temperature Dielectrometer

Having been verified at room temperature, the single frequency method was applied to a high temperature dielectric measurement in conjunction with simultaneous microwave heating. Our experimental system, as shown in Figure 6.3, consists of the self-heating dielectrometer applicator serving both as the measurement chamber and the sample heater, a 915 MHz 100 W power source with a reflected power indicator and an optical thermometer for temperature measurement.

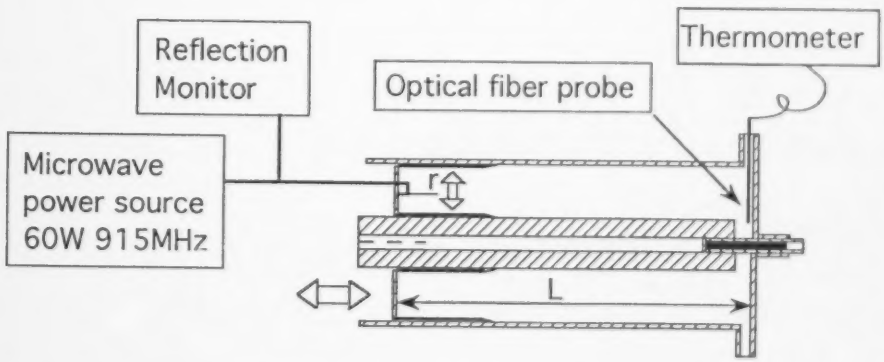

FIGURE 6.3 Passive single frequency high temperature dielectrometer system with manual tuning and matching.

This system is significantly different from the one shown in Figure 6.1. Firstly, this system operates under a pure single frequency condition, i.e., it has no swept signal source nor does it require an expensive sweeping network analyzer. Secondly, the source we used is a solid state fixed frequency high power source, used as both a measurement signal source and sample heating source. The

output power is controllable from 0 to 100W. Because of this high power source, a high sample temperature can therefore be readily established in a lossy sample. Finally, because of the high power involved, a high reflection from the cavity could cause overheating of the feed cable. Therefore the Loop Location Method is the only practical approach for this situation, for it can maintain a matched cavity during the whole measurement and heating cycle.

Upon starting the high temperature dielectric measurement, by observing the reflected power, we manually adjust the short circuit and the coupling loop to tune and to match the cavity. Their displacements, i.e., ΔL, r_{20}/r_{10} and r_2/r_1, are recorded for later determinations of the dielectric constant and the loss factor. In addition, an optical temperature sensor, aimed at the sample through the hole, and a thermometer are installed for the measurement of the sample temperature.

To demonstrate the high temperature capability of the system, the measured high temperature dielectric constant results for two samples are presented in Figures 6.4 and 6.5. One is the dielectric constant and loss factor of zeolite versus its temperature while the other shows similar data for mullite. Both the zeolite and the mullite data were taken under a matched input impedance condition.

Despite the advantages of this system in maintaining a matching condition, the required manual control over the tuning and matching makes data taking very difficult. In the case of high loss samples, heating is very rapid and the manual adjustment of the loop and the short circuit plunger positions cannot keep up with the changes in the resonant frequency and the reflection as sample temperature increases. In the case of low loss samples, on the other hand, sample heating is very slow, requiring high initial power to be applied, which must be reduced once the sample starts to heat effectively. Otherwise, thermal runaway will occur. This usually happens in a time span of a few seconds. As a result, the manual control is not satisfactory. In fact, the zeolite and the mullite samples are the only ones for which we could manage to take useful data manually.

One solution to this problem is the automation of the loop and

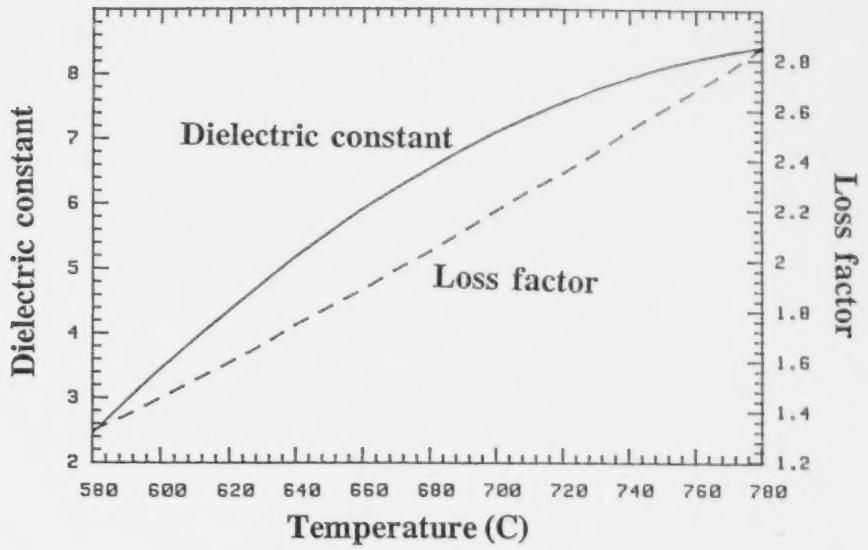

FIGURE 6.4 Dielectric constant and loss factor vs. temperature for Zeolite (13x, pellet) measured with the passive single frequency dielectrometer.

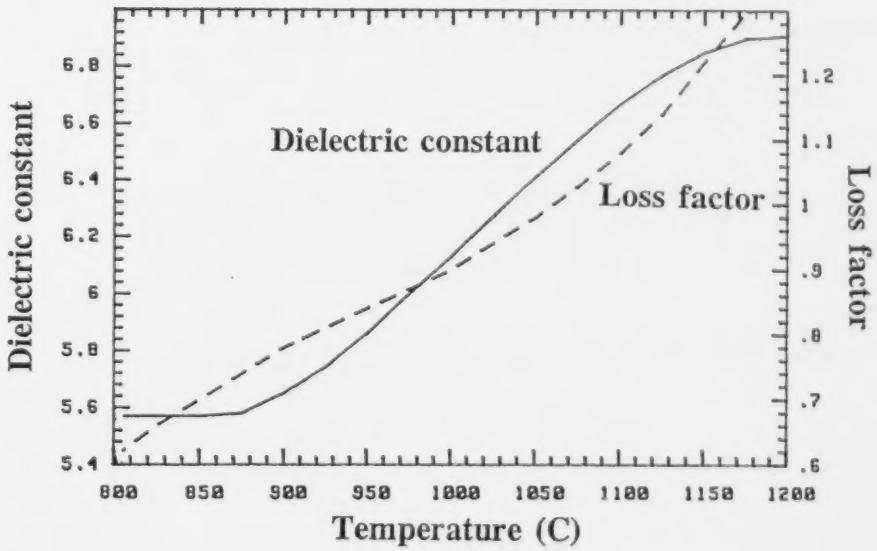

FIGURE 6.5 Dielectric constant and loss factor vs. temperature for Mullite (MV20) measured with the passive single frequency dielectrometer.

the length adjustment system. This includes two aspects. The first is an automatic temperature and power control. The speed of the temperature increase and decrease can be controlled by an electronic power level control. Secondly, automatic adjustment and measurement of the ΔL and r_2/r_1 can be accomplished using motors and displacement sensors. With the implementation of such automation, the single frequency self-heating dielectrometer is able to satisfactorily perform the high temperature dielectric measurement for a larger range of samples.

6.5 Conclusion

This chapter has focused on the realization of the single frequency high temperature dielectric measurement. We first derived the formulas for the dielectric determination. After a room temperature verification of these formulas, an experimental single frequency self-heating dielectrometer is built, which harmonizes the heating and measuring requirements, permitting the whole process to operate under a matched condition at a single frequency. The preliminary high temperature results obtained confirm the operation principle of the single frequency method.

However, the manually controlled mechanical tuning and matching have proved too slow to keep up with the rapid change in the cavity's resonant frequency and reflection caused by the dramatic variations in the dielectric properties taking place inside the sample at the high temperatures. Besides, the mechanical movement introduces additional uncertainties which reduce the measurement accuracy. In order to overcome these problems, a fundamentally different approach, namely, an active, self-tuning and self-heating approach, will be explored in the next chapter.

Reference

[6.1] Weiguo Xi and W.R. Tinga, "A High Temperature Microwave Dielectrometer", Microwaves: Theory and Application in Materials Processing, edited by David E. Clark, Frank D. Gac, and Willard H. Sutton, (Amer. Cer. Soc. Ceramic Tran., 21, 1991) pp. 215-224

Chapter 7

ACTIVE SINGLE FREQUENCY DIELECTROMETER[1]

7.1 Introduction

In response to the problems caused by the required mechanical tuning and matching in a passive single frequency dielectrometer, we will take a new approach in this chapter. To eliminate the need for a tuning and matching mechanism, we will develop an active dielectric measurement technique.

Microwave dielectric measurement methods can be generally classified into passive and active techniques. In a passive system, the dielectric being measured will not normally affect the frequency of the microwave source, as we have seen in the passive dielectrometer in the last chapter. In contrast, an active microwave dielectric measurement (AMDM) system incorporates the dielectric to be measured into its microwave oscillation mechanism, so that the properties of this dielectric are among the factors that determine the microwave oscillation parameters such as the oscillation frequency and power level.[7.1] In return, once the relations between the properties of the dielectric and the oscillation parameters are known, then the dielectric properties can be determined through measurements of the oscillation parameters. An oscillation loop consisting of amplifiers, transmission lines and the cavity including the unknown dielectric, as shown in Figure 7.1(a), is one such AMDM, in which the loop oscillation frequency is determined by the dielectric constant; in return, the dielectric constant can be deduced from the easily measurable oscillation frequency.[7.1]

We found that, based on this oscillation loop, a high temperature single frequency dielectometer, superior to a passive dielectometer in many respects, can be developed. First, being inherently different from a passive approach, the oscillation loop has its oscillation frequency regulated by the dielectric to be measured. In this sense,

---

[1] A version of this chapter has been accepted for publication. IEEE Trans. Microwave Theory and Tech., vol. 41, 1993

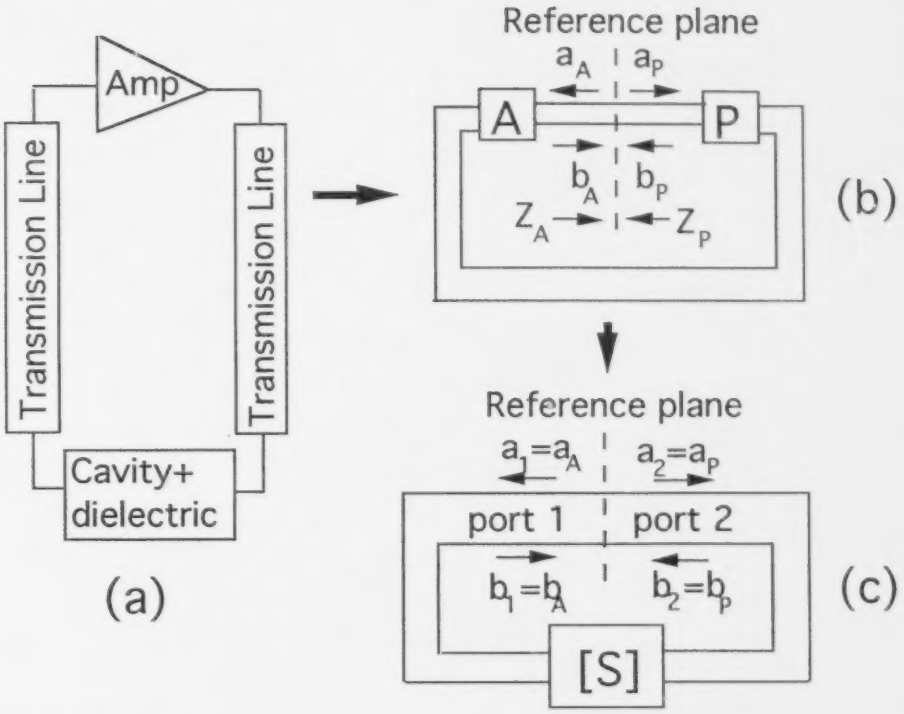

FIGURE 7.1 (a) An oscillation loop consisting of a cavity, amplifier and transmission lines for an active dielectric measurement application, which is (b), divided into an active 2-port and a passive 2-port and (c), represented by an S-parameter network with its input and output ports connected together.

the tracking and the tuning is achieved automatically, without resorting to any additional electro-mechanical facilities. Not only will the system be greatly simplified but its response to the sample property variation will also be much faster. Secondly, since the microwave signal is generated by the loop itself, separate microwave sources are no longer needed. Moreover, if a power amplifier is added in the loop, a power level high enough to heat the sample can be achieved. Consequently, the power generated inside the loop serves both the dielectric measurement and the dielectric heating, leading to

a novel self-oscillating, self-heating active single frequency high temperature dielectometer.

Formally, the use of an active oscillation loop for room temperature dielectric measurement was proposed by Ajmera in 1974,[7.1] though some similar ideas had been described elsewhere [7.2-7.5]. Since then, further discussions related to the loop oscillation behavior can also be found in the literature [7.6-7.11]. However, none of these reference papers addressed any dielectric measurement. Instead, they focused on the diagnostics of plasma and hydrogen,[7.1-7.5] the stability of a maser oscillator,[7.6-7.9] the measurement of cavity parameters[7.10] and the monitoring of a polymerization process.[7.11]

In order to design our active dielectometer, we need to understand its operational mechanism. Moreover, a theoretical model that can be used to derive the dielectric constant of the sample from the measured oscillation loop frequency must be established, which usually involves two steps. The first is to find the relation between the dielectric constant and the cavity resonant frequency. The second is to find the relation between the cavity resonant frequency and the oscillation loop frequency. The former requires the field analysis of a sample loaded cavity, which has been discussed in the previous chapters. The latter involves the oscillation loop analysis, which has not been readily available. Therefore, in this chapter, we will focus on the oscillation loop analysis.

We first will derive the S-parameter oscillation condition of an arbitrary two-port network having its input and output ports connected, as shown in Figure 7.1(c), proving that the conventional phase and gain oscillation condition is valid only for some special cases. Secondly, the active oscillation loop, treated as such a network, is analyzed, including theoretical modeling, experimental verification and a discussion of the loop characteristics. Then, based on this analysis, we design and construct a prototype for the room temperature dielectric constant measurement, demonstrating its accuracy, simplicity and dynamic range in terms of the sample's allowable loss factor. Finally, by adding a power amplifier and a

temperature measurement channel, this system is extended to allow high temperature dielectric constant measurements.

7.2. Oscillation Conditions of an Active Loop

An active loop's oscillation constraint is normally considered to be given by a phase equation and a gain equation as[7.1]

$$\text{Phase} \qquad \Phi = 2N\pi \tag{7.1}$$

$$\text{Gain} \qquad G = 0 \text{ (dB)} \tag{7.2}$$

where Φ is the phase shift of the loop in radians, G is the gain of the loop in dB and N is an integer. However, by deriving the oscillation condition in terms of the loop's S-parameters, we will prove that as a loop oscillation condition, (7.1) and (7.2) are valid only in some special cases.

It is possible to divide the loop functionally into an active two-port and a passive two-port, as shown in Figure 7.1(b). Block A represents the active two-port including amplifiers and other possible active devices. Block P represents the passive two-port including the cavity and other possible passive components such as transmission lines, directional couplers and isolators. Then $a_{A,P}$ and $b_{A,P}$ are the scattering waves into and out of the ports w r.t. a reference plane assumed between them. A natural oscillation occurs when[7.12]

$$Z_A + Z_P = 0 \tag{7.3}$$

where

$$Z_A = Z_o \frac{1+\Gamma_A}{1-\Gamma_A} \tag{7.4a}$$

$$Z_P = Z_o \frac{1+\Gamma_P}{1-\Gamma_P} \tag{7.4b}$$

and, $\Gamma_A = b_A/a_A$, is the reflection coefficient from the active two-port while $\Gamma_P = b_P/a_P$, is the reflection coefficient from the passive two-port. Z_o is the characteristic impedance of the transmission line.

Then, Eq.(7.3) can be rewritten in terms of these reflection coefficients as

$$\frac{1+\Gamma_A}{1-\Gamma_A} + \frac{1+\Gamma_P}{1-\Gamma_P} = 0 \tag{7.5}$$

To satisfy this equation requires

$$\Gamma_A = \frac{1}{\Gamma_P} \tag{7.6}$$

This means that, with respect to the reference plane, if one side appears passive($|\Gamma|<1$), the other must be active ($|\Gamma|>1$) to make an oscillation possible. From (7.6), we can obtain the oscillation condition in the form of scattering waves, namely,

$$\frac{b_A}{a_A} = \frac{a_P}{b_P} \tag{7.7}$$

In fact, (7.7) will not change if we combine the active block and the passive block into a single two-port characterized by an S-parameter matrix as shown in Figure 7.1(c), where the reference plane shown in Figure 7.1(b) now defines port1 and port2.

By definition,

$$b_1 = S_{11}a_1+S_{12}a_2 \tag{7.8a}$$

$$b_2 = S_{21}a_1+S_{22}a_2 \tag{7.8b}$$

Noting that $a_1=a_A$, $a_2=a_P$, $b_1=b_A$, $b_2=b_P$, $b_1=a_2$ and $b_2=a_1$, we obtain

$$\frac{b_1}{a_1} = \frac{S_{11}}{1-S_{12}} \tag{7.9a}$$

$$\frac{b_2}{a_2} = \frac{S_{22}}{1-S_{21}} \tag{7.9b}$$

Substituting b_A/a_A and b_P/a_P in (7.7) by b_1/a_1 and b_2/a_2 in (7.9), we derive

$$(1-S_{21})(1-S_{12}) = S_{11}S_{22} \tag{7.10}$$

This is a generalized oscillation condition for an arbitrary two-port network having its input and output ports connected. Since the position of the reference plane we previously assumed is absolutely arbitrary, then (7.10) should be valid at any position in the loop which may contain many different components. This oscillation condition is very convenient to use in a practical loop design since it is expressed in S-parameter notation.

In the special case of a unidirectional network such as a loop with a high gain amplifier, one of its transmission parameters, say S_{21}, will be zero, so that (7.10) becomes

$$1-S_{21} = S_{11}S_{22} \tag{7.11}$$

Moreover, when one of its ports, say port2, is matched, S_{22} will also be zero, reducing the oscillation condition of (7.11) to

$$S_{21}=1 \tag{7.12}$$

This equation is now equivalent to (7.1) and (7.2), that is, the phase of the transmission parameter is equal to zero (or $2N\pi$) and its magnitude is equal to unity or its gain in dB is zero, proving that the oscillation condition given in (7.1) and (7.2) is valid only for the special cases when $S_{11}=S_{21}=0$ or $S_{22}=S_{12}=0$.

In other words, as an oscillation condition, (7.1) and (7.2) are applicable only for a unidirectional loop at a matched reference plane. Therefore, using (7.1) and (7.2) for an arbitrary loop at an arbitrary plane is incorrect. Unfortunately, since these preconditions for using (7.1) and (7.2) have never been addressed before, misuse of (7.1) and (7.2) has been widespread, including the previous work referenced in this chapter, where no reference plane was set nor transmission and match conditions were specified.

Since the oscillation loop that we will use for our dielectric constant measurement includes high gain amplifiers and a matched isolator at its port2, the condition of $S_{22}=S_{12}=0$ is well satisfied, as will also be verified by our later measurements. Therefore, we can properly use (7.12) as the oscillation condition in the modeling which follows. In addition, for our given reference plane, the loop phase shift is actually the phase, ϕ_{21}, of S_{21}. Consequently, for simplicity, we will no longer distinguish between the loop phase and ϕ_{21}.

7.3. Modeling of the Oscillation Loop Formed by A Cavity, Amplifiers and Transmission Lines

To use the derived S-parameter oscillation condition to model the loop, we need the S-parameters of each component in that loop. An oscillation loop of this kind should consist, at least, of a cavity, amplifiers and transmission lines. In practice, the loop may need a few more components such as attenuators for adjusting the gain, directional couplers for coupling signals from the loop and isolators for improving the impedance match to certain components. However, it is noted that an attenuator can be included in an amplifier as a gain adjustment device, while a directional coupler or an isolator can be treated approximately as a section of transmission line. Therefore,

from a theoretical modeling point of view, a cavity, an amplifier and a transmission line are the basic elements which need to be characterized. For convenience, the cascade or transmission matrix, designated as [A], will also be employed in our modeling, since all the components are configured in a cascade fashion in the loop.

It is well known that the matrix [A] of a section of transmission line can be expressed as[7.13]

$$[A^T] = \begin{bmatrix} \cos\beta L & j\sin\beta L \\ j\sin\beta L & \cos\beta L \end{bmatrix} \tag{7.13}$$

where $\beta=2\pi/\lambda$ is the propagation constant, and L is the electric length of the transmission line. Their corresponding S-parameters can be obtained by converting $[A^T]$ to $[S^T]$ using the standard formulas[7.13]

$$S_{11}^T = \frac{a^T+b^T-c^T-d^T}{a^T+b^T+c^T+d^T} \tag{7.14a}$$

$$S_{12}^T = \frac{2|A^T|}{a^T+b^T+c^T+d^T} \tag{7.14b}$$

$$S_{21}^T = \frac{2}{a^T+b^T+c^T+d^T} \tag{7.14c}$$

$$S_{22}^T = \frac{a^T+b^T-c^T-d^T}{a^T+b^T+c^T+d^T} \tag{7.14d}$$

where a^T, b^T, c^T and d^T are the elements of $[A^T]$ in the positions defined by

$$[A^T] = \begin{bmatrix} a^T & b^T \\ c^T & d^T \end{bmatrix} \tag{7.15}$$

The superscript T designates a Transmission line matrix. Similarly, superscripts A and C will designate an Amplifier matrix and a Cavity matrix respectively in the following.

Being an active device, an amplifier's S-parameters may vary from one unit to another. We determined the frequency dependence of the S-parameters for our amplifier experimentally using an automatic S-parameter measurement system and converted these to the cascade

matrix parameters, $[A^A]$. (See Appendix A). Using polynomial curve fitting on that data resulted in the following equations,

$$\begin{aligned} a^A &= 24.224-0.0531919f+2.89236*10^{-5}f^2+j(2.91463-0.00316638f) \\ b^A &= 25.528-0.0564754f+3.08759*10^{-5}f+j(6.07467-0.00992886f \\ &\quad +3.5937*10^{-6}f^2) \\ c^A &= 25.0559-0.0550109f+2.9917*10^{-5}f+j(2.90077-0.00315084f) \\ d^A &= 24.3153-0.0537048f+2.93626*10^{-5}f^2+j(6.78937-0.0114867f \\ &\quad +4.4431*10^{-6}f^2) \end{aligned} \tag{7.16}$$

A cavity can be represented by an equivalent resonant circuit with two transformers simulating its two coupling ports, as shown in Figure 7.2. Their cascade matrices are[7.13]

$$A_0=\begin{bmatrix} 1 & 0 \\ Y & 1 \end{bmatrix} \tag{7.17a}$$

$$A_1=\begin{bmatrix} \frac{1}{n_1} & 0 \\ 0 & n_1 \end{bmatrix} \tag{7.17b}$$

$$A_2=\begin{bmatrix} n_2 & 0 \\ 0 & \frac{1}{n_2} \end{bmatrix} \tag{7.17c}$$

respectively, where n_1 and n_2 are the coupling transformer ratios of ports 1 and 2, Y is the normalized admittance of the cavity, expressed as[7.13]

$$Y=G_0\left[1+Q_0\left(\frac{f}{f_c}-\frac{f_c}{f}\right)\right] \tag{7.18}$$

where G_0 is the normalized characteristic conductance of the cavity,

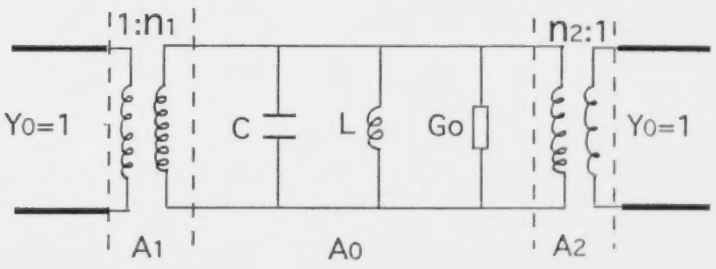

FIGURE 7.2 Equivalent circuit of a cavity with two coupling ports.

f_c is the cavity resonant frequency, f is the frequency of interest and Q_0 is the Q factor of the cavity.

Then the cavity matrix, $[A^c]$, will be the product of the three individual circuit matrices, namely,

$$[A^c]=[A_1][A_0][A_2] \tag{7.19}$$

Furthermore, the total cascade matrix of the loop will be the product of the individual component matrices, that is

$$[A]=[A^c][A^T][A^A] \tag{7.20}$$

Finally, the S-parameters of the complete loop can be obtained by applying (7.14) to convert [A] to [S], where a^T, b^T, c^T, d^T and S_{11}^T, S_{12}^T, S_{21}^T, S_{22}^T should be replaced by the a, b, c, d, elements of [A], and the S_{11}, S_{12}, S_{21}, S_{22}, elements of [S] respectively.

7.4. Programming and Experimental Verification

All of the above model equations have been implemented, in HP BASIC, on an HP200 computer to meet different needs in our loop analysis and to predict the cavity resonant frequency, f_c, from the loop oscillation frequency, f_L. For example, to calculate f_L, we can first calculate the [S] of the loop, then search for the zero of the phase, ϕ_{21}, of S_{21}, because, according to the oscillation condition (7.12), the loop oscillation frequency, f_L, is that frequency which makes $\phi_{21}=0$. (See Appendix B).

To verify the model, we used the experimental setup shown in Figure 7.3, where the cavity is the coaxial re-entrant cavity, a detailed analysis of which has been given in a previous chapter. Amp is a cascade of amplifiers UTO1001 and UTO2021 (Avantek, G≅56 dB). The limiter is a UTL1001 (Avantek). The attenuator is the combination of a MIDWEST MICROWAVE 291-1-10dB attenuator and a type L4410-10 (PRD, 10 dB coupling factor) directional coupler. We also used a variety of flexible transmission lines. Among these components, the cavity, the amplifier and the transmission lines are needed to establish an oscillation. As the S-parameters of an amplifier vary with the signal's power level, the limiter and the attenuator are used to adjust the amplifier input power level to that used to find the previously measured S-parameters. The directional coupler is used to

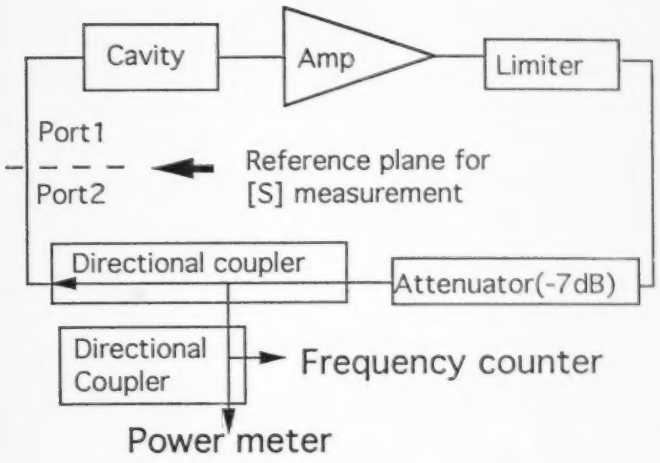

FIGURE 7.3 Diagram of the experimental setup for verification of the theoretical model based on S-parameter oscillation condition.

sample the signal in order to measure the loop signal's frequency and power level via the instruments outside the loop.

From the results in Table 7.1, it is clear that the measured S-parameters of the loop shown in Figure 7.3 confirm the general oscillation condition we derived. The reference plane for this measurement is located at the front of the cavity, where the cavity faces port1 while port2 sees a matched 7 dB attenuator, through the directional coupler. Therefore, the $|S_{22}|$ values are approximately zero, indicating a good match, whereas the $|S_{11}|$ values vary with the measurement frequency, reflecting the input frequency spectrum characteristics of the cavity. A high gain amplifier (>50 dB) in the loop results in a highly unsymmetrical S-matrix, where the $|S_{12}|$ values are all equal to zero while the $|S_{21}|$ values are all close to unity, particularly in the region around f_L. Taking the set of the S-parameters at $f=f_L$, in Table 7.1, and substituting them for S_{11}, S_{12}, S_{21}, S_{22} in the oscillation condition (7.10), it is apparent that this equation is well satisfied with these measured data.

To verify the model's prediction of f_L as calculated from a given

Table 7.1 Measured [S] of the experimental active oscillation loop over the 915MHz ISM band.

f(MHz)	S_{11}		S_{12}		S_{21}		S_{22}	
	Magn	Degr	Magn	Degr	Magn	Degr	Magn	Degr
939.80	0.891	-80.4	0.000	51.6	0.888	112.0	0.032	88.0
940.20	0.876	-87.8	0.000	41.1	0.907	111.3	0.033	87.9
940.60	0.835	-101.9	0.000	56.7	0.936	109.5	0.033	87.8
941.00	0.663	-140.0	0.000	53.5	0.926	90.9	0.033	87.6
941.40	0.447	59.7	0.000	-6.4	0.900	32.4	0.033	88.4
f_L 941.60	**0.668**	**5.9**	**0.000**	**33.1**	**0.913**	**4.2**	**0.034**	**88.8**
942.00	0.840	-30.6	0.000	-38.7	0.923	-25.9	0.034	88.3
942.40	0.881	-44.0	0.000	18.2	0.895	-44.6	0.035	88.4
942.80	0.895	-51.3	0.000	46.6	0.876	-55.8	0.035	88.6

f_c, we measured the f_L with a Frequency counter for a number of different f_c. These are compared with the model's calculated f_L in Table 7.2. Their maximum relative difference is shown to be 0.041%.

Table 7.2 Comparison of the measured and calculated f_L for different f_c

fc(MHz)	fL(meas)	fL(calc)	Difference(%)
957.51	957.20	957.37	0.019
963.01	962.36	962.71	0.040
952.06	951.93	952.05	0.013
946.59	946.68	946.71	0.003
941.36	941.46	941.62	0.017
936.09	936.35	936.55	0.021
930.89	931.36	931.74	0.041

Up to this point, the S-parameter oscillation condition and the model for the loop have been verified. In the following, we will use this model to investigate the active loop's characteristics.

7.5. Discussion of Active Loop Characteristics

Figure 7.4(a) shows the frequency dependence of the magnitude of the loop phase which varies periodically from 0^0 to 180^0. As suggested by (7.12), loop oscillations occur at the frequencies corresponding to the zeros in the phase locus. Therefore, each valley of the loop phase represents an oscillation mode of the loop. In order to explain the effects of f_c on the loop phase, we also label the location of f_c in this figure, and indicate it by a circle. Among these oscillation modes, there is only one which is closest to, and possibly coincident with f_c. We call this oscillation mode the cavity mode. Clearly, the phase valley of the cavity mode is much sharper than that of a non-cavity mode. Owing to this steep phase slope, the stability of the loop frequency of a cavity mode is much higher than that of a non-cavity mode. Our experiments have shown that f_L of a cavity mode drifts only 100Hz while that of a non-cavity mode may drift more than 10kHz. Therefore, our active loop for the dielectric measurement will be designed to operate in a cavity mode.

Let us now consider the cavity mode oscillation in greater detail. Figure 7.4(b) compares the phase patterns of a cavity mode for different given cavity frequencies, f_{c0}, f_{c1}, etc., indicated by the vertical lines. The loop frequencies, f_{L0}, f_{L1},...., are still located at the zeros in the phase valleys. Firstly, the sharpest and most symmetrical phase valley, i.e., curve 0, results when the loop frequency coincides with the cavity frequency. Naturally, this will cause the most stable loop oscillation. Secondly, the farther apart the cavity and the loop frequencies are, the wider the valleys. One common feature to all these valleys or phase loci is that their steepest slope always occurs when the loop phase curves cross the vertical lines which represent the cavity frequencies. Therefore, in any case, an f_c can always be found by searching for the maximum loop phase variation as was done by Akyel et al [7.10].

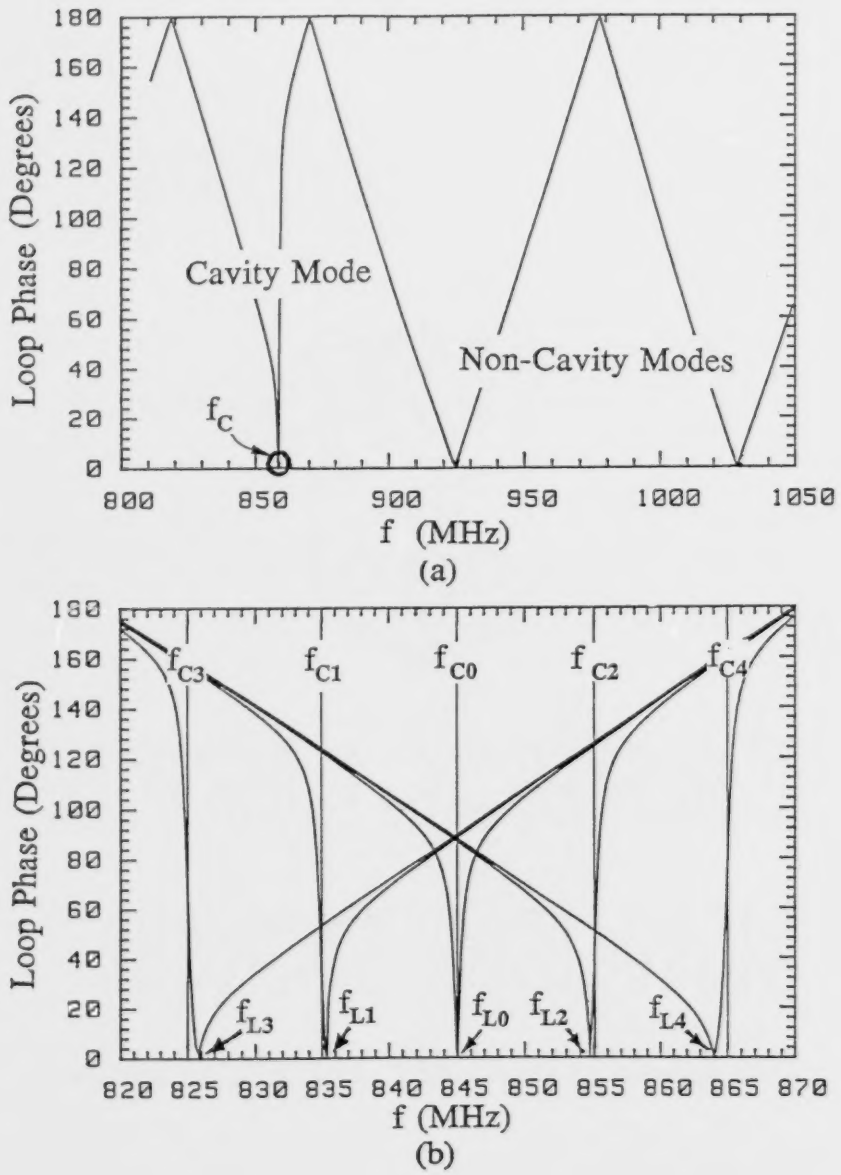

FIGURE 7.4 Magnitude of the loop phase vs. frequency (a) for a fixed f_c of 859MHz, labeled by 0, and (b) of a cavity mode for different f_c, indicated by the vertical lines. (Loop oscillations occur at frequencies where the loop phase =0)

Using this loop for a dielectric constant measurement requires a quantitative relation between f_L and f_c, since, in our case, it is f_L which will be measured while it is f_c which will be used to determine the dielectric constant of a sample in the cavity. Even though some authors directly used an f_L as f_c,[7.5] our results show that, for a given cavity mode, f_c is only equal to f_L at one particular frequency, as shown in Figure 7.5(a). When f_c shifts 20 MHz, typical when a dielectric sample is introduced, the difference between f_L and f_c may exceed 0.4 MHz. Plotting the ratio of loop to cavity frequency change as done in Figure 7.5(b) shows further properties of the f_c and f_L interdependence. It is observed that, firstly, the shift of f_L can never be more than that of f_c, since $\Delta f_L/\Delta f_c<1$. This conclusion agrees with that drawn in [7.1]. Secondly, the range over which $\Delta f_L/\Delta f_c>0.9$ is about 40MHz. As we will see later, this range is sufficient to accommodate samples with a dielectric constant from 1 to 80. If a 10% frequency error is tolerable, approximately corresponding to a 10% error in ε',[7.14] use of the f_L shift in place of the f_c shift is still acceptable. Finally, reducing the cavity Q results in a smaller frequency ratio or a larger frequency difference and a smaller dynamic measurement range for ε'.

As revealed by a study of Figure 7.6, the relationship between f_L and the loop length is actually dominated by f_c. Curves 2 and 3 show the behavior of f_L with loop length variation when $f_c \simeq f_L$ while curves 1 and 4 are for the cases when $f_c \neq f_L$. Curves 2 and 3 show that, f_L, when coincident with f_c, is hardly influenced by the loop length variation. However, curves 1 and 4 show that the loop length will significantly affect f_L when f_L and f_c are relatively far apart. Therefore, to minimize the susceptibility of f_L to the uncertainty in the loop length, the loop should be designed to operate at a frequency as close to the chosen f_c as possible. The optimum loop length range can be determined using the model.

7.6. Dielectric Constant Measurement at Room Temperature

Based on the previous analysis, a dielectrometer system using this active loop has been constructed, as shown in Figure 7.7, where

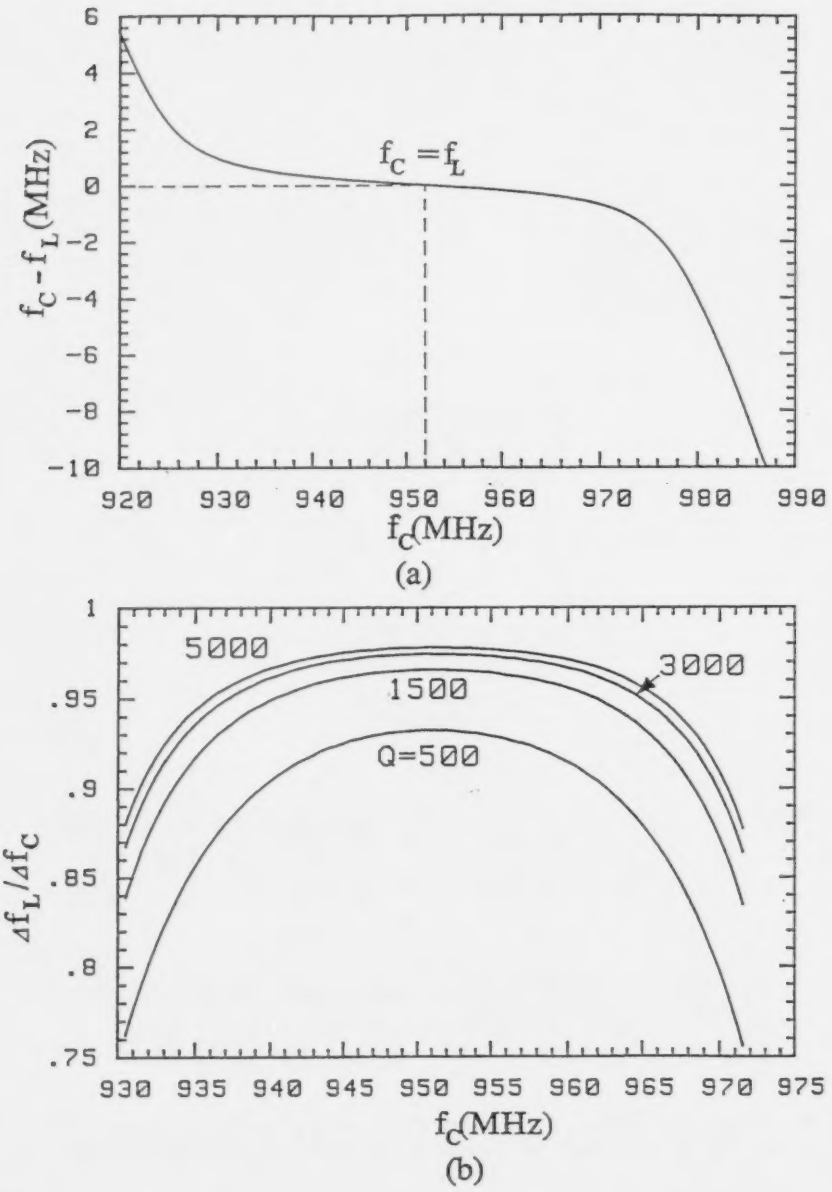

FIGURE 7.5 (a) Difference between f_L and f_c vs. f_c for a given cavity mode. $f_L=f_c$ is possible only at one particular frequency, i.e., 951MHz in this case. (b) Ratio of Δf_L to Δf_c as a function of f_c with cavity Q as a parameter.

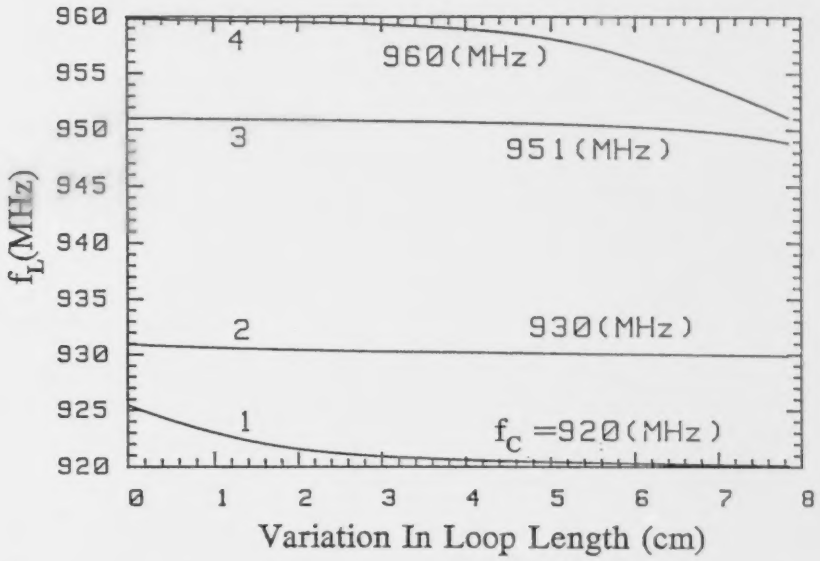

FIGURE 7.6 f_L vs. variation in loop length for different f_c. The closer f_L is to f_c, the smaller the influence of the length variation on f_L.

the cavity is again the re-entrant coaxial cavity, Amp is an AM2002N amplifier (Avantek) with the input and output characteristics shown in Figure 7.8, the limiter is an Avantek UTL-1001. Its limiting level, depending on its DC bias, can be adjusted from 0dBm to -13dBm. We set it at -10dBm to enable the amplifier to achieve its maximum output, as suggested by Figure 7.8, where the output power reaches its peak for an input power of -10dBm. The corresponding idealized input and output characteristic of the limiter is also shown in Figure 7.8. A circulator (RTY-300014) provides a matched input as seen from the cavity while isolating the cavity from the amplifier and providing the frequency counter with a measurement signal through its port 3. A dual directional coupler (HP775D) forms a reflectometer to monitor the reflection from the cavity. Two power meters (HP436A), a frequency counter (EIP575) and an HP200 computer, interconnected by an HPIB bus, form a data acquisition system, which records the forward and the reflected power as well as the loop frequency for analysis by the

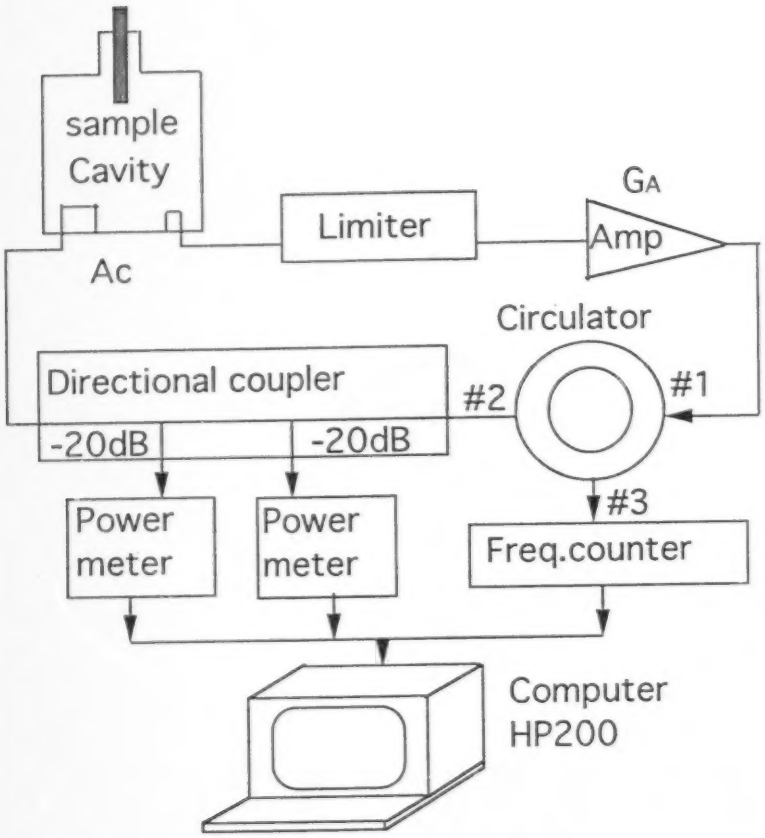

FIGURE 7.7 Diagram of the active room temperature dielectric constant measurement system.

computer.

With the aid of this system, we can now discuss how the gain condition is applied and how it affects the dynamic range of a sample's allowable dielectric loss factor. Considering the directional coupler and the circulator as part of the transmission line, the total gain around the loop should be the summation of the gain of the cavity, the amplifiers and the attenuation in the rest of the loop and, according to (7.2), should equal zero when the loop oscillates, i.e.,

$$A_C + A_L + G_A = 0 \qquad (7.21)$$

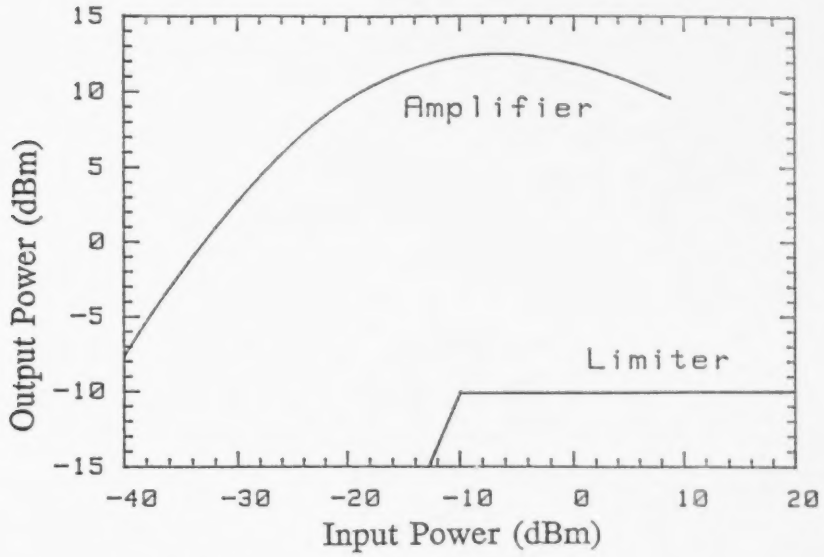

FIGURE 7.8 Input and output characteristic of the Avantek AM2002N amplifier, and an idealized input and output characteristic of the Avantek UTL-1001 limiter.

where A_C is the cavity attenuation (a reduction in gain) including sample loss, G_A is the amplifier gain, A_L is the attenuation in the rest of the loop (a reduction in gain) made up of the limiter and transmission lines.

Besides having to satisfy (7.21), in a practical case, a stable oscillation cannot be established unless the amplifier is saturated. Therefore, the dynamic range of the attenuation in the loop should equal this saturation range. For example, in our case, the saturation range of the amplifier used is -10dBm to 0 dBm as shown in Figure 7.8. Then, the dynamic attenuation range allowed in this loop must be 10 dB. However, the limiter placed ahead of the amplifier can greatly extend this range due to its much wider saturation range, which, as shown in Figure 7.8 again, is 30dB from -10dBm to 20 dBm. Usually, during a measurement, the cavity is the only component changing its loss (due to the inserted sample). Consequently, this 30dB dynamic range will all be allocated to the cavity. Our experiments have shown

that the attenuation is about 15 dB when a lossy sample such as water is inserted into the cavity for a given re-entrant gap width. This implies that the dielectric constant of most lossy dielectrics can be measured using this active dielectrometer with plenty of margin in the available attenuation range.

Initially, f_L is measured for the empty cavity. After a sample is inserted into the cavity, the HP200 data acquisition program determines the average of 10 f_L readings. From this averaged f_L, a corresponding f_c is calculated. Finally, the Δf_L and the Δf_c are used to calculate the dielectric constant, ε', using Eq. (6.1).

We obtain the dielectric constant data for 8 different samples, as shown in Table 7.3. For comparison, the data obtained with a standard passive swept method are also given. Table 7.3 shows that the errors in the results obtained from f_c are smaller than those

Table 7.3 Dielectric constant data measured with the active oscillation loop system, compared to data from a passive swept frequency system [7.15]. Two different sets of results are shown, which are calculated using (6.1) with $f=f_L$ and $f=f_c$ respectively.

Sample No.	ε'			Difference(%)	
	Swept method	This work		using f_L	using f_c
		using f_L	using f_c		
1	2.32	1.96	2.28	16.0	1.7
2	3.30	3.00	3.33	9.1	0.9
3	3.53	3.27	3.65	7.4	3.4
4	4.00	3.67	4.05	8.3	1.0
5	4.52	4.24	4.66	5.8	3.1
6	6.37	5.95	6.42	6.6	0.8
7	14.62	14.15	15.15	3.2	3.6
8	88.64	75.83	97.25	14.45	10.4

obtained from f_L, showing the significant role played by the model for f_c used in the dielectric constant prediction. The differences between the data obtained from the active dielectrometer and the data from a passive swept frequency dielectrometer are less than 4% for medium ε' (<20) and 11% for high ε' (up to 80) samples.

7.7. Dielectric Constant Measurement at High Temperature

We now extend the application of this active loop to a high temperature dielectric measurement. Adding a power amplifier and a temperature measurement channel, as shown in the new system diagram of Figure 7.9, allows us to use this active loop to both rapidly heat the sample and measure its dielectric constant.

Now three amplifiers are used, namely, an Avantek UTO1001 preamplifier (maximum 50 dB gain), an Avantek AM-2002N preamplifier (maximum 30 dB gain) and an American Microwave Technology Inc. multi-channel power amplifier (>40dB gain). The preamplifiers enable the loop oscillation to start from the system noise level and supply the power amplifier with the required input driving power ($\cong$ 10 dBm). An attenuator between the two preamplifiers ensures a proper input power level for the AM-2002N amplifier. The output of the power amplifier, controllable from 0 to 100W, boosts the power to a level high enough to heat up the sample. Loop frequency and the sample temperature are measured with a frequency counter (EIP 757) and an optical fiber thermometer (Accufiber 100C) respectively. This data is then logged and processed using the HP200 computer. The input signal for the frequency counter is coupled through the directional coupler, while the sample temperature is sensed through a light pipe aimed at the hot sample.

Observe that there are two different power regions in the active loop, i.e., a high power (maximum 100W) and a low power (maximum 4mW) region. It is clearly advantageous that only the sample, needing heating, be located in the high power region while the rest of the components are in the low power region, avoiding high power related problems such as over-heating, performance deterioration and damage to

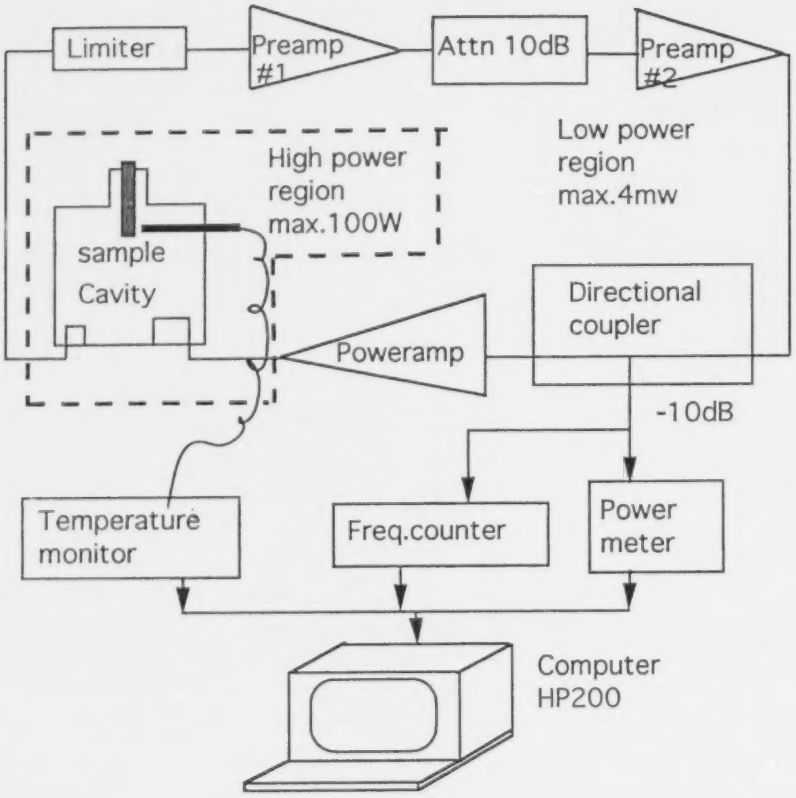

FIGURE 7.9 Diagram of the active high temperature dielectric constant measurement system, where the sample is heated in the high power region while the measuring components are all in the low power region.

the measurement instruments.

We start the measurement by adjusting the empty cavity's frequency and the output of the power amplifier to establish a proper oscillation in the loop, then measure the loop oscillation frequency of the empty cavity, which serves as the reference for the subsequent frequency shift due to the introduction of the sample. The sample is inserted through the endplate of the re-entrant cavity in which it will be heated by the highly focused microwave fields in the cavity's gap region. When the desired sample temperature is reached, the automatic data acquisition program starts to log the temperature and frequency data. As in the room temperature case, this program will

calculate the dielectric constant of the sample from the measured average loop frequency shift, Δf. In this manner, the temperature dependence of the dielectric constant can be obtained within one minute, depending on the sample's heating rate.

We have performed some preliminary high temperature dielectric constant measurements. Results are shown for mullite (MV20) and machinable alumina (Cotronics 960) in Figure 7.10. Data obtained using a passive high temperature method in [7.15] are also presented for comparison. Even though measurement uncertainties increase with temperature because of cavity expansion and parameter variation in the power amplifier, the good agreement of these data confirms the feasibility of the active high temperature dielectrometer.

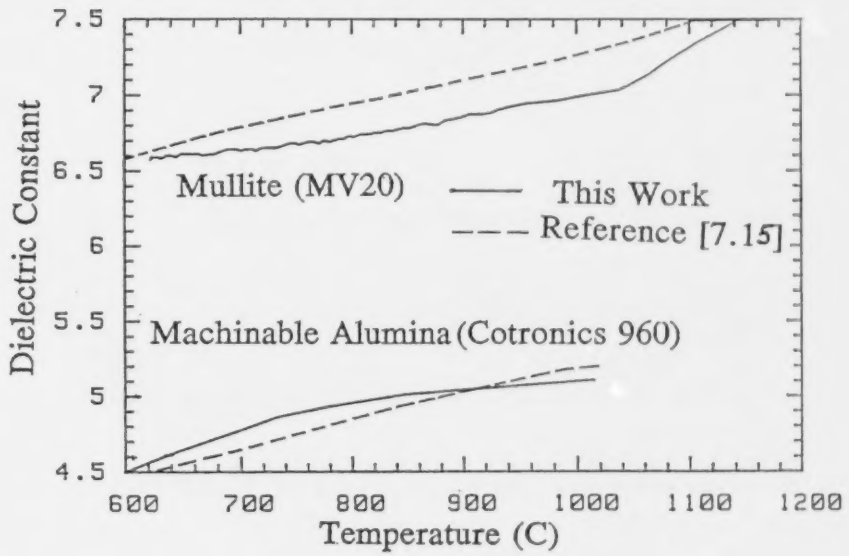

FIGURE 7.10 Dielectric constant vs. temperature for Mullite (MV20) and Machinable Alumina (Cotronics 960), measured with the self-oscillating, self-heating single frequency active dielectrometer.

7.8. Conclusions

We have derived a generalized oscillation condition, in S-parameter notation, for an arbitrary two-port having its input and output ports connected. The oscillation condition can be used for the analysis of an arbitrary oscillation loop. It is proved that the commonly used phase and gain oscillation condition defined in (7.1) and (7.2) is only a special case of the S-parameter condition. An active oscillation loop formed by a cavity, amplifiers and transmission lines has been analyzed using the S-parameter oscillation condition. The analysis includes theoretical modeling, programming, experimental verification and discussion of the loop characteristics, thereby providing better understanding of the loop's operation and laying the foundation for active loop dielectrometer design.

We have also developed prototypes of two active loop dielectrometers, one for room temperature measurements and the other for high temperature measurements. Compared to the results from a standard swept frequency dielectrometer method, the active dielectrometers exhibit discrepancies of less than 4% for medium dielectric constant and 11% for high dielectric constant samples. Using the power generated inside the loop to heat the dielectric sample leads to a novel high temperature dielectrometer. Owing to its self-oscillating and self-heating nature, this dielectrometer needs no external tuning nor separate microwave sources. A normal high temperature dielectric measurement can be completed within one minute. Compared to existing systems, this high temperature dielectrometer system measures more rapidly, requires much simpler instrumentation and is therefore more economical.

References

[7.1] C.Ajmera, D.B.Bachelor, D.C.Moody and H.Lashinsky, "Microwave Measurements With Active Systems", Proc.IEEE. vol.62, pp 118-127, Jan. 1974.an. 1974.

[7.2] R.C.Ajmera and H.Lashinsky, "Plasma Impedance Element In an Active Fabry-Perot Microwave Resonator", Appl. Phys. Lett.,

vol.13, pp 96-98, March, 1968.

[7.3] R.B.Hall, "Microwave Measurements on Laser-Produced Blast Waves, J. Appl. Phys. vol.40, pp 36-43, Jan. 1969.

[7.4] R.C.Ajmera and H.Lashinsky, "Microwave Diagnostics of a Transient Plasma With an Active Fabry-Perot Resonator", J. Appl. Phys., vol.40, pp 4869-4471, Dec. 1969.

[7.5] N.C.Wenger and J.Smetana, "Hydrogen Density Measurements Using an Open-Ended Microwave Cavity", IEEE Trans. Instrum. Meas., Vol. IM-21, pp 105-114, May, 1972.

[7.6] M.Tetu, R.Brousseau and J. Vanier, "Frequency-Domain Measurement of the Frequency Stability of a Maser Oscillator", IEEE Trans. Instrum. Meas., Vol. IM-29, pp 94-97, Feb. 1980.

[7.7] P.Lesage and C.Audoin, "Frequency Stability of an Oscillating Maser: Analysis of the Effect of an External Feedback Loop", IEEE Trans. Instrum. Meas., Vol. IM-30, pp 182-186, March, 1983.

[7.8] M.Tetu, P.Tremblay, P.Lesage and P.Petit, "Experimental Study of the Frequency Stability of a Maser Oscillator Operated With an External Feedback Loop", IEEE Trans. Instrum. Meas., Vol IM-32, pp 410-414, March, 1983.

[7.9] B.Villeneuve, P.Tremblay, A.Michaud and M.Tetu, "RF Spectrum of Thermal Noise and Frequency Stability of a Microwave Cavity-Oscillator", IEEE Trans. Microwave Theory Tech., Vol. MTT-32, pp 1565-1572, Dec.,1984.

[7.10] C.Akyel, R.G.Bosiso and G.April, "An Active Frequency Technique for Precise Measurements on Dynamic Microwave Cavity Perturbation", IEEE Trans. Instrum. Meas. Vol. IM-27, pp 364-368, Apr., 1988.

[7.11] M.Martinelli, P.A.Rolla and E. Tombari, "A Method for Dynamic Dielectric Measurements at Microwave Frequencies: Applications to Polymerization Process Studies", IEEE Trans. Instrum. Meas. Vol. IM-34, pp 417-422, March, 1985.

[7.12] M.J.Howes and D.V.Morgan, *Microwave Devices, Device Circuit Interactions,* John Wiley&Son, 1976, p 210

[7.13] D.M.Pozar, *Microwave Engineering*, Addison-Wesley Publishing Company, New York, 1990, pp233-235

[7.14] W.Xi and W.R.Tinga, "A High Temperature Microwave Dielectrometer", Ceramic Trans. Microwaves: Theory And Applications In Material Processing, vol. 21, Cincinnati, p. 215-224, 1991.

[7.15] W.Xi, "High Temperature Microwave Dielectrometer Using A Re-Entrant Cavity", Ph.D. dissertation, Dept. Elec.Eng., Univ. Alberta, Edmonton, Fall, 1992.

Chapter 8
CONCLUSIONS

Eventhough, the heating of a dielectric sample or its dielectric constant measurement at room temperature is not so difficult, combining simultaneous sample heating and measuring has presented considerable technical challenges. Conventional sample heating approaches have the disadvantages of a slow heating rate, excessive heating of components other than the sample and thermal expansion of the measuring equipment. No doubt the recently developed two channel microwave heated dielectrometer[8.1] has significantly reduced these difficulties. Unfortunately, that system contains rather complex instrumentation and is not simple to optimize. In response, this thesis is devoted to the development of a one channel single frequency high temperature dielectrometer.

A re-entrant coaxial cavity with a gap in its hollow center conductor has proven to be very suitable as the applicator for the high temperature dielectrometer. This structure has been employed successfully not only in the single frequency dielectrometer but also in the two channel version.[8.1] This thesis summarizes its characteristics and gives a field and an equivalent circuit analysis of the cavity with the gap arbitrarily positioned in its center conductor. The artificial electric wall concept along with the equivalent circuit analysis have greatly simplified the extremely complex boundary value problem, presenting a better physical understanding of the operation of the re-entrant structure. Also, the analysis of a movable coupling loop adds another option for loss factor measurement —— a measurement that can be performed at a matched impedance condition regardless of the variation in the cavity loading.

To be able to measure the loss factor at a single source frequency, we developed a new way to determine the relative Q factor from a single frequency measurement. We proved that, if the perturbation stipulation is satisfied, the Q factor is directly or inversely proportional (depending on coupling condition) to the

cavity's input resonant resistance. As a result, relative cavity Q can be determined by a single reflection measurement at the resonant frequency.

Based on these concepts, a prototype of a passive single frequency high temperature dielectrometer has been constructed. The dielectric constant is deduced from the mechanical displacement of a movable short circuit and a movable coupling loop at a fixed frequency condition. The system includes a fixed frequency power source, a cavity, and a temperature measurement system. The performance of the system with discrepancies less than 10% in dielectric constant and 16% in loss factor compared to the 2 channel swept frequency dielectrometer system has convinced us of the feasibility of using the single frequency measurement methodology for high temperature dielectric measurements. Since the tuning and matching adjustments in this scheme are used to calculate the dielectric sample properties, this system harmonizes the heating and measuring requirements. However, the manual tuning and matching adjustments are too slow to respond to the fast variation of dielectric parameters in a rapidly heated high temperature sample.

To overcome this problem, an active oscillation loop for high temperature dielectric constant measurement is developed. The essence of this approach is to incorporate the cavity including the dielectric to be characterized into a microwave oscillation loop so that the microwave loop oscillation frequency is regulated by this dielectric. This has led to some unique features. Firstly, the dielectric constant can be determined from the loop oscillation frequency shift. Secondly, the loop frequency always follows the cavity frequency so that a cavity tuning mechanism is no longer needed. Thirdly, because of the positive feedback in the loop, the external oscillator can be eliminated. In addition, the microwave power generated in this loop can be used to heat the sample. This approach is therefore much simpler than any existing systems, and the system response is much faster than that of a passive system.

We designed and analyzed a microwave oscillation loop formed by a dielectric loaded cavity, amplifiers and transmission lines for the

dielectric constant measurement of samples at both room and very high temperatures. An oscillation condition for an arbitrary loop is derived in S-parameter notation, by which the commonly used oscillation condition in loop phase and gain notation is proved to be valid only in the special case when either $S_{11}=S_{21}=0$ or $S_{22}=S_{12}=0$. Based on this S-parameter oscillation condition, a theoretical model is established and verified with a discrepancy of less than 0.041% between the calculated and the measured oscillation frequencies. With this model, the loop characteristics are investigated. From the measured loop oscillation frequency, the cavity resonant frequency, and thereby the dielectric constant of the sample in the cavity, can be predicted. The discrepancies of the measured dielectric constant between the passive and active systems are less than 4% for $\varepsilon'<20$ and less than 11% for $\varepsilon'<80$.

In summary, the five initiatives, i.e., the single frequency Q measurement method, the coaxial re-entrant cavity with a gap in its hollow center conductor as a high temperature microwave applicator, the S-parameter analysis of an active oscillation loop, the passive and active high temperature dielectrometers, together with the theoretical model of the movable coupling loop and its application in the loss factor measurement, constitute the main contributions of this thesis. By means of these passive and active single frequency microwave heating and measuring systems, a dielectric sample can be heated and measured simultaneously using one power channel under a single frequency condition. Owing to the removal of the normally required swept frequency channel in the passive dielectrometer, the external power source and the mechanical tuning in the active dielectrometer, the dielectrometer instrumentation has been greatly simplified.

In exploring the single frequency high temperature dielectric measurements, this thesis emphasizes the theoretical basis, the operational principles and the feasibility rather than the perfection of a specific experimental system. Nevertheless, it will be beneficial for further research to point out some of the remaining problems.

1. Arcing In the gap Area As microwave fields approach the breakdown strength, the air in the gap will be ionized and arcing occurs. Due to the highly focused fields in the gap of the re-entrant cavity, arcing occurs in the gap region when a low loss dielectric sample is loaded. Once arcing starts, the whole heating and measuring process becomes unpredictable. Therefore, the use of the coaxial re-entrant cavity structure as a microwave heater is less suitable for low loss samples.

2. Sample temperature control for the active system. In microwave dielectric heating, the control of the sample temperature is usually achieved by a temperature monitor which can feed back an electric signal to adjust the microwave source power, so that the temperature can be maintained at a desired value or changed in a desired fashion. Similarly, in the active system, the sample temperature can be controlled by adjusting the output power of the power amplifier. But, to execute a change in the power level, certain amplifier parameters have to be altered, which will affect the loop oscillation frequency. Considering the relatively small frequency shift caused by the sample, such an added frequency shift effect cannot be tolerated. For this reason, in our prototype active system, the power level is kept at a fixed level during a measurement. Therefore, the sample temperature rises in a free running fashion, which, from an application point of view, is not an ideal operational condition.

3. Q measurement in the active system. We can prove (see appendix C) that the Q factor can be determined theoretically using the single frequency Q method in an active system. It is noted that measurement of the reflection coefficient is not performed at the exact cavity resonant frequency (the bottom of the resonant reflection curve) but at the loop oscillation frequency (different by several hundred kHz). Since the reflection on the steep slope part of the resonant curve is highly sensitive to frequency, a small measurement error in frequency or in reflection will result in a large Q factor error. On the other hand, several hundred kHz error in frequency prediction (including the measured and the calculated errors) is highly possible. This may cause a larger than 100% error in a Q measurement, making the loss

factor measurement rather inaccurate.

Reference

[8.1] Weiguo Xi and W.R. Tinga, "A High Temperature Microwave Dielectrometer", Microwaves: Theory and Application in Materials Processing, edited by David E. Clark, Frank D. Gac, and Willard H. Sutton, (Amer. Cer. Soc. Ceramic Tran., 21, 1991) pp. 215-224.

APPENDIX A

MEASUREMENT OF THE AMPLIFIER S-PARAMETERS USING AUTOMATIC NETWORK ANALYZER SYSTEM

The most convenient equipment available in our laboratory for an S-parameter measurement is the Automatic S-parameter Network Analyzer System, which is composed of the following instruments: an EIP 575 source locking microwave counter, an HP8620A sweeper with various RF plug-ins, an HP8410A network analyzer, an HP8746A test set, an HP3421A data acquisition/control unit, an HP80 desktop computer, as well as an HP82901M disk drive and an HP82905B printer. These units are interconnected as shown in Figure A1. The measurement is controlled by a BASIC program called "SPARAMS". Use of this system for an automatic measurement of S-parameters was initiated by M.Chau in 1984[A1] and modified by subsequent users[A2]. The details of the concept, the operational principles and the measurement procedures of this system can be found in [A1]. At the time I used it, its frequency range was 1-18GHz with a resolution of 1MHz. In order to be suitable for our frequency range (915MHz band) and to be able to measure the detailed resonant frequency response of a cavity (typical bandwidth of a resonant curve in our application is less than 1MHz), I modified "SPARAMS" to extend its lower frequency to 600MHz and improved its frequency resolution to 0.01MHz.

The procedures for the measurement of the equivalent S-parameters of the amplifier used in Figure 7.3 is as follows.

1) Set up an active oscillation loop as shown in Figure A2(a). An oscillation is expected to be built up at a frequency set by the cavity. Adjust the DC bias of the limiter in front of the amplifier so that the power level at the reference plane is close to the power level at which the automatic S-parameter system operates.

2) We wish to measure $[S^A]$ at that fixed power level corresponding to the power level of the active loop when it oscillates. Therefore, to accomplish the measurement of $[S^A]$ in an open loop, we removed the very narrow band cavity and replaced it by a broad band attenuator of a value equal to the cavity's insertion loss.

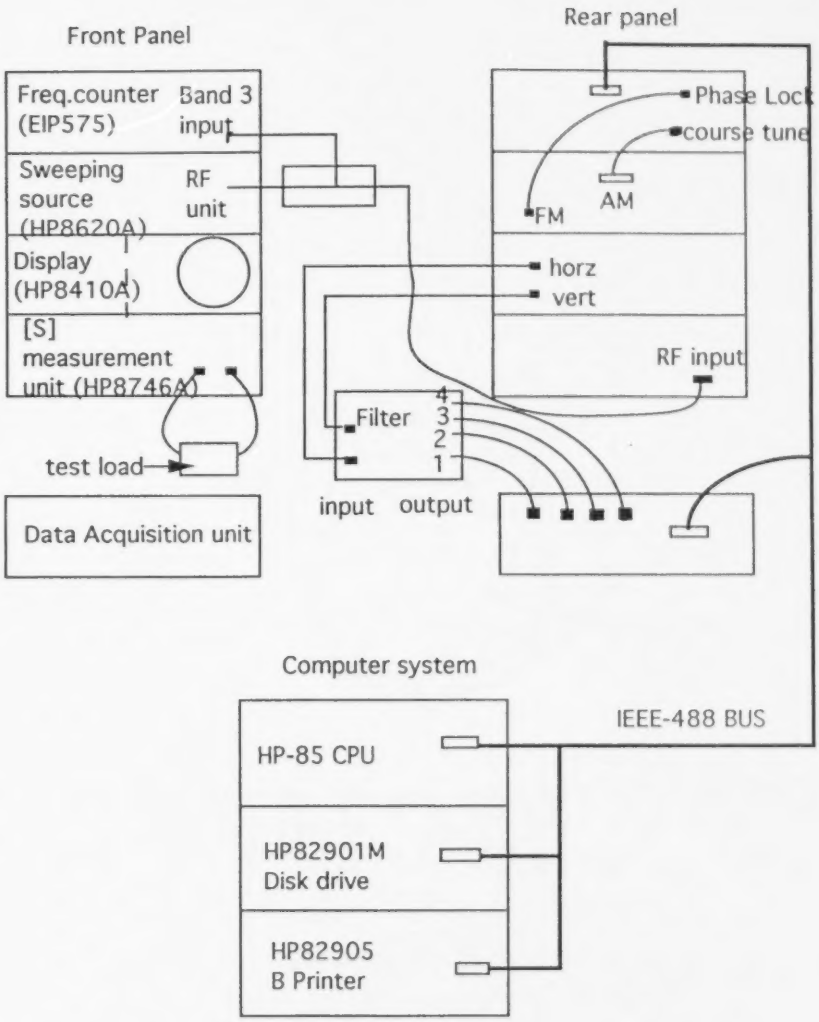

FIGURE A1 Equipment connection diagram of the automatic S-parameter network analyzer.

3) Measure the total [S] of the loop at the reference plane given, and that of the attenuator, $[S^B]$, separately.

4) Convert [S] and $[S^B]$ to their corresponding [A] and $[A^B]$ respectively using (7.14).

5) The [A] matrix of the amplifier including a limiter, $[A^A]$, can be obtained using

$$[A^A]=[A^B]^{-1}[A] \qquad (A1)$$

The frequency dependence of the $[A^A]$ given in (7.16) is the polynomial curve fitting of the measured numerical data.

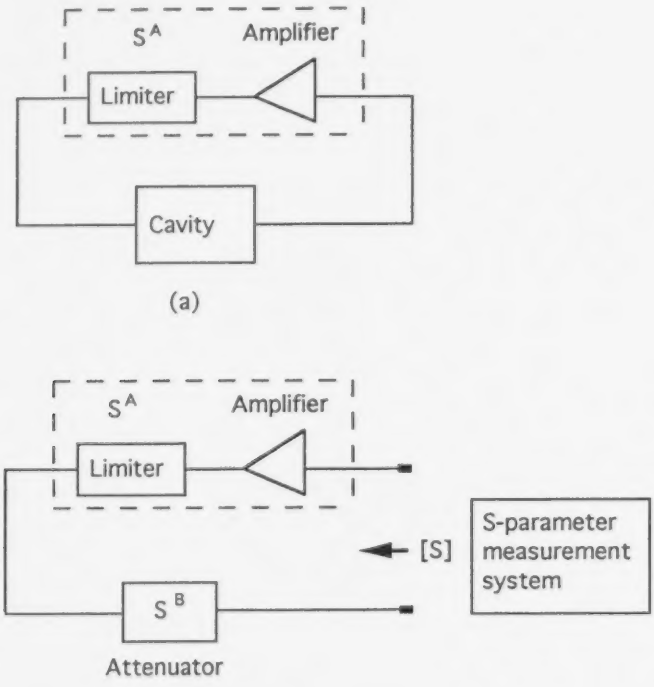

FIGURE A2 Active oscillation loop for the measurement of the equivalent S-parameters of the amplifier. (a) Closed loop for adjusting the oscillation loop power level, (b) measuring the S-parameters at the same amplifier lower level.

References

[A1] M.C.Chau, "Microprocessor-Controlled ANA System For D-Embedding FET Parameters", M.Sc. Thesis, Dept. of Electrical Engineering, Univ. of Alberta, Edmonton, Alta, Canada, fall, 1984.

[A2] H.Johansen, "A 4 GHz Cryogenic Noise Parameter Measurement System", ibid, 1991.

APPENDIX B

THE HP-BASIC PROGRAMS FOR ANALYSIS OF THE OSCILLATION LOOP FORMED BY AMPLIFIERS, A CAVITY AND TRANSMISSION LINES

All the formulas in chapter 7 have been coded in five subprograms. They are

Root —— Search for the root of a one variable equation defined in a subprogram called Function

Searchmin —— Search for the minimum of a multi-variable function

Acavity —— Calculate [A] matrix of a cavity

Atransline —— Calculate [A] matrix of a transmission line

Aamplifier —— Calculate [A] matrix of the amplifier used

A-to-S —— Convert [A] to [S]

Sloop —— Calculate [S] matrix of the loop

In addition, there are some general purpose subprograms such as

Input —— Input required initial values

Print —— Print out results in a required format

Datasaver —— Save data in the format readable by a graph program for the HP200 computer

The above subprograms can be organized flexibly to meet different needs in the loop analysis. We have developed a total of eight programs for the analysis of the loop's characteristics, including the loop oscillation frequency versus the cavity frequency at a given cavity Q factor, the loop oscillation frequency versus the loop length, the loop oscillation frequency versus the cavity Q factor and the cavity resonant frequency versus the loop oscillation frequency.

As an example, here we give the program for calculating the loop oscillation frequency versus the cavity frequency at a given cavity Q factor. To obtain the loop oscillation frequency for a given loop, we need to first find the loop [S] using Sloop, then search for the frequency that makes the phase of S_{21}=0. This frequency, according to (7.12), is the oscillation frequency. The HP-BASIC program used is listed below.

```
10    !*****************************************************
20    !*                                                   *
30    !* LOOP-FREQ(Updated by Baiqiang Tian on Nov.13,92)*
40    !*                                                   *
50    !*    This program calculates the oscillation      *
51    !* frequency of a loop formed by a cavity,amplifier*
52    !* and transmission lines,versus cavity resonant    *
53    !* frequency with a changable caity Q factor.       *
54    !*    The meanings of all variables are explained   *
55    !* when they first appear. Required input parameter*
56    !* -s and output data are explained on the screen   *
57    !* while this program is running.                   *
110   !*    Call:Input                                     *
120   !*         Printer                                   *
130   !*         Print                                     *
140   !*         Searchmin                                 *
150   !*         Datasaver                                 *
160   !*****************************************************
161   !
170   CALL Printer
180   PRINTER IS 1
190   DIM Freq(1:400)
200 COM /Loop/ Lcable1,Lcable2
210 COM /Cavity/ F_resonant,Qcavity,Cmp_cp_fact,Ncoup1,Nco
up2,Fcavity,Lcvtport1,Lcvtport2
220 COM /Atransline/ Fline,Lline
230  COM /Aamp/ Famp
240 COM /Input/ Nd,Ncv,Para(1:6),Vinitial,Vfinal
250   COM /Print/ Variable(1:400),Data(399,6),Variable$[40
],Function$[40],Para$[20]
260   COM /Data/ Ddata(399,6)
270   DIM Dname$[80]
280 COMPLEX A(1:2,1:2),S(1:2,1:2)
290 Function$="Floop(MHz)"     ! give function name
300 Variable$="Fcavity(MHz)"     ! give variable name
310 Para$="Q-factor"          ! give parameter name
320 !*********************************************
330 !*   You may change following parameters     *
340 !*********************************************
350!( All the cable lengths given must be the electric len
gth in centermeter!)
360!----------------The cavity parameter set-------------
370 Cmp_cp_fact=14 ! The comprehensive coupling factor (WA
RN!! This value has
380!                  been calibrated, don't change arbitar
ily!)
390 Ncoup1=11.3   !Coupling transformer ratio at cavity po
rt1 (WARN!! the ratio
400!                has been calibrated, don't change arbit
arily)
410 Ncoup2=40.0  !coupling transformer ratio at cavity por
```

```
t2 (WARN!! the ratio
420!              has been calibrated,don't change arbitar
ily)
430 Lcvtport1=49.05 !Cable length used at port1(WARN:the l
ength has been calibe-
440!                   rated. Do not change arbitarily !)
450 Lcvtport2=50.05 !Cable length used at port1 (Calibrate
d,do not change arbtar
460!                   ily)
470 Lcable1=0          !Cable length between the cavity po
rt2 (the output of
480                        !the cavity)
490                        !and the input of the amplifier
 in centermeter.
500 Lcable2=103.31   !Cable length between the amplifier o
utput and cavity port1
510                    !(the input of the cavity) in centerm
eter.
520!
530!        ================Input parameters===========
540 CALL Input
550!
560!        ================Calculation=============
570!
580 Vincr=(Vfinal-Vinitial)/Nd  ! Variable increment
590 FOR Nn=1 TO Ncv
600 FOR N=1 TO Nd
610 Variable(N)=Vinitial+(N-1)*Vincr
620 Qcavity=Para(Nn)         !give Q-factor value which is
given through INPUT
630 F_resonant=Variable(N)  !give cavity resonant frequenc
y which is given
640                          ! through INPUT
650 Low=F_resonant-10   !Limiting the searching range with
in +/-1MHz
660 High=F_resonant+10  !around the given resonant frequen
cy
670 CALL Searchmin(Low,High,Fmin,Xmin)     ! Searching osc
illation frequency
680 IF Fmin>1 THEN Error1
690  F_osc=Xmin
700 Data(N-1,Nn)=F_osc               !the calculated F_osc
is
710                                  ! converted to Data ar
ray for output
720 Data(N-1,0)=F_resonant           ! the resonant frequen
cy is converted
730                                  ! to Data array for ou
tput
740 NEXT N
750 NEXT Nn
```

```
760!CLEAR SCREEN
770 BEEP 600,1
780 ! PRINT "Fmin";Fmin
790 INPUT "Print out (Y/N) ?",Answer$
800 IF Answer$="N" THEN Screen
810 PRINT "Connect the printer,then press 'cont'!"
820 BEEP 600,5
830 PAUSE
840 INPUT "Enter a title(one line max.):",Dname$
850       INPUT "Date:dd/mm/yy=?",Date$
860 CALL Printer
870 PRINTER IS 9
880 GOTO Print
890 Screen:PRINTER IS 1
900 Print:PRINT "                    ";Dname$
910       PRINT "----------------------------------------
--------------------"
920       PRINT "
 DATE:";Date$
930       PRINT "
 Program:LOOP_FREQ"
940       PRINT "----------------------------------------
--------------------"
950 PRINT "Lcable1=";Lcable1,"Lcable2=";Lcable2,"Lcvtport1
=";Lcvtport1,"Lcvtport2=";Lcvtport2,
960  PRINT "Ncoup11=";Ncoup1,"Ncoup12=";Ncoup2,"Cmp_cp_fac
t=";Cmp_cp_fact
970  PRINT "----------------------------------------
--------------------"
980  PRINT
990  CALL Print
1000 !
1010 !
1020 !
1030 !====================Save data================
1040 INPUT "Do you want to save data ? (Y/N)",Answer$
1050 IF Answer$="N" THEN Exit
1060 CALL Datasaver
1070 GOTO Exit      !Skip error trap
1080 Error1:BEEP 600,3
1090     !  CLEAR SCREEN
1100        PRINT "The minimun is larger than 1 degree at"
;F_resonant
1110        GOTO 690
1120 Exit:END
1130!
1140!=========================Subprograms================
====
1150!
1160 SUB Acavity(COMPLEX Acvt(*))
1170 !*****************************************************
```

```
**********************
1180!*Calculate [A] matrix of a two-port cavity with two t
ransformers simulati *
1190!*ng the coupling device and two transmission lines co
nnecting with the two*
1200!*ports.  The output is the [A] matrix,Acvt(*).
                     *
1210!*The inputs through COM/Cavity are
                     *
1220!*F_resonant----cavity resonant freqency
                     *
1230!*Qcavity---- cavity unloaded Q-factor
                     *
1240!*Cmp_cp_fact----a comprehensive coupling factor defin
ed by myself(see     *
1250!*               B.Q.Tian's note on this)
                     *
1260!*Ncoup1 and Ncoup2-----coupling transformer ratios of
 the port1 and       *
1270!*                       the port2
                     *
1280!*Lcvtport1 and Lcvtport2-----lengths of the transmiss
ion lines,           *
1290!*Lcvtport1=L and Lcvtport2=0 gives S-parameters of th
e cavity itself.     *
1300!*Fcavity-----Freqency of interest
                     *
1310!*****************************************************
**********************
1320 COM /Cavity/ F_resonant,Qcavity,Cmp_cp_fact,Ncoup1,Nc
oup2,Fcavity,Lcvtport1,Lcvtport2
1330 COMPLEX Y,A0(1:2,1:2),Acvt1(1:2,1:2),Acvt2(1:2,1:2),A
line1(1:2,1:2),Aline2(1:2,1:2)
1340 DIM A1(1:2,1:2),A2(1:2,1:2)
1350 Yreal=Cmp_cp_fact/Qcavity
1360 Yimg=Yreal*Qcavity*(Fcavity/F_resonant-F_resonant/Fca
vity)
1370 Y=CMPLX(Yreal,Yimg)
1380 Beta=2*PI*Fcavity/30000
1390 A0(1,1)=1
1400 A0(1,2)=0
1410 A0(2,1)=Y
1420 A0(2,2)=1
1430 A1(1,1)=1/Ncoup1
1440 A1(1,2)=0
1450 A1(2,1)=0
1460 A1(2,2)=Ncoup1
1470 A2(1,1)=Ncoup2
1480 A2(1,2)=0
1490 A2(2,1)=0
1500 A2(2,2)=1/Ncoup2
1510 Aline1(1,1)=COS(Beta*Lcvtport1)
```

```
1520 Aline1(1,2)=CMPLX(0,SIN(Beta*Lcvtport1))
1530 Aline1(2,1)=CMPLX(0,SIN(Beta*Lcvtport1))
1540 Aline1(2,2)=COS(Beta*Lcvtport1)
1550 Aline2(1,1)=COS(Beta*Lcvtport2)
1560 Aline2(1,2)=CMPLX(0,SIN(Beta*Lcvtport2))
1570 Aline2(2,1)=CMPLX(0,SIN(Beta*Lcvtport2))
1580 Aline2(2,2)=COS(Beta*Lcvtport2)
1590 MAT Acvt1= Aline1*A1
1600 FOR I=1 TO 2
1610 FOR J=1 TO 2
1620 Acvt2(I,J)=Acvt1(I,J)
1630 NEXT J
1640 NEXT I
1650 MAT Acvt1= Acvt2*A0
1660 FOR I=1 TO 2
1670 FOR J=1 TO 2
1680 Acvt2(I,J)=Acvt1(I,J)
1690 NEXT J
1700 NEXT I
1710 MAT Acvt1= Acvt2*A2
1720 FOR I=1 TO 2
1730 FOR J=1 TO 2
1740 Acvt2(I,J)=Acvt1(I,J)
1750 NEXT J
1760 NEXT I
1770 MAT Acvt= Acvt2*Aline2
1780 SUBEND
1790!
1800!
1810!=========================================
1820!
1830 SUB Atransline(COMPLEX Aline(*))
1840 !*******************************************************
**********************
1850 !*For calculating [A] matrix of a piece of a transmis
sion line. The input *
1860 !*are Fline---the frequency
                    *
1870 !*    Lline---the length of the transmission line.
                    *
1880 !*The output is Aline----[A] matrix of the line.
                    *
1890 !*******************************************************
**********************
1900 COM /Atransline/ Fline,Lline
1910 Beta=2*PI*Fline/30000
1920 Aline(1,1)=COS(Beta*Lline)
1930 Aline(1,2)=CMPLX(0,SIN(Beta*Lline))
1940 Aline(2,1)=CMPLX(0,SIN(Beta*Lline))
1950 Aline(2,2)=COS(Beta*Lline)
1960 SUBEND
```

```
1970 !
1980 !
1990 SUB Aamplifier(COMPLEX Aamp(*))
2000 !
2010 !****************************************
2020 !* For amplifier [A] matrix calculation.*
2030 !****************************************
2040 !
2050 COM /Aamp/ Famp
2060 Realpart=24.224-.0531919*Famp+2.89236E-5*Famp*Famp
2070 Imgpart=2.91463-.00316638*Famp
2080 Aamp(1,1)=CMPLX(Realpart,Imgpart)
2090 Realpart=25.582-.0564754*Famp+3.08759E-5*Famp*Famp
2100 Imgpart=6.07467-.00992886*Famp+3.5937E-6*Famp*Famp
2110 Aamp(1,2)=CMPLX(Realpart,Imgpart)
2120 Realpart=25.0559-.0550109*Famp+2.9917E-5*Famp*Famp
2130 Imgpart=2.90077-.00315084*Famp
2140 Aamp(2,1)=CMPLX(Realpart,Imgpart)
2150 Realpart=24.3153-.0537048*Famp+2.93626E-5*Famp*Famp
2160 Imgpart=6.78937-.0114867*Famp+4.4431E-6*Famp*Famp
2170 Aamp(2,2)=CMPLX(Realpart,Imgpart)
2180 SUBEND
2190 !
2200 !
2210 !
2220 !
2230 SUB A_to_s(COMPLEX S(*),COMPLEX A(*))
2240 !*********************************************
2250 !*Conversion of the [A] matrix to [S] matrix *
2260 !*********************************************
2270 COMPLEX Da,Addition
2280 Da=DET(A)
2290 Addition=A(1,1)+A(1,2)+A(2,1)+A(2,2)
2300 S(1,1)=(A(1,1)+A(1,2)-A(2,1)-A(2,2))/Addition
2310 S(1,2)=2*Da/Addition
2320 S(2,1)=2/Addition
2330 S(2,2)=(-A(1,1)+A(1,2)-A(2,1)+A(2,2))/Addition
2340 SUBEND
2350 !=====================================================
==
2360 !
2370 !
2380 SUB Sloop(COMPLEX Sloop(*))
2390 !*********************************
2400 !* Calculate the [S] of the loop  *
2410 !*********************************
2420! OPTION BASE 1
2430 COM /Loop/ Lcable1,Lcable2
2440 COM /Cavity/ F_resonant,Qcavity,Cmp_cp_fact,Ncoup1,Nc
oup2,Fcavity,Lcvtport1,Lcvtport2
2450 COM /Atransline/ Fline,Lline
```

```
2460 COM /Aamp/ Famp
2470 COMPLEX Aloop(1:2,1:2),Acvt(1:2,1:2),A1(1:2,1:2),A2(1
:2,1:2),Aline(1:2,1:2),Aamp(1:2,1:2)
2480 CALL Acavity(Acvt(*))       ! [A] of the cavity
2490 Lline=Lcable1
2500 CALL Atransline(Aline(*))    ! the [A] of cable1
2510 MAT A1= Acvt*Aline
2520 CALL Aamplifier(Aamp(*))     ! [A] of the amplifier
2530 MAT A2= A1*Aamp
2540 Lline=Lcable2
2550 CALL Atransline(Aline(*))    ! [A] of the cable2
2560 MAT Aloop= A2*Aline
2570 CALL A_to_s(Sloop(*),Aloop(*)) ! converting the loop
[A] to [S]
2580 SUBEND
2590 !
2600 !
2610 !
2620 Printer:SUB Printer! used for listing to serial print
er WRT/12/16/91
2630 !==========================================================
===============
2640 !
2650 CONTROL 9,3;9600   ! set baud rate=9600
2660 CONTROL 9,12;128+16! disable carrier detect, disable
CTS
2670 CONTROL 9,4;3+0+0+0! 8 bits+1 st.bit+parity disabled+
odd parity
2680 CONTROL 9,5;0+1! toggle DTR, force RTS=active=ready
2690   ! LIST #9 ! list to printer via serialport
2700 SUBEND
2710!
2720!
2730!
2740!=========================================================
====================
2750!
2760  SUB Input
2770!*********************************
2780!* Input the initial parameters *
2790!*********************************
2800 COM /Input/ Nd,Ncv,Para(*),Vinitial,Vfinal
2810 INPUT "Inintial value,final value=?",Vinitial,Vfinal
2820 INPUT "Curve number=?(< 6 !!)",Ncv
2830 INPUT "Data number per curve =?( < 399 !!)",Nd
2840 FOR N=1 TO Ncv
2850 PRINT "Value of parameter #";N;"=?"
2860 INPUT Para(N)
2870 NEXT N
2880 PRINT "Calculating........"
2890  SUBEND
```

```
2900  !
2910  !
2920 SUB Datasaver    !  B.Tian 23/6/92
2930 ! ************************************************
**
2940 ! * save data in the format readable by GRAPH program
 *
2950 ! ************************************************
**
2960 !
2970 COM /Input/ Nd,Ncv,Para(*),Vinitial,Vfinal
2980  COM /Print/ Variable(*),Data(*),Variable$,Function$,
Para$
2990  COM /Data/ Ddata(*)
3000 DIM Title$(0:9)[30],Ppara$(1:7)[20]
3010 REDIM Ddata(Nd,Ncv)
3020 FOR N=0 TO Nd
3030 FOR Nn=0 TO Ncv
3040 Ddata(N,Nn)=Data(N,Nn)
3050 NEXT Nn
3060 NEXT N
3070 FOR N=1 TO Ncv
3080 Ppara$(N)=Para$&VAL$(Para(N))
3090 NEXT N
3100!CLEAR SCREEN
3110 PRINT
3120 PRINT TABXY(10,8),"Put a data disk on Drive 0, then p
ress 'cont'!"
3130 PAUSE
3140 BEEP 800,.5
3150 INPUT "Enter a name for the datafile (WARNING! Do not
 use a DUPLICATED name)",Fname$
3160 INPUT "Enter the title(max.30 characters): ",Title$(8
)
3170 INPUT "Enter the date(mm/dd/yy): ",Title$(9)
3180 Title$(0)=Variable$
3190 Title$(1)=Function$
3200 FOR N=1 TO Ncv
3210 Title$(N+1)=Ppara$(N)
3220 NEXT N
3230 Size=INT((366+(Ncv+1)*Nd*8)/256)+1        ! estimated
 size of the datafile
3240 Size1=Nd       ! number of data in each curve
3250 Size2=Ncv      ! number of curves
3260 CREATE BDAT Fname$,Size              ! creat a datafil
e
3270 PRINT TABXY(10,10),"Saving datafile of ";CHR$(34);Fna
me$;CHR$(34);"..."
3280 ASSIGN @Diskdrive TO Fname$
3290 OUTPUT @Diskdrive;Size1,Size2
3300 OUTPUT @Diskdrive;Title$(*)
3310 ON END @Diskdrive GOTO Close
```

```
3320 OUTPUT @Diskdrive;Ddata(*)
3330 Close:ASSIGN @Diskdrive TO *
3340 SUBEND
3350 !
3360 !
3370!=========================================================
====================
3380!
3390  SUB Root(X0,Root)
3400 !  ***************************************************
**********
3410  ! * Subprogram"Root"
        *
3420 !  * Finding root of the function specified in Sub "F
unction" *
3430  ! * Call "Function"
        *
3440  ! ***************************************************
**********
3450  ! INPUT PARAMETERS: (1)Y---Function defined in SUB "
Function"
3460  !                   (2) X0--Initial value of X
3470  !                   (3) A---Accuracy
3480  ! OUTPUT VARIABLE:X0---Root of the Function Y
3490    A=.00001
3500    D1=.01*X0
3510    FOR I=1 TO 200
3520      X=X0
3530      CALL Function(X,Y)
3540      Y0=Y
3550      IF ABS(Y0)<A THEN Exit1
3560      X=X0+D1
3570      CALL Function(X,Y)
3580      Y1=Y
3590      Y2=(Y1-Y0)/D1
3600      IF Y2=0 THEN 3660
3610      Y3=Y0/Y2
3620      X0=X0-Y3
3630      D2=ABS(Y3)
3640      D1=.1*D2
3650    NEXT I
3660    PRINT "Y2=0"
3670    SUBEXIT
3680 Exit1:Root=X0
3690   ! PRINT "ROOT=",Root,Y0
3700  SUBEND
3710 !-------------------------
3720 !
3730 !-------------------------
3740 SUB Function(X,Y)
3750 COM /Loop/ Lcable1,Lcable2
```

```
3760 COM /Cavity/ F_resonant,Qcavity,Cmp_cp_fact,Ncoup1,Nc
oup2,Fcavity,Lcvtport1,Lcvtport2
3770 COM /Atransline/ Fline,Lline
3780 COM /Aamp/ Famp
3790  COMPLEX Func(1:2,1:2)
3800 Freq=X
3810   Fcavity=Freq
3820 Fline=Freq
3830 Famp=Freq
3840 CALL Sloop(Func(*))   !Send [S] of the loop to [Func]
3850 Y=ABS(ARG(Func(2,1))*180/PI)    ! Absolute value of p
hase of S21 to Y
3860 SUBEND
3870!
3880!
3890!---------------------------------------
3900  SUB Searchmin(Low,High,Fmin,Xmin)
3910 !*****************************************************
*********************
3920 !* Search the minimun Y defined in Function(X,Y). Low
 and High determine*
3930 !*the searching range of variable X
                   *
3940 !*****************************************************
*********************
3950 !-----------------------------------------------
3960  X1=Low+.618*(High-Low)
3970  X2=High-.618*(High-Low)
3980 Comparing: IF (High-Low)<.001 THEN Out
3990                   CALL Function(X1,Y1)
4000                   CALL Function(X2,Y2)
4010                   IF Y1<Y2 THEN Case1
4020                        High=X1
4030                        X1=X2
4040                        X2=High-.618*(High-Low)
4050                        GOTO Comparing
4060 Case1:                 Low=X2
4070                        X2=X1
4080                        X1=Low+.618*(High-Low)
4090                    GOTO Comparing
4100 Out:          CALL Function(X1,Y1)
4110               CALL Function(X2,Y2)
4120               IF Y1>Y2 THEN
4130                  Fmin=Y2
4140                  Xmin=X2
4150                ELSE
4160                  Fmin=Y1
4170                  Xmin=X1
4180                END IF
4190   SUBEND
4200   !
```

```
4210   !
4220  SUB Print
4230  !*********************************
4240  !* Print data in a required form *
4250  !*********************************
4260  COM /Print/ Variable(*),Data(*),Variable$,Function$,
Para$
4270 COM /Input/ Nd,Ncv,Para(*),Vinitial,Vfinal
4280  !---------Printing data--------
4290  PRINT Para$;
4300  FOR Nn=1 TO Ncv
4310  Para(Nn)=DROUND(Para(Nn),6)
4320  PRINT TAB((Nn-1)*11+12),Para(Nn);
4330  NEXT Nn
4340  PRINT
4350  PRINT "-----------------------------------------------
--------------------"
4360  PRINT "=";Variable$;"=";TAB(Ncv*5+12),"===";Function
$;"==="    ! Print name of variables
4370  PRINT
4380  FOR N=1 TO Nd
4390  Data(N-1,0)=DROUND(Data(N-1,0),7)
4400  PRINT Data(N-1,0);
4410  FOR Nn=1 TO Ncv
4420  Data(N-1,Nn)=DROUND(Data(N-1,Nn),7)
4430 PRINT TAB((Nn-1)*11+11),Data(N-1,Nn);
4440 NEXT Nn
4450 PRINT
4460 NEXT N
4470  PRINTER IS 1
4480  SUBEND
4490  !
4500  !                          **************
4510  !                          *   THE END  *
4520  !                          **************
```

APPENDIX C

METHOD FOR Q MEASUREMENT FOR A CAVITY

IN AN ACTIVE LOOP AND ASSOCIATED PROBLEMS

With the active system discussed in chapter 7, we only measured the dielectric constant not the loss factor. Because the error in the required cavity Q measurement is too large to allow us to calculate the loss factor with reasonable accuracy, in this appendix, we will give the formulation of the active oscillation loop Q-measurement method to illustrate the associated accuracy problems.

I. Method Formulation

It is well known that the magnitude of reflection coefficient at port 1 of the cavity in Figure 7.2 is[7.13]

$$|\Gamma(f)|^2 = \frac{\Gamma_o^2 + (2Q_L\frac{f-f_c}{f_c})^2}{1 + (2Q_L\frac{f-f_c}{f_c})^2} \qquad (C1)$$

where Γ_o is the reflection coefficient at the cavity resonance, f is the loop oscillation frequency, f_c is the cavity resonant frequency, Q_L is the system Q of the cavity, which is related to the cavity Q by

$$Q_L = \frac{Q}{\beta + 1} \qquad (C2)$$

where Q is the sample loaded cavity Q factor when the loading of port 2 is neglected, β is the coupling factor of the port 1, which can be expressed by

$$\beta = \frac{1}{\bar{G}} \qquad (C3)$$

where $\bar{G}$ is the normalized input conductance of the cavity at its resonant frequency and can be related to the reflection coefficient by

$$\Gamma o = \begin{cases} \dfrac{1 - \bar{G}}{1 + \bar{G}} & \text{for } \bar{G} < 1 \qquad \text{(C4a)} \\ \dfrac{\bar{G} - 1}{1 + \bar{G}} & \text{for } \bar{G} > 1 \qquad \text{(C4b)} \end{cases}$$

According to (2.14), we have

$$Q = \frac{Co}{\bar{G}} \qquad \text{(C5)}$$

where Co is a constant and can be determined easily. For example, according to (C5), Co will equal Q when $\bar{G}$=1. Remembering that coupling for this case is fixed, one can make $\bar{G}$=1 by changing the cavity Q through increasing or reducing the loss in the cavity until the cavity is matched. In other words, Co can be determined by measuring the Q at a matched condition.

There are 8 unknown parameters in the above five equations, namely, $|\Gamma|$, f, fo, Q, Q_L, β, Γo and $\bar{G}$. Using the setup shown in Figure 7.7, $|\Gamma|$ can be measured with the reflectometer and f with the frequency counter. Moreover, f_c can be calculated from the measured loop oscillation frequency, f, using the theoretical model developed in chapter 7. Eventually the cavity Q, along with the other four remaining unknowns, Q_L, β, Γo and $\bar{G}$, can be determined using the five equations (C1) to (C5). Note that Q is derived from the measure $|\Gamma|$ and f.

II. Results and Problems

The same set of 8 samples used in the dielectric constant measurement in chapter 7 were used here for the Q measurement to test the above method. The Q values obtained using this method are listed in Table C1, along with the measured Q values using a swept frequency method for comparison. Since the swept frequency method is a standard Q measurement method, its results are used as our reference, showing the active method Q factor results differ by as much as 190%. Obviously, with such a large error in Q factor prediction, no reliable loss factor measurement is possible.

Table C1 Q-factor data measured in the active system, compared with data obtained using the passive swept frequency system.

Sample No.	f_L(MHz)	f_c(MHz)	$\|\Gamma\|$	Q_L		
				Sweeping	Active	Difference(%)
1	945.85	945.99	0.327	3141	6453	105
2	946.72	946.90	0.298	3069	4828	57
3	945.59	945.73	0.299	2747	5848	113
4	945.20	945.33	0.313	2681	6416	139
5	944.10	944.19	0.312	2566	7462	191
6	946.03	946.20	0.245	2475	4195	70
7	939.21	939.06	0.277	422	591	40
8	956.66	956.66	0.755	342	137	60

This large error is due to the high sensitivity of Q with respect to the cavity's resonant frequency shift, Δf_c, as demonstrated in Table C2, An error of 0.4 MHz in Δf_c can cause an error of 676% in Q_L. Q values may vary for different reflection coefficients at which

Table C2 Q-factor vs. Δf_c, showing the sensitivity of Q to the frequency change ($|\Gamma|$=0.3 and f_c=1000MHz).

Δf_c(MHz)	Q_L	
	Values	Difference(%)
0.1	7044	676
0.2	4639	411
0.3	2802	209
0.4	1565	72
0.5	908	0

a given Δf_c is measured and calculated. However, the tendency remains similar. In our case, the error in the Δf_c calculation alone may be

as much as 0.4MHz (equivalent to 0.04% at 1000MHz as stated in chapter 7), which is enough to cause the large Q error, not to mention other errors such as those in the measurements of Δf_L and $|\Gamma|$.

Improvement of the amplifier modeling is the key to reducing the error. In the current theoretical loop model, the S-parameters of the amplifier are obtained using an Automatic Network Analyzer System at a given power level. However, variations in these parameters are expected as the amplifier power level fluctuates. This will cause an error in our f_c prediction. Therefore, incorporating a power level dependent amplifier model into the loop oscillation model would reduce the error in f_c and consequently in the loss factor. In addition, any measures which can stabilize the amplifier parameters, such as a power leveling feedback loop, will definitely help to improve the predictability in f_c.